Charles University,

Faculty of Science

Study program: Experimental Plant Biology

MLOs and EXO70H4 interplay in trichomes cell wall development

Author:

George A. Caldarescu

Supervisor:

Viktor Žárský

Consultant:

Peter Sabol

Doctoral thesis

Prague, 2024

Student's declaration:

I hereby declare that I have witten this PhD thesis by myself, that I have listed all information sources and literature used and that this thesis was submitted only once and has not been used to apply for another academic title

Prohlášení studenta:

Prohlašuji, že jsem závěrečnou práci zpracoval samostatně a že jsem uvedl všechny použité informační zdroje a literaturu. Tato práce ani její podstatná část nebyla předložena k získání jiného nebo stejného akademického titulu.

In Prague/V Praze: George Alexandru Caldarescu

Supervisor's declaration:

I hereby confirm that the contribution of George A. Caldarescu to the published work corresponds to what he has declared here.

Prohlášení školitele:

Prohlašuji, že podíl George A. Caldarescu na předložených publikacích odpovídá tomu, co v této disertační práci deklaruje.

In Prague/V Praze: Prof. RNDr. Viktor Žárský, CSc.

Acknowledgements

I would like to thank my supervisor, Viktor Zarsky, who gave me the opportunity to do my PhD in his lab and introduced me to the world of research with all his passion for science.

I also want to thank Peter Sabol for all the comments and corrections of the text, and together with Michal Hala, for all the teaching in the lab.

I would like to thank my colleagues in our lab and not for all the constructive discussions and collaborations we had during this time.

Lastly, I want like to thank my two- and four-legged family :) for all the support I have received, and a special thanks goes to Karolina for her support and encouragement during challenging moments.

Research presented in this thesis was supported by these grants:

- Czech Science Foundation/GACR international project number **GC19-02242J**
- START student grant: Grant Schemes at CU
  (reg. no. CZ.02.2.69/0.0/0.0/19_073/0016935) project number **START/SCI/136**

Contents

Abbreviations

BHLH	Basic helix-loop-helix
CAMTA3	CALMODULIN-BINDING TRASCRIPTION ACTIVATOR 3
Callose	β-1,3-glucan
CATCHR	Complexes associated with tethering containing helical rods
CW	Cell wall
EDS	Energy Dispersive X-ray Spectroscopy
FTIR	Fourier transform Infrared spectroscopy
GSL	Glucan synthase-like
HM	Heavy metals
LOF	Loss-Of-Function
MLO	Mildew Resistance Locus O
OR	Ortmmanian ring
PM	Plasma membrane
PMR4	Powdery Mildew Resistant 4
SNARE	*N-ethylmaleimide-sensitive-factor* attachment receptor
SCW	Secondary cell wall
TM	Transmembrane

Abstract

EXO70H4 subunit of the exocyst complex plays a crucial role in vesicle tethering during secondary trichome cell wall biogenesis. This thesis investigates the intricate relationship between MLO protein, which function as plasma membrane calcium channels, and the exocyst complex in driving secondary cell wall synthesis in Arabidopsis thaliana trichomes. Analysis of three *mlo* mutants trichomes revealed disrupted callose deposition and thinner cell walls, with MLO6 isoform playing the most significant role. The mislocalization of PMR4, a callose synthase, in *exo70H4-1* and *mlo* triple mutants highlights the complex interaction between MLO proteins and EXO70H4 in callose deposition. Furthermore, ROS and heavy metals localisation are compromised in all mutants studied, indicating the role of MLO proteins as positive regulators of these trichome features. Interestingly, Raman spectroscopy revealed a lack of calcium carbonate in the cell wall of all mutants, providing insights into the role of MLO proteins along with the EXO70H4 in biomineralisation and cell wall hardening. These findings shed light on the cellular function of MLO proteins and their integral role in the fundamental cellular process of cell wall formation in Arabidopsis thaliana trichomes. And lastly, the introduction of the proximity-labelling methods in our laboratory and the study of the Arabidopsis proteome under biotic stress.

Abstrakt

EXO70H4 podjednotka komplexu exocyst hraje klíčovou roli při vázání vezikul během biogeneze sekundární buněčné stěny trichomu. Tato práce zkoumá složitý vztah mezi proteiny MLO, které fungují jako vápníkové kanály plazmatické membrány, a kom-

plexem exocyst při řízení syntézy sekundární buněčné stěny v trichomech Arabidopsis thaliana. Analýza tří trichomů mutantů *mlo* odhalila narušené ukládání kalózy a tenčí buněčné stěny, přičemž nejvýznamnější roli hrála izoforma MLO6. Chybná lokalizace PMR4, kalosové syntázy, u *exo70H4-1* a trojitých mutantů *mlo* poukazuje na složitou interakci mezi proteiny MLO a EXO70H4 při ukládání kalosy. Kromě toho je u všech studovaných mutantů narušena lokalizace ROS a těžkých kovů, což naznačuje roli proteinů MLO jako pozitivních regulátorů těchto vlastností trichomu. Zajímavé je, že Ramanova spektroskopie odhalila nedostatek uhličitanu vápenatého v buněčné stěně všech mutantů, což poskytuje pohled na roli proteinů MLO spolu s EXO70H4 v biomineralizaci a zpevňování buněčné stěny. Tato zjištění vrhají světlo na buněčnou funkci proteinů MLO a jejich nedílnou úlohu v základním buněčném procesu tvorby buněčné stěny v trichomech Arabidopsis thaliana. A konečně zavedení metod proximitního značení v naší laboratoři a studium proteomu Arabidopsis v podmínkách biotického stresu.

1. Published article

The work in this thesis is based on the following published article in collaboration with Ralph Panstruga's laboratory in Aachen.

My contribution to the paper: generation of constructs of fluorophore-labelled proteins, established transgenic lines, performed histochemical staining of leaf-attached trichomes, generated the mlo6 CRISPR line, performed microscopy, yeast-two hybrid experiments, and FRET-FLIM experiments, and conducted image analysis and statistical analysis.

In the results chapter of this thesis, are present some experiments that Jan W Huebbers did in collaboration with the co-authors (cell wall matrix monosaccharides, FTIR analysis, cell wall transcription data and luciferase complementation). David Ušák (Laboratory of Integrative Structural Biology) performed the molecular dynamic simulation of MLO6 trimer.

https://doi.org/10.1093/plcell/koad319 THE PLANT CELL 2024: 36: 1007–1035

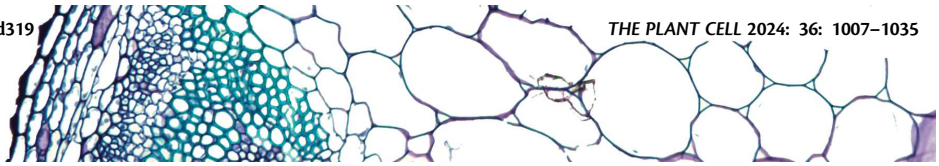

Research Article

Interplay of EXO70 and MLO proteins modulates trichome cell wall composition and susceptibility to powdery mildew

Jan W. Huebbers [1,†] George A. Caldarescu [2,†] Zdeňka Kubátová [2] Peter Sabol [2] Sophie C.J. Levecque [1] Hannah Kuhn [1] Ivan Kulich [2,‡] Anja Reinstädler [1] Kim Büttgen [1] Alba Manga-Robles [3] Hugo Mélida [3] Markus Pauly [4] Ralph Panstruga [1,*] and Viktor Žárský [2,5,*]

1 Unit of Plant Molecular Cell Biology, Institute for Biology I, RWTH Aachen University, Worringerweg 1, 52056 Aachen, Germany
2 Department of Experimental Plant Biology, Faculty of Science, Charles University, Viničná 5, 128 44 Prague, Czech Republic
3 Área de Fisiología Vegetal, Departamento de Ingeniería y Ciencias Agrarias, Universidad de León, 24071 León, Spain
4 Institute for Plant Cell Biology and Biotechnology, Heinrich-Heine-University Düsseldorf, Universitätsstr. 1, 40225 Düsseldorf, Germany
5 Institute of Experimental Botany of the Czech Academy of Sciences, Laboratory of Cell Biology, Rozvojová 263, 165 02 Prague 6 Lysolaje, Czech Republic

*Author for correspondence: panstruga@bio1.rwth-aachen.de (R.P.), viktor.zarsky@natur.cuni.cz (V.Ž.)
†These authors contributed equally to this work.
‡Present address: Institute for Science and Technology Austria (ISTA), Am Campus 1, 3400 Klosterneuburg, Austria.
The authors responsible for distribution of materials integral to the findings presented in this article in accordance with the policy described in the Instructions for Authors (https://academic.oup.com/plcell/pages/General-Instructions) are: Ralph Panstruga (panstruga@bio1.rwth-aachen.de) and Viktor Žárský (viktor.zarsky@natur.cuni.cz).

Abstract

Exocyst component of 70-kDa (EXO70) proteins are constituents of the exocyst complex implicated in vesicle tethering during exocytosis. MILDEW RESISTANCE LOCUS O (MLO) proteins are plant-specific calcium channels and some MLO isoforms enable fungal powdery mildew pathogenesis. We here detected an unexpected phenotypic overlap of *Arabidopsis thaliana exo70H4* and *mlo2 mlo6 mlo12* triple mutant plants regarding the biogenesis of leaf trichome secondary cell walls. Biochemical and Fourier transform infrared spectroscopic analyses corroborated deficiencies in the composition of trichome cell walls in these mutants. Transgenic lines expressing fluorophore-tagged EXO70H4 and MLO exhibited extensive colocalization of these proteins. Furthermore, mCherry-EXO70H4 mislocalized in trichomes of the *mlo* triple mutant and, vice versa, MLO6-GFP mislocalized in trichomes of the *exo70H4* mutant. Expression of GFP-marked PMR4 callose synthase, a known cargo of EXO70H4-dependent exocytosis, revealed reduced cell wall delivery of GFP-PMR4 in trichomes of *mlo* triple mutant plants. In vivo protein–protein interaction assays in plant and yeast cells uncovered isoform-preferential interactions between EXO70.2 subfamily members and MLO proteins. Finally, *exo70H4* and *mlo6* mutants, when combined, showed synergistically enhanced resistance to powdery mildew attack. Taken together, our data point to an isoform-specific interplay of EXO70 and MLO proteins in the modulation of trichome cell wall biogenesis and powdery mildew susceptibility.

Received September 07, 2023. Accepted December 15, 2023. Advance access publication December 20, 2023

Open Access

2. Introduction and Aims

1.1 Trichomes

Trichomes are outgrowths of epidermal cells that are found on the surface of plant organs, including leaves. They can be unbranched or branched, and are either uni- or multicellular.

These structures play a critical role in enabling plants to cope with and adapt to various abiotic stresses, such as regulating transpiration, providing mechanical resistance against wind and sand damage, and mitigating the effects of salt and excessive light **(X. Wang et al., 2021)**.

Additionally, trichomes play a vital role in defending against biotic stressors by serving as the first line of defence against herbivore attacks, containing and secreting secondary metabolites that act as deterrents, and forming a physical barrier **(Kaur et al., 2020)**. Guo *et al.* **(2022)** observed an accumulation of cadmium ions in *A. thaliana* and *Brassica rapa L.* subsp. pekinensis, suggesting a probable role of trichomes in heavy metals detoxification in soils. In the context of biotic and abiotic stress, trichomes can be seen as "antennas" and first receptors out of the plant. The disruption of glandular trichomes by herbivorous insects has been observed to trigger the expression of defence transcripts regulated by jasmonic acid **(Peiffer et al., 2009)**. Furthermore, it has been observed that touching trichomes serves as an initial receptor for external signals, which initiates calcium propagation from the base of the trichome through the CALMOLDULIN-BINDING TRANSCRIPTION ACTIVATOR 3 (CAMTA3), ultimately resulting in leaf movement **(Matsumura et al., 2022; Pantazopoulou et al., 2023)**. The same study has suggested the adaptive value for this

trichome-mediated calcium signalling in environments where crowding causes mutual shading **(Pantazopoulou et al., 2023)**.

In A. thaliana the development of trichomes originates from rapidly dividing pro-epidermal cells in new leaf bases **(Larkin et al., 1993)**.Their development is characterised by six primary stages: initiation (including DNA endoreduplication), polar expansion, branching, branch growth, diffuse growth, and cellular maturation **(Folkers et al., 1997; Hülskamp et al., 1994; Szymanski et al., 1998)**. Trichome development is controlled by three main transcription factor groups, the R2R3 MYB, basic helix-loop-helix (BHLH) and WD40 repeat protein (WDR), which form a trimeric activator complex that positively regulates trichome development **(Pattanaik et al., 2014)**.

According to Jakoby **(2008)**, the EXO70H4 is the eleventh most highly expressed gene in mature trichomes compared with rosette leaves with detached trichomes. Recent research by Kulich et al. **(2015; 2018)** has demonstrated that EXO70H4 plays a critical role in trichome maturation, particularly in the deposition of the secondary cell wall (SCW) in the apical region. The mature trichomes of exo70H4 loss-of-function (LOF) mutants exhibited less cell wall autofluorescence and a more flexible phenotype, which can be attributed to the thinner secondary cell wall than wild-type plants. The flexibility is related to the absence of the inner callose-rich cell wall layer, leading to a decrease in trichome rigidity in the exo70H4 mutant compared to the wild type. Additionally, the absence of a callose-rich Ortmannian ring (OR) in exo70H4 mutant trichomes was observed **(Kulich et al., 2015)**. OR is a structure composed by callose, which divides trichomes into two major domains, the apical and basal domains. The presence of different EXO70 isoforms has also been observed in these domains, with EXO70A1 recruited by the basal domain and EXO70H4 recruited by the apical domain **(Kubátová et al., 2019a)**.

In trichomes, GSL5 also known as POWDERY MILDEW RESISTANT 4 (PMR4) is one of the most highly expressed callose synthase in trichomes **(Jakoby et al.,**

2008). Kulich and colleagues **(2018)** demonstrated the importance of the EXO70H4 in proper docking and delivery of the PMR4 to the plasma membrane (PM), and found that EXO70H4, among the closely related isoforms, was the only one capable of rescuing aberrant callose deposition in mutant trichomes.

1.2 Plant cell wall

The plant cell wall is a complex and dynamic structure that changes throughout the lifespan of a cell. There are two distinct types of cell wall (CW): primary and secondary. The primary cell wall is continuously altering, growing and elongating. Its functions extend beyond mere structural support, as it may contain molecules that influence a cell's position within a plant and participate in cell-to-cell communication through the transmission of signalling molecules. In contrast, the secondary cell wall plays a more significant structural and protective role in comparison to the primary one, and together with the primary cell wall, it contributes to defence mechanisms, not only as a passive barrier but also as secreting molecules that play a role against pathogens. **(Bacete et al., 2018)**

Despite their initial similar appearance, the primary and secondary cell walls exhibit distinct differences in structure, function and synthesis. The primary cell wall is a dynamic structure that provides initial support for the plant, composed primarily of cellulose and a cellulose-hemicellulose network embedded in a pectin matrix. The secondary cell wall, on the other hand, is thicker and deposited after the cell has reached maturity, providing additional strength and protection. It comprises cellulose, hemicellulose (xylan, glucomannan), lignin and callose **(Varner et al., 1989)**.

All cell wall constituents, including pectins and hemicellulose, are synthesised *de novo* in the Golgi apparatus and secreted into the apoplast **(Mohnen, 2008; Scheller et al., 2010)**. However, cellulose and callose differ in that they are directly synthesised on the plasma membrane, which indicates a crucial step in delivering the enzymes

involved in their synthesis to the appropriate location.

The formation of the secondary cell wall is a complex process that requires the coordination of gene regulation, biosynthesis, and targeted secretion to the site of synthesis and assembly of the secondary cell wall. Studies involving fluorescence microscopy, knockout genes, and cytoskeletal drugs have shown that microtubules and their organisation are crucial in the patterned deposition of the secondary cell wall, especially for the main constituent, cellulose **(Zhong et al., 2015)**.

1.3 Callose

Callose is a plant-derived β-1,3-glucan polysaccharide with β-1,6 branches synthesised on plant plasma membranes. It can be categorised into two primary forms: wound callose and developmental callose. Wound callose is produced in response to various stressors, such as pathogen infection or wounding, and is deposited at the site of injury in the plant cell wall to play a role in defence mechanisms. On the other hand, developmental callose is associated with various stages of plant development, such as the development of the cell plate in dividing cells and the growth of pollen tubes. Callose plays a vital role in plant growth, development and stress response. During cell plate development, callose ensures the correct assembly of the cell wall during cytokinesis **(Zonglie Hong et al., 2001)**.

Callose is synthesised on the plasma membrane by *glucan synthase-like* (GSL) proteins, , called synthase, using UDP-glucose as the initial substrate. In *A. thaliana*,, there are 12 GSL proteins, referred to as either GSL or CalS (callose synthase). This confusion is due to the inconsistent numerical designation in annotations and different functions **(Richmond et al., 2000; Verma et al., 2001)**.

Experimental evidence has demonstrated the crucial role of GSL proteins in various plant developmental processes. For instance, GSL1, GSL2, GSL8, and GSL10 are required for callose formation during pollen grain maturation **(Enns et al., 2005;**

Grobei et al., 2009; Töller et al., 2008). Additionally, GSL8, GSL6 and GSL12 play a role in callose deposition during cell plate formation, plasmodesmata formation, and stomatal patterning **(Guseman et al., 2010; Han et al., 2014; Z. Hong et al., 2001; Sevilem et al., 2013; Thiele et al., 2009)**.

GSL5, also known as PMR4 or CalS12, has been shown to play an essential role in the pathogen response by depositing callose in papillae, which are localised cell wall reinforcements that restrict the invasion of germinating pathogen spores on the leaf surface, at sites of pathogen attack, and at wound sites **(Jacobs et al., 2003)**. Furthermore, the pmr4 LOF mutant exhibited enhanced resistance to pathogens, attributed to a higher concentration of salicylic acid. This suggested that PMR4 is a negative regulator of this hormone **(Nishimura et al., 2003)**.

Although a significant amount of experimental data has been collected, the regulation of GSL proteins remains to be determined. For instance, GSLs are believed to form complexes similar to cellulose synthase, which interacts with monomeric GTPases, UDP-glucose transferase, and sucrose synthase **(Zonglie Hong et al., 2001)**. Additionally, EXO70H4 has been shown to play a role in delivering GSL5 to the synthesis site **(Kulich et al., 2018)**.Phosphorylation is another crucial player in the regulation of callose synthase, as observed in yeast **(Qadota et al., 1996)**. Secondary messengers such as calcium and reactive oxygen species (ROS) are also involved in callose deposition in response to stress **(German et al., 2023)**. For instance, GSL4 was identified as the key enzyme for callose deposition in response to ROS. However, the enzyme was not affected by hydrogen peroxide treatment, indicating that its activity may be controlled by receptor-like proteins or receptor-like kinases that link ROS signalling to GSL4 activation **(W. Cui et al., 2016; B. Wang et al., 2022)**.

It is also known that external calcium is essential for callose deposition, and many plants can increase callose synthase activity by up to 50 times in the presence of calcium chloride **(H. Kauss et al., 1990; Heinrich Kauss, 1985; Nedukha, 2015)**. Shikanai *et al.* **(2020)** demonstrated the relationship between callose synthase

activity and calcium concentration and how inhibiting the enzyme increases sensitivity to low-calcium conditions, resulting in leaf necrosis. The severity of the symptoms was more significant in the *gsl10* mutant, indicating that GSL10 plays a crucial role in mitigating the defects caused by calcium deficiency.

1.4 Reactive oxygen species

Reactive oxygen species (ROS) are actively produced e.g. by respiratory burst oxydase homologues (RBOH) in a higly regulated manner or might be by-products of the photosynthetic or aerobic metabolism of plants. Although often preceived as deleterious, ROSs are essential as signalling molecules in plant growth and development, primarily involved in cell elongation, cell division, differentiation and organogenesis **(H. Huang et al., 2019; Mhamdi et al., 2018; Mittler et al., 2022)**. There are several sources of ROS production in plants - photosynthesis in shoot, particularly the electron transport chain and photorespiration, but also mitochondria, but importantly at the PM RBOHs. At cellular level, they can be found in multiple forms such as superoxide, hydrogen peroxide, hydroxyl radicals, and singlet oxygen **(Dumanović et al., 2021)**.

Despite the beneficial roles, ROSs are toxic to plants, causing oxidative damage. Plants have developed mechanisms to regulate ROS levels and mitigate potential damaging effects, which are essential for maintaining redox homeostatis within plant cells. There are antioxidant systems in place to neutralise excess ROS. These systems use enzymes such as superoxide dismutase, catalase, peroxidase and glutathione reductase **(Mittler et al., 2022)**.

Two enzymes localised on the the cell wall are crucial in producing ROS. The peroxidase (POX), and NADPH oxidases, also known in plants as RBOHs. Among other enzymes, POX generates ROS through preocesses such as the oxidative cycle, wherein it reduces O_2 to O_2^- or H_2O_2, utilising reducing agents present in the apoplast.

In contrast, RBOHs produce O_2^- via electron transfer from the cytosol to oxygen present in the apoplast **(Podgórska et al., 2017)**. Instead in terms of the functions of these two enzymes, POX are responsible more in the structural changes of the cell wall such as the cross-linking of the structural proteins and polysaccharides, strengthening the overall cell wall. Importantly, if the substrate is depleted, hydroxyl radicals are formed, causing polymer cleavage and therefore cell wall loosening. Contributing to this dynamic balance, ROS allows plants to adapt their growth in response to the environment **(Mhamdi et al., 2018)**; on the other hand RBOHs are involved more in the oxidative burst in response to pathogens an abiotic stress.

1.5 Exocyst complex

The exocyst is a conserved multi-subunit protein complex in all eukaryotes. It comprises eight subunits: SEC3, SEC5, SEC6, SEC8, SEC10, SEC15, EXO70, and EXO84, which form a hetero-oligomeric complex **(TerBush et al., 1996)**. Exocysts function as CATCHR-type (complexes associated with tethering containing helical rods) vesicle-tethering complexes and play a crucial role in the tethering and docking of post-Golgi secretory vesicles to the plasma membrane and regulation of soluble *N-ethylmaleimide*-sensitive-factor (SNARE) complex formation, including vesicle fusion at the plasma membrane. In addition to its core function, individual subunits or subcomplexes have been reported to contribute to cellular processes such as autophagy and cytoskeleton regulation **(Heider et al., 2012)**.

After the initial discovery of the exocyst complex in yeast **(TerBush et al., 1996)**, it was later found in all eukaryotes, including plants **(Elias et al., 2003)**. In non-plant eukaryotes, exocyst members are typically present as solitary isoforms encoded by single-copy genes. The plant exocyst complex is divided into two modules composed of SEC3, SEC5, SEC6, SEC8, SEC10, SEC15, EXO70, and EXO84 **(Lukáš Synek et al., 2021)**. However, in land plants, the EXO70 subunit family exhibits a unique pattern of expansion and divergence, giving rise to three subfamilies (EXO70.1,

EXO70.2, EXO70.3) and rapidly evolving paralogues **(Cvrčková et al., 2012; Lukás Synek et al., 2006; Žárský et al., 2020)**.

The exocyst complex is fundamental to developing and maintaining plant cell polarity. It is well established that the cell polarity is regulated by small GTPases **(Yang et al., 2020)** and the connection between small GTPases and the exocyst complex in yeast is well described/known **(Rossi et al., 2020)**. In yeast and mammals, the proper recruitment of the vesicle to the plasma membrane is mediated by the interaction between Sec3 and Exo70 and their direct binding to phospholipids **(He et al., 2007; Liu et al., 2007)**. However, in plants, the two exocyst modules are connected through a specific interaction between the SEC3 and EXO70 subunits, which differs from what occurs in yeast and animals, where mutated plant SEC3a is unable to bind *phosphatidylinositol 4,5-biphosphate* (PIP2), or inhibition of EXO70A1 results in decreased secretion to the plasma membrane **(X. Li et al., 2023; Lukáš Synek et al., 2021)**.

In plants, several exocyst subunits play essential roles in protein polarisation. For instance, EXO84B regulates the polar localisation of PEN3 and NIP5;1 **(Mao et al., 2016)**. Members of the larger EXO70 subunit are actively involved in the localised secretion of plasma membrane and cell wall components in various plant tissues, such as pectin **(Kulich et al., 2010)** and callose **(Kubátová et al., 2019a; Kulich et al., 2015, 2018)**, cellulose synthase **(Vukašinović et al., 2017)**, PIN auxin transporters **(Drdová et al., 2013)**, CASP1 **(Kalmbach et al., 2017)**.

The significance of specific isoforms within the more prominent EXO70 family extends to crucial roles in cellular defence and innate immunity. EXO70B1 and B2, in particular, play pivotal roles in the distribution of FLS2, a receptor kinase involved in the recognition of bacterial flagellin **(W. Wang et al., 2020)**. Furthermore, EXO70B2 has been implicated in PAMP-triggered immunity, and recent research has revealed its role in delivering the callose used to form cell wall structures known as papillae, which act as barriers to restrict the entry of pathogens. **(Ortmannová et al., 2022;**

Pečenková et al., 2011).

1.6 Mildew resistance Locus O

The Mildew Resistance Locus O (Mlo in barley) proteins are a group of seven transmembranes (TM) proteins well known for reducing susceptibility against the barley powdery mildew pathogen, *Blumeria hordei*. The LOF mutation of this gene results in resistance to powdery mildew pathogens The Mlo gene family, first described by Buschgens *et al.* **(1997)**, comprises approximately 10 - 20 paralogs per plant species, encoding plant-specific and sequence-diversified integral membrane proteins. Mlo proteins are divided into seven clades, with clade V mainly found in dicotyledonous plants and clade IV mainly found in monocotyledonous **(Devoto et al., 1999; Jørgensen, 1992; Kusch et al., 2016)**.

Several studies on *A. thaliana* have reported that MLO (in *A. thaliana*) proteins from clade V are involved in processes linked to polar secretion, such as thigmomorphogenesis. For example, *mlo4* and *mlo11* mutant plants exhibit severe root curling in response to tactile stimuli, indicating a defect in thigmomorphogenesis **(Bidzinski et al., 2014; Z. Chen et al., 2009)**. Additionally, MLO7, MLO5, and MLO9 are involved in the dialogue between the ovule and pollen tube, reducing fertility **(Ju et al., 2021; Kessler et al., 2010; J.-g. Meng et al., 2020)**.

The loss-of-function of MLO2, MLO6, and MLO12 of the 15 MLO genes of A. thaliana resembles the near-complete resistance of barley mlo mutants **(Consonni et al., 2006)**. This is because of the unequal genetic redundancy of these genes, resulting in the encoded proteins contributing unevenly to the susceptibility of *A. thaliana* to the powdery mildew pathogens *Golovinomyces orontii* and *G. cichoacearum*, with MLO2 being the major contributor and MLO6 and MLO12 being minor contributors **(Consonni et al., 2006)**. In addition to reduced susceptibility to powdery mildew disease, barley *mlo* and *A. thaliana mlo2 mlo6 mlo12* exhibit indiscriminate callose-rich de-

positions at the cell wall and feature spontaneous death of mesophyll cells associated with premature leaf senescence **(Consonni et al., 2010; Piffanelli et al., 2002; Wolter et al., 1993)**. MLO2 also plays a decisive role in regulating ozone sensitivity **(F. Cui et al., 2018)** and mediating systemic acquired resistance, a form of induced and systemically acting plant defence **(Gruner et al., 2018)**.

Recently, a study reported that MLO proteins function as calcium channels **(Gao et al., 2022)**. Although this discovery provides further insight into the biochemical function of MLO proteins, the relationship between the calcium channel activity of MLO proteins and their impact on cellular processes and mediated powdery mildew susceptibility remains unclear. Conserved sequence regions among all MLO proteins include a binding site for the ubiquitous calcium sensor calmodulin in the proximal part of the intracellular MLO carboxyl terminus **(M. C. Kim et al., 2002)**, and four invariant cysteine residues in two of the extracellular loops, which form two disulphide bridges that are crucial for the stability of MLO proteins **(ELLIOTT et al., 2004)**. Mutations in the POWDERY MILDEW RESISTANT gene of *A. thaliana* have been linked to decreased susceptibility to these fungal pathogens **(J. Vogel et al., 2000)**. The respective forward genetics approach was used to identify PR1-independent defence mechanisms, and PMR2 was identified as allelic to MLO2 **(Consonni et al., 2006)**. To date, all other discovered PMR genes (PMR4-PMR6) encode proteins that play a role in the biogenesis and/or modification of the cell wall **(Jacobs et al., 2003; Nishimura et al., 2003; J. P. Vogel et al., 2002, 2004)**, consequently it is plausible that MLO2 or other MLO proteins participate in processes crucial for trichome secondary cell wall biogenesis as observed with PMR4 **(Kulich et al., 2018)**.

1.7 Machine learning in plant research

In recent years, machine learning/AI has dramatically influenced numerous scientific disciplines, including plant biology. This computational approach allows for analysing intricate biological data, outperforming conventional methods in precision and speed. Recently, there has been a surge in the use of machine learning across various plant biology fields, such as genomics, physiology, and ecology. By employing extensive datasets and advanced algorithms, researchers have obtained unparalleled insights into plant growth, development, and responses to environmental stresses **(Dijk et al., 2020; Gill et al., 2022)**.

A notable illustration of the transformative influence of machine learning in the field of plant biology is the emergence of AlphaFold (now in version 3), a pioneering protein structure prediction tool **(Abramson et al., 2024; Jumper et al., 2021)**. By employing deep learning approaches **(LeCun et al., 2015)**, AlphaFold has attained exceptional precision in predicting protein structures from amino acid sequences. This challenge has baffled scientists for several decades. This breakthrough significantly impacts plant biology as protein structure is intrinsically connected to function. By elucidating the protein structures, researchers can gain invaluable insights into molecular underpinning plant processes.

By integrating the protein structures obtained from AlphaFold with tools utilised in molecular dynamics simulations **(J. Huang et al., 2017)**, significantly more information could be extracted that would facilitate the study of our protein/complex of interest.

1.8 Proximity labelling techniques used in plant research

Proximity labelling has emerged as a powerful tool for elucidating protein-protein interactions and studying the proteome in plants. Multiple techniques have been developed and subsequently applied to plant-based research.

BioID and its derivates TurboID and MiniTurbo are widely used proximity-labelling approaches in plants. These methods utilise bacterial biotin ligase (BirA) fused to a bait protein, which covalently binds biotin on lysine residue, resulting in the biontinylation of nearby protein **(Roux et al., 2012)**. It was observed that BioID requires longer incubation time (16-24 h) at higher temperatures (37°) **(D. I. Kim et al., 2016)**, and MiniTurbo, a smaller version of TurboID, is half active compared with TurboID **(Mair et al., 2022)**. It was observed that TurboID is the most efficient variant in several plant model systems, allowing for the capture of membrane-associated protein interactomes **(Arora et al., 2020)**.

Although biotin-based methods are commonly used, they may have some labelling-related drawbacks, such as long incubation times and higher temperatures. A pupylation-based proximity labelling (PUP-IT) system has shown promise for overcoming these limitations. This system is based on the prokaryotic enzyme PafA, which mediates the ligation of a small PUP(E) peptide to lysin residues of proteins in close proximity. This new method has demostrated increased detection of specific interactions compared to biotin-based proximity labelling systems and has been used to identify protein interactions in the cellulose synthesis complex **(Persson et al., 2024)**.

Proximity labelling techniques such as TurboID and PUP-IT are valuable tools for studying the plant proteome. These methods allow the detection of weak and transient interactions, and when combined with machine learning-based methods, they can provide deeper insights into complex cellular processes in plant biology.

1.9 Aims

1. Phenotypic analysis and comparison of Arabidopssi trichomes in *exo70H4* and *mlo* loss-of-function mutants (including preparation of new MLO6 CRISPR/Cas9 mutant allele).

2. Molecular-mechanistic analysis of EXO70H4 and MLO proteins functional interconnection.

3. Bioinformatic modelling and prediction of functional MLO proteins membrane complex

4. Introduction of the TurboID methodology (START grant) in our laboratory and study of the exocyst proteome under biotic stress

2. Results

2.1 Phenotypic deviations of leaf trichomes in MLOs mutants

In the course of examining callose deposition in trichomes of the triple mutant *mlo2-5 mlo6-1 mlo12-1*, it was observed that the deposition was highly reminiscent of the phenomenon observed in the *exo70h4-1* mutant, as described by Kulich *et al.* **(2015; 2018)**. To quantify this possible new characteristic, we categorised the trichomes based on the degree of callose deposition (confined, erratic, and absent, as illustrated in **Fig. 1**) and calculated the percentage of trichomes in each category. Our findings revealed that approximately 68% of rosette leaf trichomes in Col-0 displayed confined callose deposition, distinguished by aniline blue fluorescence in the OR region. Approximately 14% and 17% of trichomes exhibited delocalised callose deposition or no callose deposition, respectively. This variability can be mostly attributed to the distribution of various developmental stages of trichomes on the leaves **(Hülskamp et al., 1994)**. The mutants we analysed showed that *exo70h4-1* had significantly altered callose deposition patterns, with the majority of trichomes displaying erratic or absent callose deposition. This pattern was also observed in the two MLO triple LOF mutants we analysed (*mlo2-5 mlo6-2 mlo12-1* and *mlo2-6 mlo6-4 mlo12-8*).

To explore whether there are any additional shared traits between the *exo70h4-1* mutant and MLO triple mutants, we measured the cell wall autofluorescence and cell wall thickness. Our findings revealed that the trichomes of both MLO triple mutants displayed reduces autofluorescence and a thinner cell wall when compared to the wild type, both characteristics reminiscent of the *exo70h4-1* mutant.

To determine whether the observed phenotypic variability is attributed to a particular MLO gene or whether it is the result of the combined effects of three mutated genes, we carried out the same assays as previously mentioned on single and double mutants. The results showed that mutation in the *mlo6-2*, in conjunction with mutations either in *mlo2-5* or *mlo12-1* resulted in a phenotype deviation similar to that observed in both MLOs triple mutants with regard to callose deposition. On the other hand, *mlo2-5* and *mlo12-1* single and the combined double mutants exhibited a callose phenotype similar to the Col-0 WT (**Fig. 2A**). Concerning the cell wall autofluorescence - only the double mutant *mlo2-5 mlo6-2* displayed significantly reduced autofluorescence compared to the other genotypes, which showed WT-like autofluorescence (**Fig. 2C**). All *mlo* single and double mutants displayed thinner cell wall compared to the Col-0 WT as in the case for the *exo70h4-1* mutant(**Fig. 2B**).

To corroborate dominant MLO6's isoform in the earlier observed phenotypic alteration, we generated a new CRISPR-Cas9 *mlo6-6* mutant. In combination with several controls, including Col-0 WT, *exo70h4-1*, and *mlo6-2* mutants, was observed the same *mlo6-2* phenotype also in *mlo6-6* for all the phenotypic characteristics examined previously (**Fig. 3**).

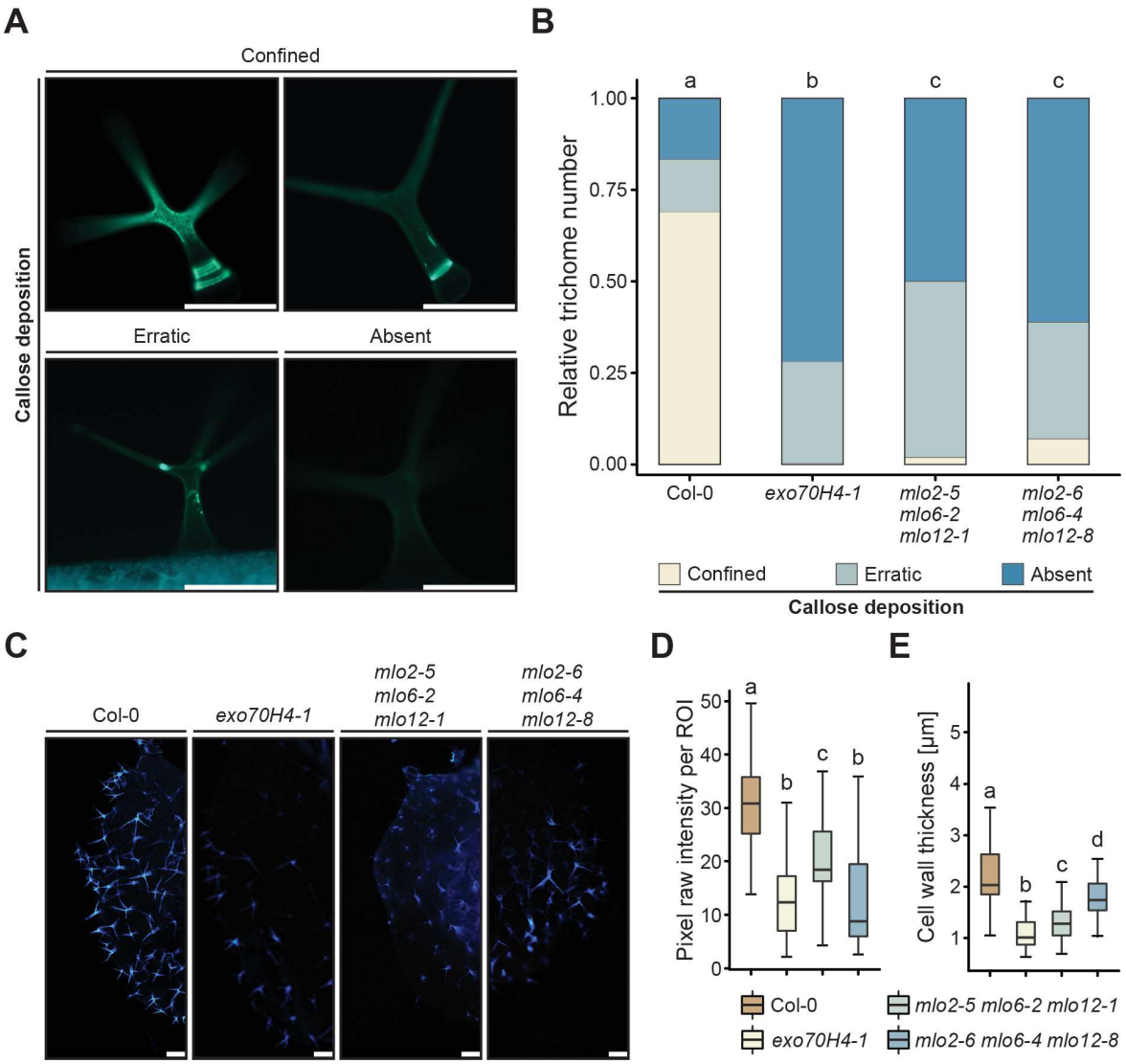

Figure 1: The *exo70h4-1* mutant and 2 independent *mlo2 mlo6 mlo12* triple mutants share similar rosette leaf trichome phenotypes. **A** Representative micrographs illustrating the trichome-associated callose phenotype categories (confined, erratic, and absent) following staining with aniline blue. **B** Frequencies of trichome callose patterns defined in **A** in trichomes of Col-0 WT and the indicated mutants following staining with aniline blue. Values are based on 4 experiments with $\approx$ 150 trichomes inspected per experiment and genotype, i.e. $\approx$ 600 trichomes per genotype in total. Data were analysed by chi-square test. the *P*-values were corrected by FDR ($\alpha = 0.05$), letters denote statistically significant differences between genotypes. **C** Representative micrographs depicting trichome cell wall autofluorescence in rosette leaves of Col-0 WT plants and indicated mutant plants. **D** Quantification of trichome cell wall autofluorescence. Shown is the pixel intensity per randomly chosen regions of interest (ROIs), calculated based on autofluorescence micrographs as those exemplarily shown in **C**. Box plots represent the probability distribution of data as described in the Material and methods chapter. Values are based on 2 experiments with $\approx$ 20 trichomes inspected per experiment and genotype, i.e. $\approx$ 40 trichomes per genotype in total. Letter assign differences of statistical significance (pairwise Wilcoxon-Mann-Whitney test corrected by FDR, $\alpha = 0.01$).

Figure 1: (continued) **E** Quantification of trichome cell wall thickness. Cell wall thickness was measured in proximity of the OR. Box plots represent the probability distribution of data as described in the Material and methods chapter. Values are based on 4 experiments with ≈ 20 trichomes inspected per experiments and genotype, i.e. ≈ 80 trichomes per genotype in total. Letters represent differences of statistical significance (pairwise Wilcoxon-Mann-Whitney test corrected by FDR, $\alpha = 0.01$). Scale bars in **A** and **C** represent 200 μ m

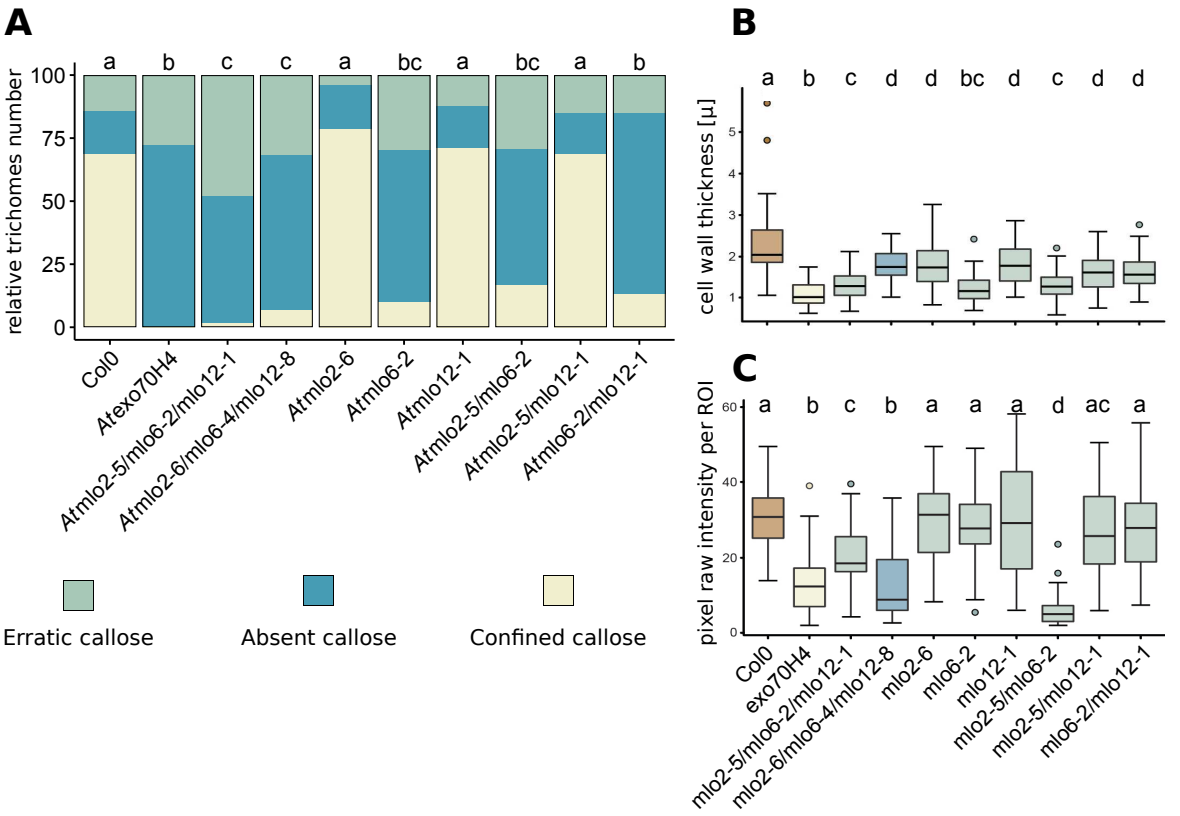

Figure 2: **A** Quantification of callose deposition in all mutants involved in the study, frequencies of callose deposition pattern are based on four experiments with ≈ 150 trichomes inspected per experiment and genotype, i.e., ≈ 600 trichomes per genotype in total. **B** cell wall thickness, measured in proximity to the OR, is based on four experiments with ≈ 20 trichomes inspected per experiment and genotype, i.e. ≈ 80 trichomes per genotype in total. **D** quantification of trichome CW autofluorescence. The pixel intensity per randomly chosen region of interest (ROI) is shown. Data in **A** were analysed by chi-square test, and the p-values were corrected by FDR (α=0.05). Boxplots (**B** and **C** represent the probability distribution of data as described in the Material and Methods chapter. Data in **B** and **C** were analysed by pairwise Wilcoxon-Mann-Whitney test, and p-values were corrected by FDR ($\alpha = 0.01$). Letters represent differences of statistical significance.

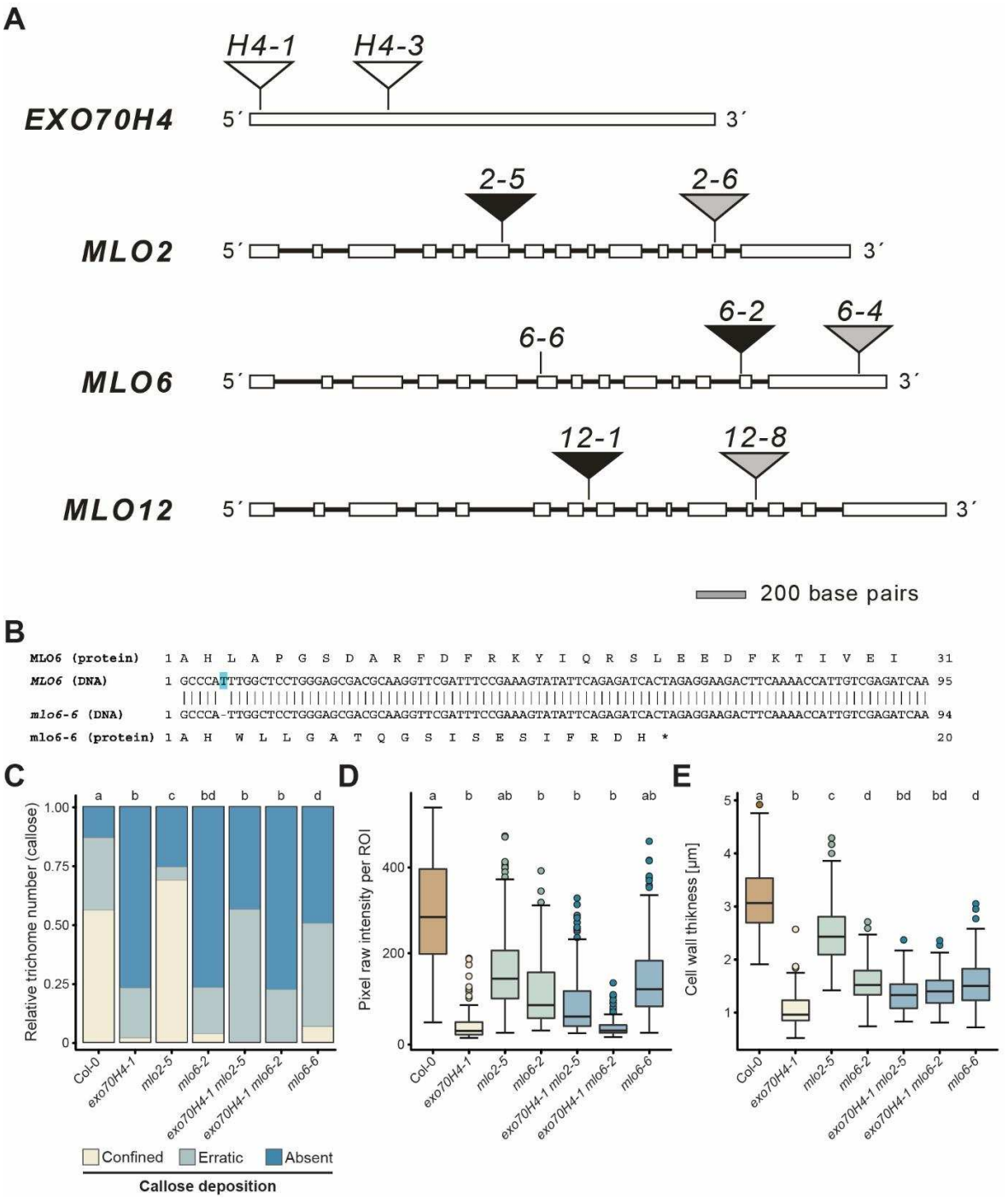

Figure 3: **A** schematic representing the exon-intron structure of EXO70H4, MLO2, MLO6, MLO12 and derived mutants. White boxes indicate exons and black lines introns. Triangles symbolise the insertion sites in the various T-DNA mutants; the mutation site of the CRISPR-Cas9-based *mlo6-6* allele is also shown. Note that T-DNA mutants specified by the black triangles are combined in the triple mutant *mlo2-5 mlo6-2 mlo12-1*, and T-DNA mutants designated by the grey triangles are combined in the triple mutant *mlo2-6 mlo6-4 mlo12-8*. The scheme is a modified version of a similar graphic published in **(Acevedo-Garcia et al., 2017)**, including information given in Kulich *et al.* **(2015)**. **B** multiple sequence alignment of the DNA and derived protein sequences (above and below the DNA sequence, respectively) of MLO6 and the CRISPR-Cas9 based *mlo6-6* allele. The DNA sequence corresponding to exon 7 of MLO6 is shown.

Figure 3: (continued) The nucleotide missing in *mlo6-6* (one of three consecutive T nucleotides) is highlighted in blue. The 1-bp deletion in *mlo6-6* causes a frameshift, resulting in a premature stop codon (indicated by an asterisk) in the MLO6 coding sequence. **C, D, E** quantification of callose deposition **(C)**, autofluorescence **(D)** and CW thickness **(E)** in trichomes of Col-0 WT, *exo40h4-1* and various *mlo* single, and *exo70h4-1 mlo* double mutants. Frequencies of callose deposition patterns **(C)** are based on two experiments with five leaves per genotype, in which $\approx$ 1240 trichomes were inspected per leaf, i.e. $\approx$ 1400 trichomes per genotype in total. Values for autofluorescence **(D)** and CW thickness **(E)** are based on three experiments using three leaves per genotype, in which $\approx$ 20 trichomes (autofluorescence) and $\approx$ 10 trichomes (CW thickness), respectively, were inspected per leaf, i.e. $\approx$ 180 trichomes for autofluorescence and $\approx$ 90 trichomes for CW thickness in total. Data in C were analysed by chi-square test, and the p-values were corrected by FDR ($\alpha = 0.05$). Box plots **(D)** and **(E)** represent the probability distribution of data as described in the Materials and Methods chapter. Pairwise Student's t-test analysed data in **(D)** and **(E)**, and p-values were corrected by FDR ($\alpha = 0.01$). Letters represent differences of statistical significance.

2.2 Exploring and comparison of the localisation of reactive oxygen species and heavy metals in trichome cell wall of WT and mutants

Due to the similar phenotypic peculiarities exhibited by the two MLO triple mutants and *exo70h4-1* as well as the involvement of the reactive oxygen species (ROS) in callose deposition during stress responses **(Xiao et al., 2018)**,we conducted histochemical staining on rosette leaves to confirm the in situ accumulation of ROSs and heavy metals in leaf trichomes. Similar to callose, we established phenotypic categories (confined, diffused, or absent) to classify these features. Most Col-0 WT ($\approx$ 53%) trichomes analysed exhibited a confined pattern of ROS accumulation in the proximity of the OR region, whereas $\approx$ 43% lacked ROS accumulation, and $\approx$ 3% showed a diffuse ROS pattern. Conversely, the *exo70h4-1* and the two MLO triple mutants showed either diffused ROS distribution ($\approx$ 39%) or complete absence of ROS ($\approx$ 59%) **(Fig. 4B)**.

The deposition of heavy metals followed a pattern similar to that observed for ROS. In the wild-type plants, the majority of trichomes ($\approx$ 30%) showed confined basal accumulation (close to OR), around half of the trichomes analysed showed no accumulation while only a small proportion ($\approx$ 16%) exhibited a diffused pattern. In contrast, the mutants displayed a diffuse distribution of HM in the majority of trichomes ($\approx$ 40%) (**Fig. 4B**).

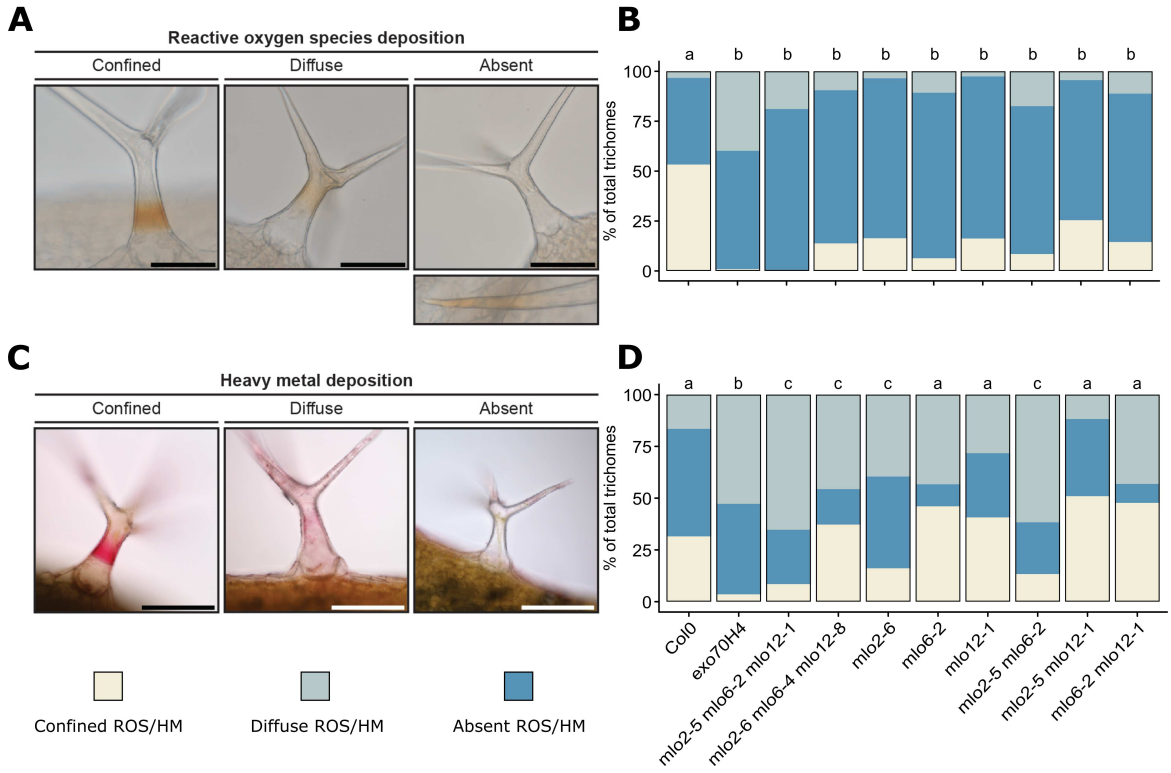

Figure 4: The *exo70h4-1* mutant and all the MLOs mutants investigated share similar aberrant ROS and HM localisation patterns in rosette leaf trichomes. **A** representative micrographs illustrating categories of trichome-associated ROS occurrence (confined, diffuse, and absent). Trichomes lacking ROS accumulation in the trichome's basal part and the branches' proximal areas occasionally exhibited weak DAB staining in the branch tips. **B** frequencies of trichome ROS accumulation patterns as defined in A in Col-0 WT and indicated mutant plants. Values are based on three experiments with $\approx$ 50 trichomes inspected per experiment and genotype, i.e. $\approx$ 150 trichomes per genotype in total. Data were analysed by chi-square test, the p-values were corrected by FDR ($\alpha = 0.05$), and letters denote statistically significant differences between genotypes. **C** representative micrographs illustrating categories of trichome-associated HM phenotypes (confined, diffuse, absent). **D** frequencies of trichome HM deposition patterns defined in **C**, in Col-0 WT and the indicated mutant plants. Values are based on three experiments with $\approx$ 50 trichomes inspected per experiment and genotype, i.1. $\approx$ 150 trichomes per genotype in total. Data were analysed by chi-square test, the p-values corrected by FDR ($\alpha = 0.05$), and letters denote statistically significant differences between genotypes. Scale bars in **A** and **C** represent 200 μm

2.3 Trichome cell wall composition

We were interested in whether this phenotypic deviation observed in the *exo70h4-1* and the two MLOs triple mutants from the Col-0 WT were symptoms of alterations in cell wall composition as indicated by changes in callose deposition. Considering the characteristics of MLO proteins, which are recently identified as calcium channels, and the vital role of calcium in the cell wall, we performed the following analyses to elucidate the trichome cell wall composition: analysis of the cell wall matrix monosaccharides (rhamnose, arabinose, galactose, mannose, fucose, xylose and glucose) (*experiment performed by co-authors*), Fourier transformed infrared (FTIR) (*experiment performed by co-authors*) spectroscopy for the global analysis of the cell wall composition, Energy Dispersive X-ray Spectroscopy (EDS), and Raman Spectroscopy.

While most of the methods used for the analysis are destructive or require sample preparation, Raman Spectroscopy is a noninvasive and nondestructive method that can be used directly without any sample preparation.

Raman Spectroscopy is a non-destructive analytical technique that provides information about molecular vibrations and the chemical composition of materials by detecting inelastically scattered light from a laser-illuminated sample. The energy difference between the incident and scattered light, known as Raman shifts, is a characteristic of the molecular bonds and structure of the sample. This technique is valuable for analysing organic and inorganic compounds, offering detailed insights into materials' molecular structure, chemical bonding, and crystallinity **(Smith et al., 2004)**.

Examining the cell wall composition, monosaccharides revealed a decline in arabinose levels in the trichomes of the triple *mlo2-5 mlo6-2 mlo12-1* mutant plants, whereas both triple MLO mutant plants demonstrated a decrease in galactose **Fig5 B**. These differences decreased the overall total amount of neutral monosaccharides in the *mlo2-5 mlo6-2 mlo12-1* triple mutant compared to the other genotypes. However, no substantial differences were observed in the crystalline cellulose and uronic acid levels

between the mutant and Col-0 WT trichomes **(Fig. 5)**. The results of FTIR analysis revealed significant changes in the composition of cell walls of both single exo70h4-1 and triple MLO mutant trichomes **(Fig. 5D)**.

Employing EDS (unpublished results), we observed the accumulation of chemical elements in the trichome cell wall. Given the nature of MLO proteins function, we specifically focused on calcium accumulation. We observed a significant decrease in calcium levels on both branches and trunk in the mlo2-5 mlo6-2 mlo12-1 and exo70h4-1 mutants compared to Col-0 WT trichomes, results which are presently unpublished **(Fig. 6)**.

By observing the trichomes using Raman spectroscopy (unpublished results), we achieved outcomes analogous to those obtained through EDS for calcium. Rather than obtaining results for an individual element, we received the calcite spectra at approximately 1080 cm^{-1} (symmetric C-O stretching) **(Donnelly et al., 2017)** deposited in a specific pattern in the cell wall of trichomes. For Col-0 WT, calcite was negligible or present in a significantly smaller amount near the OR and then increased as it progressed towards the tips of the trichomes branches. Conversely, the three mutants examined displayed the absence of calcite in their cell walls **(Fig. 7)** and **(Fig. 8)**. As for the other cell wall components, such as pectins, lignin, and cellulose, none of the mutant trichomes analysed differed from the Col-0 WT control plant. An 855 cm^{-1} peak characterises pectins. Lignin has a distinguishable peak at 1604 cm^{-1} assigned to acyl stretching vibrations. Since there is no overlap with carbohydrate peaks, it can be used as a lignin fingerprint, while an intense peak characterises cellulose at 1097 cm^{-1} (C-O-C stretching). The intensity of the cellulose peak can also help us to distinguish their orientation **(Gierlinger, 2018)**.

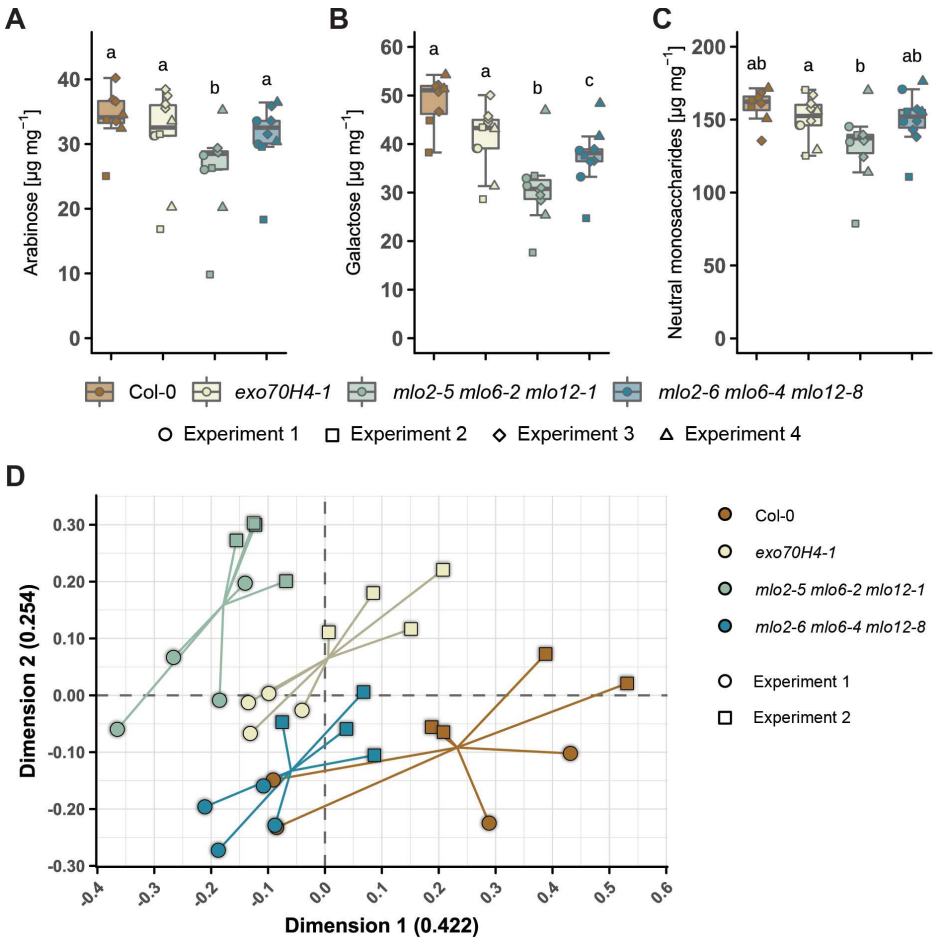

Figure 5: Cell walls of isolated *exo70h4-1* and *mlo2 mlo6 mlo12* triple mutant rosette leaf trichomes have altered carbohydrate composition. **A to C** Quantification of neutral matrix monosaccharides in the indicated genotypes. Different geometric shapes denote samples that arose from the same independent experiment, as indicated in the legend below the box plots. **A, B** Abundance of the neutral monosaccharides arabinose **A** and galactose **B** in the alcohol-insoluble residue recovered from trichomes of the various genotypes. Box plots represent the probability distribution of data as described in the Materials and methods section. Values are based on at least 3 independent experiments. Each independent experiment comprised at least 2 replicates, representing trichomes that were retrieved from the same round of trichome isolation. Letters assign differences of statistical significance (pairwise Student's t-test corrected by FDR, $\alpha = 0.05$). **C** Total abundance of neutral monosaccharides in the cell wall matrix of the various genotypes. Box plots include the amounts of the monosaccharides indicated in panels **A** and **B**. Letters assign differences of statistical significance (pairwise Student's t-test corrected by FDR, $\alpha = 0.05$). **D** Principal component analysis of FTIR spectra of rosette leaf trichomes isolated from the various genotypes (2 experiments with 4 samples each). The plot shows the first and second dimensions, which accounted for 42.2% and 25.4% of the variability between samples, respectively. The intersection point of the lines indicates the mean of the data points per genotype.

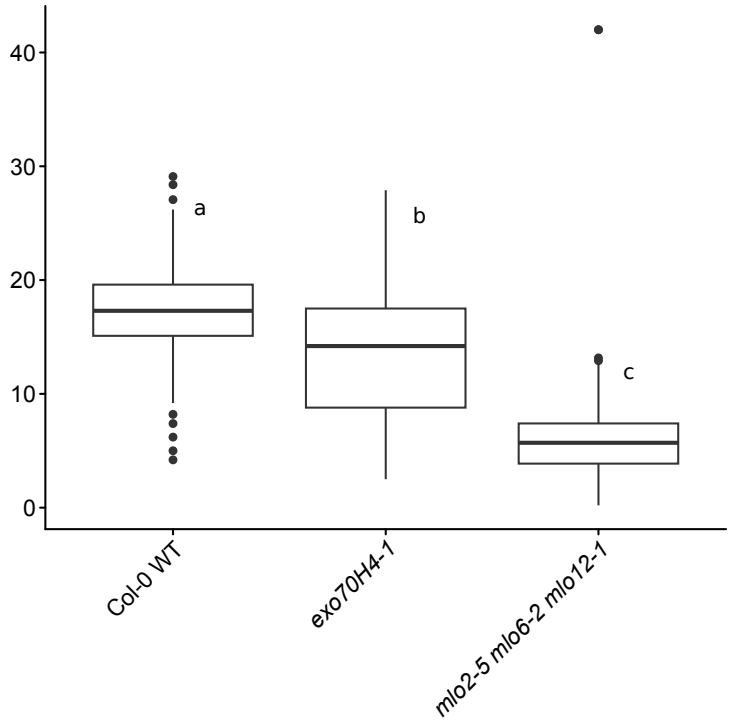

Figure 6: Calcium distribution analysed by EDS in exo70h4-1 and mlo2-5 mlo6-2 mlo12-1 compared against Col-0. On the x-axis the sum of the percentage of calcium measured in the vicinity of OR, on the trunk and branches of the trichomes. Data were analysed by pairwise Wilcoxon-Mann-Whitney test, and p-values were corrected by FDR ($\alpha = 0.01$). Letters represent differences of statistical significance.

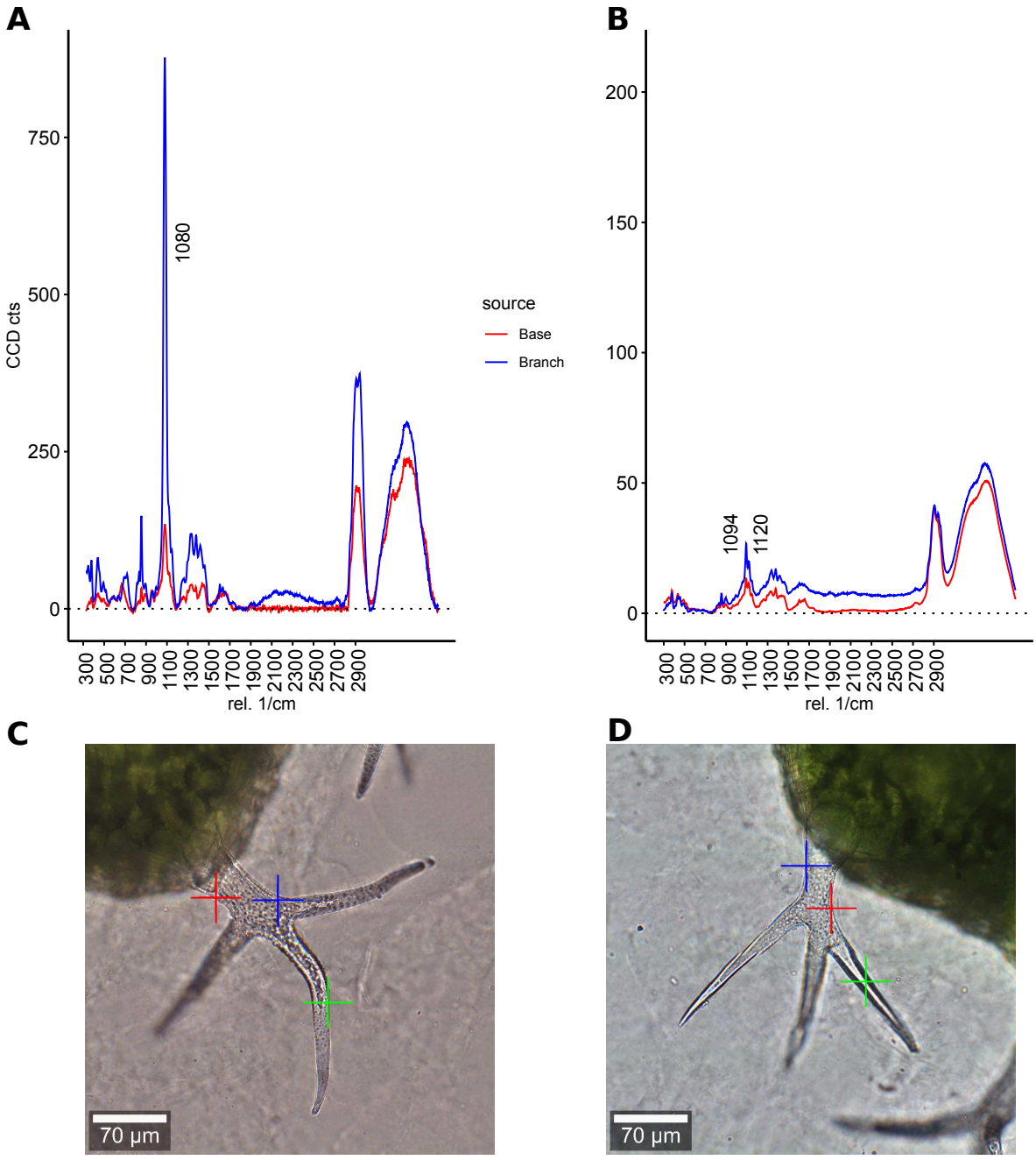

Figure 7: Raman single point spectra acquisition comparing Col-0 (**A**) and *mlo2-5 mlo6-2 mlo12-1* (**B**) trichomes showing the differences between branches and base. Peak at 1080 cm^{-1} indicate the presence of calcium carbonate that is missing in MLO triple mutant, in this case visible the cellulose spectra (1094 and 1120 cm^{-1}) that are covered by the higher signal of calcium carbonate in Col-0 trichome. Spectra are averages of three single acquisition for each base or branch of three different trichomes. Spectra were analysed as shown in Material and Methods chapter. Example of the spectra position in Col-0 trichome (**C**) and*mlo2-5 mlo6-2 mlo12-1* (**D**)

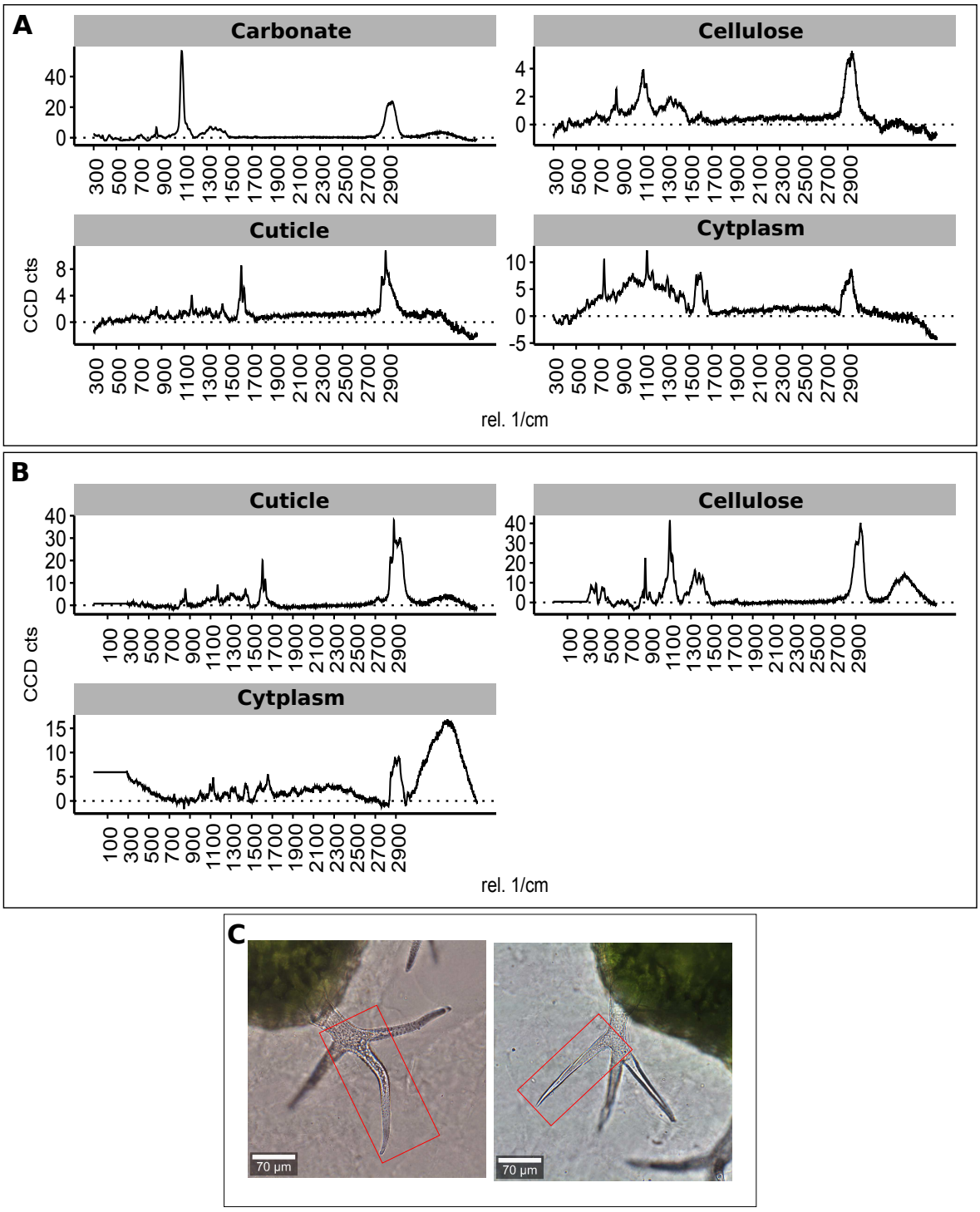

Figure 8: Decomposition of Raman spectra maps of Col-0 (**A**) and *mlo2-5 mlo6-2 mlo12-1* (**B**). The single spectra shows the different chemical composition of the trichome cell wall. Calcium carbonate (1080 cm^{-1}), pectins (855 cm^{-1}), cellulose (1094 and 1120 cm^{-1}), ligning (1604 and 1630 cm^{-1}). In **C** example of the map position for Col-0 (left) and MLO triple mutant (right)

2.4 Co-localisation of fluorophore-tagged EXO70H4 and MLO proteins in trichomes

The subcellular localisation of EXO70H4 is well known and has been described by Kulich *et al.* **(2018)**, but this is not the case regarding MLO2, MLO6, and MLO12 proteins localisation in trichomes. Therefore, to elucidate and study the localisation of MLO proteins in A. thaliana trichomes, we transformed mCHerry-EXO70H4 expressing plants in the *rdr6* background **(Kulich et al., 2018)**, which reduces transgene silencing, with constructs expressing GFP-tagged version of MLO, MLO6, and MLO12 under the EXO70H4 promoter, which confers preferential expression in trichomes.

The examination of the transgenic lines using confocal laser scanning microscopy revealed that all three MLO proteins were co-localised with EXO70H4 mainly in the domain of the OR and above it at the PM, delineating the thickened secondary cell wall of trichomes branches **(Fig. 9)**. Additionally, both EXO70H4 and all three fluorescent MLO fusion proteins were visible in the cell wall channels, which were oriented perpendicular to the trichome surface. This observation was also confirmed following plasmolysis **(Fig. 10)** and suggests trapping a portion of the fluorophore-labelled EXO70H4 and MLO proteins within the cell wall. This finding is supported by visualising membrane remnants within the cell wall via electron microscopy **(Kubátová et al., 2019a)**.

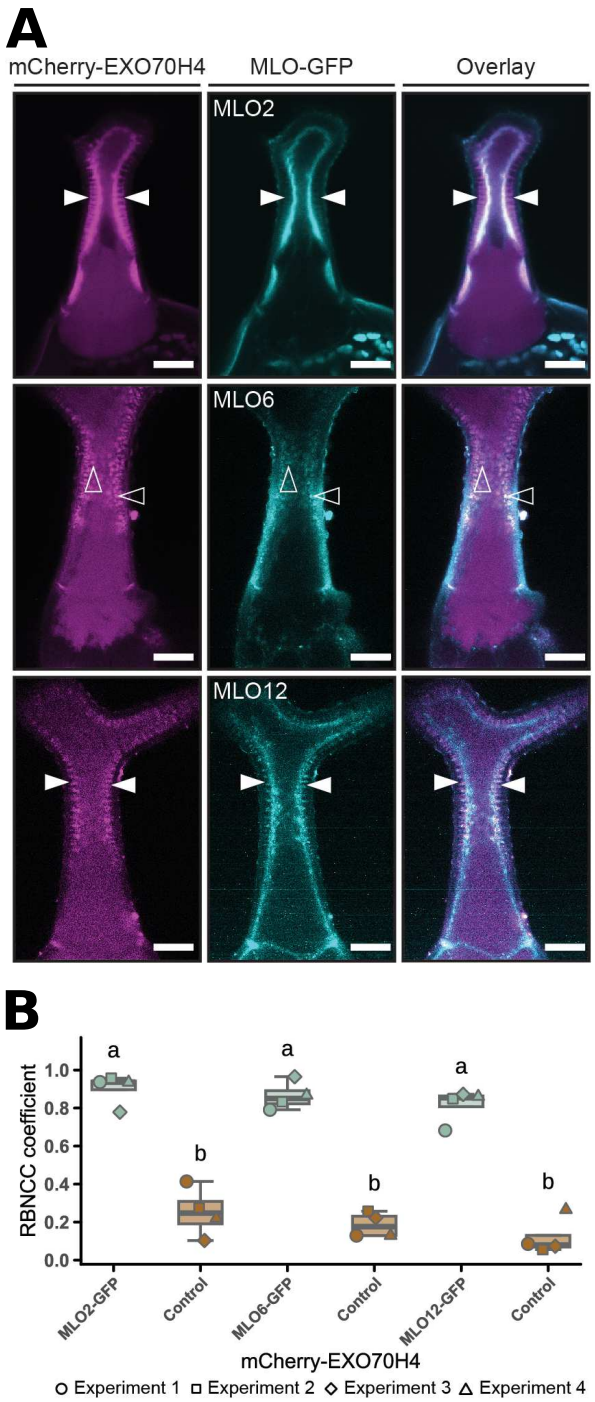

Figure 9: Subcellular localisation of fluorophore-labeled EXO70H4, MLO, in rosette leaf trichomes of *exo70H4* and *mlo2 mlo6 mlo12* transgenic lines. **A** Colocalisation of mCherry-EXO70H4 and GFP-tagged MLO proteins in trichomes of transgenic *A. thaliana lines*. mCherry-EXO70H4 and MLO-GFP (MLO2, MLO6, and MLO12) were expressed in transgenic *A. thaliana* lines (Col-0-derived *rdr6* background) under the control of the EXO70H4 promoter. In each micrograph, a single confocal plane is shown. Filled and open arrowheads point to examples of the fluorophore-labeled cell wall channels and PM speckles, respectively. Note that the ellipsoid structures seen in the GFP channel in the case of the MLO2-GFP trichome likely are chloroplasts present in mesophyll cells beneath the trichome cell. Scale bars represent 20 μm.

Figure 9: (continued) **B** Replicate-Based Noise Corrected Correlation (RBNCC) coefficient, indicating a correlation between the localisation of GFP-tagged MLO proteins and mCherry-EXO70H4 in mature trichomes of the transgenic lines shown in **A**. Control values are based on rotating the mCherry images by 90 degrees counterclockwise. Box plots represent the probability distribution of data as described in the Materials and methods section. Values are based on micrographs taken in 4 experiments, with 5 trichomes per experiment and transgenic line. Letters assign differences of statistical significance (pairwise Wilcoxon–Mann–Whitney test corrected by FDR, $\alpha = 0.05$).

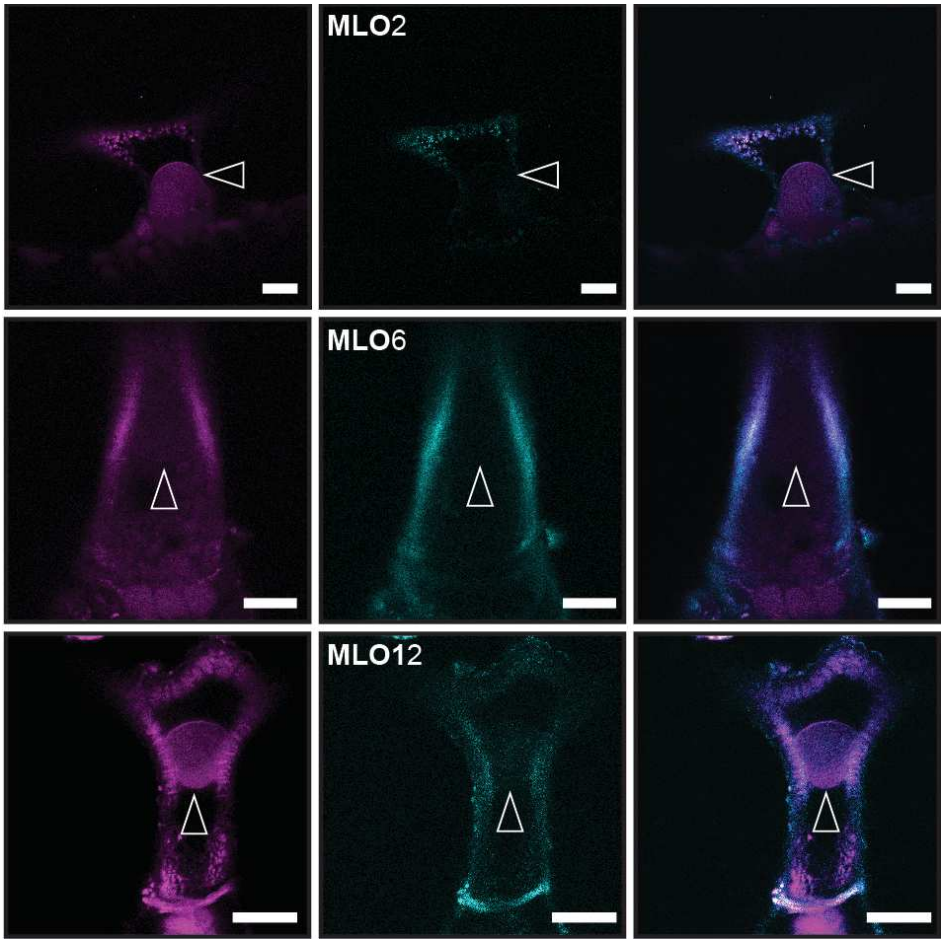

Figure 10: Plasmolysis experiment with trichomes of transgenic lines. Rosette leaf trichomes of transgenic lines co-expressing mCherry-EXO70H4 and MLO2-GFP, MLO6-GFP or MLO6-GFP were plasmolyzed by incubation in 20% sucrose solution and subsequently imaged by confocal microscopy. After plasmolysis, the signal from both EXO70H4 and MLO was still visible on the CW (CW speckles) and PM, indicating that both proteins were localized to the cell wall. In each micrograph, a single confocal plane is shown. Arrows point to the retracted cytoplasm. Scale bars represent 20 μm.

2.5 Effect of LOF mutation of either EXO70H4 or MLO proteins on the partner localisation

After obtaining positive co-localisation results, we were also interested in examining the potential impact of EXO70H4 and MLO proteins on each other's localisation. To achieve this, we first transformed Col-0 WT and *mlo2-5 mlo6-2 mlo12-1* plants with the mCherry-EXO70H4 construct previously used in co-localisation experiments. Our expectations were corroborated in Col-0 WT plants, as EXO70H4 was primarily located at the plasma membrane and within the thickened secondary cell wall of the apical part of the trichome, as well as on the cell wall papillae that decorate the surface of the trichome branches and trunk. However, in the MLO triple mutant, EXO70H4 exhibited predominantly cytoplasmic localisation and was absent from the plasma membrane and the cell wall **(Fig. 11A)**. Concerning MLO proteins, we chose to express only MLO6 due to its primary role in causing the aberrant trichome phenotype (see above). We produced A. thaliana transgenic plants carrying the MLO6-GFP fusion protein under the control of the native promoter (ProMLO6) in both Col-0 WT and exo70h4-1 mutant plants. In the control plants, MLO6-GFP localised to the plasma membrane, cell wall, cell wall channels, and stationary PM-associated speckles. However, in the *exo70h4-1* mutant, the signal was less pronounced in the cell wall, possibly due to the reduced thickness of the secondary cell wall. MLO6-GFP was partially visible in the cytoplasm, and the PM-associated speckles were smaller and appeared more mobile in the mutant background **(Fig. 11B)**.

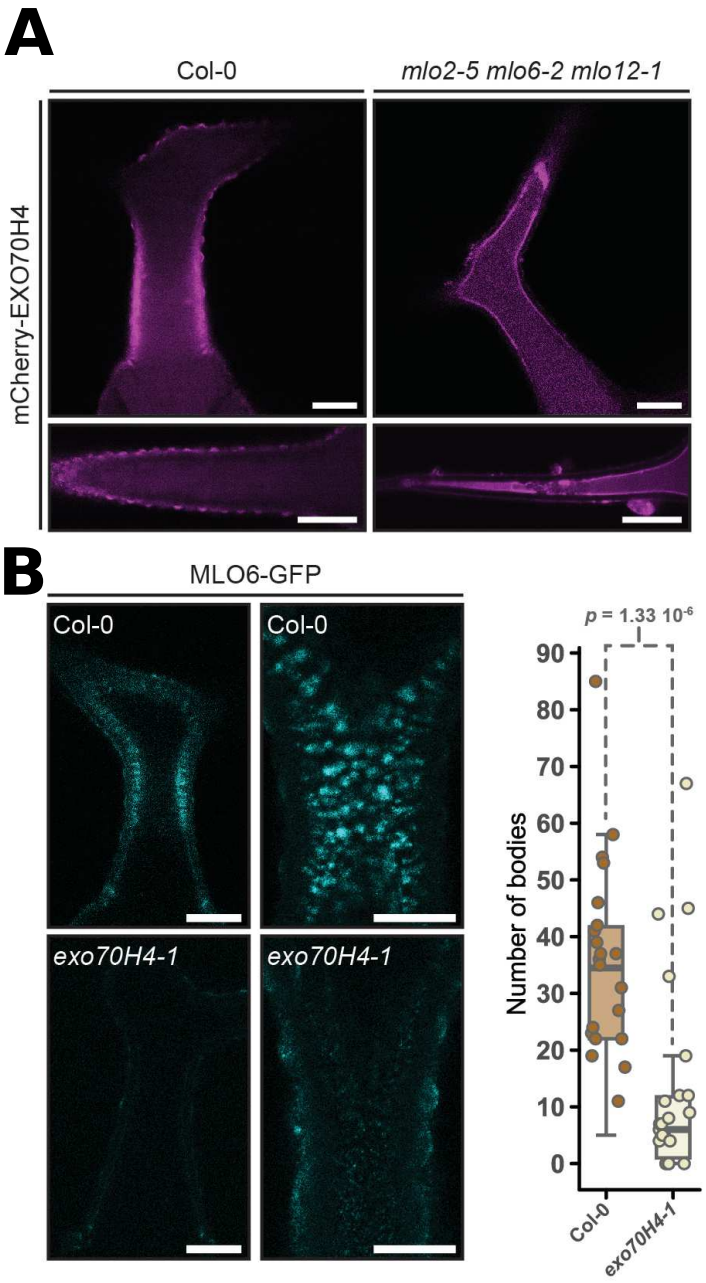

Figure 11: **A** Subcellular localisation of mCherry-EXO70H4, expressed under the control of the EXO70H4 promoter in either a transgenic Col-0 WT plant (left panels) or a mlo2-5 mlo6-2 mlo12-1 triple mutant plant (right panels). The upper panels show the trichome stalk region, and the lower panels depict an individual trichome branch. Scale bars represent 20μm. **B** Subcellular localisation of MLO6-GFP, expressed under the control of the MLO6 promoter, in either a transgenic Col-0 WT plant (upper panels) or the exo70h4-1 mutant plant (lower panels). The left panels show single planes focused on the cell wall, and the right panels show single planes focused on the PM. Scale bars represent 20μm each. Left panerl in **B** Quantification of the number of stationary MLO6-GFP-labeled intracellular dot-like compartments as calculated from the minimal-intensity projection images (see Materials and methods for further details). Box plots represent the probability distribution of data as described in the Materials and methods section. Values are based on 2 experiments with a total of 30 images analyzed per genotype. The p-value was computed according to Wilcoxon–Mann–Whitney and indicates the statistical difference between the mobility of MLO6-GFP in the Col-0 WT background and the exo70h4-1 background.

2.6 Localisation of PMR4 callose synthase in *mlo2-5 mlo6-2 mlo12-1* mutant trichomes

PMR4 is widely acknowledged to be the primary callose synthase expressed in *A. thaliana* trichomes, with studies indicating its predominant localisation in these structures **(Jacobs et al., 2003)**. Moreover, a previous study has shown that in the *exo70h4-1* mutant, PMR4 is delocalised **(Kulich et al., 2018)**. Given the similarities in callose deposition phenotype between exo70h4-1 and *mlo2-5 mlo6-2 mlo12-1* mutants, we examined the subcellular localisation and dynamics of PMR4 in the mutant mentioned above. In stable transformants of *mlo2-5 mlo6-2 mlo12-1* expressing GFP-PMR4, we did not observe the typical cell wall localisation pattern of PMR4 seen in Col-0 WT **(Fig. 12)**. Instead, GFP-PMR4-marked endomembrane bodies exhibited increased dynamics in the triple mlo mutant compared to Col-0 WT. This finding mirrors the behaviour observed previously in the *exo70h4-1* mutant. This suggests that the delivery of the callose synthase to the plasma membrane is perturbed in the mlo triple mutant in the same manner as observed in the *exo70h4-1* mutant by Kulich *et al.* **(2018)**.

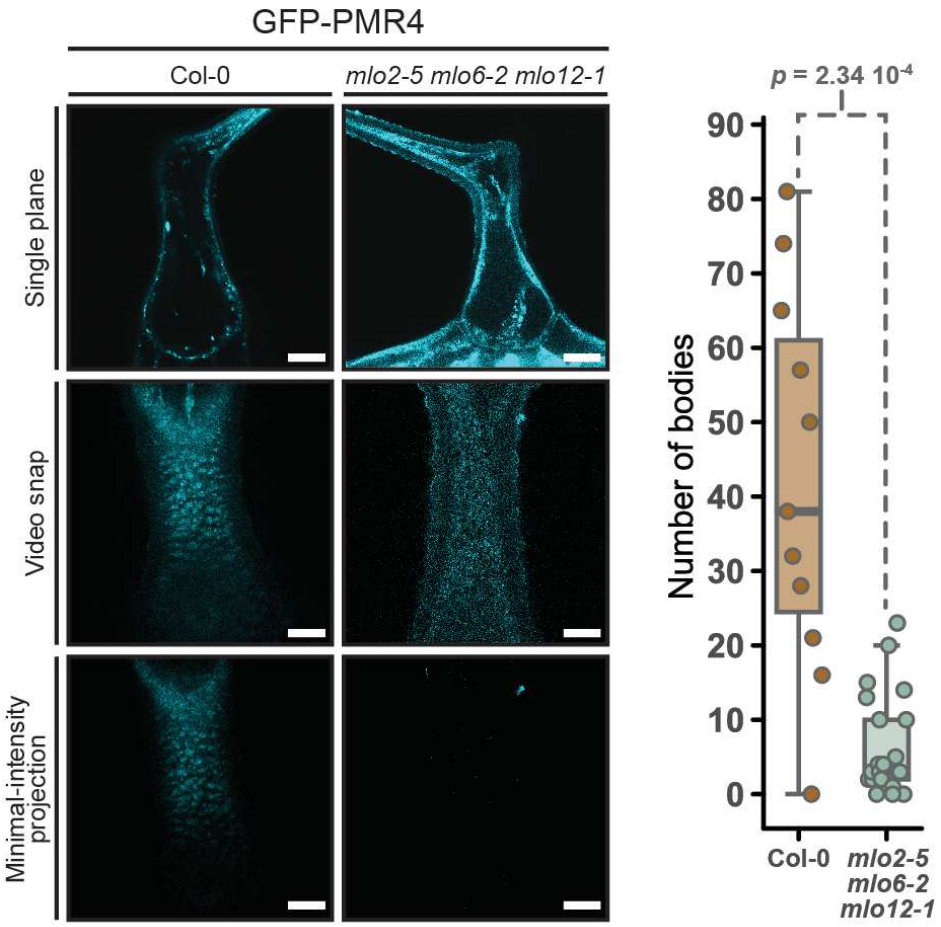

Figure 12: Subcellular localisation of GFP-PMR4, expressed under the control of the EXO70H4 promoter in either a transgenic Col-0 WT plant (left panels) or a *mlo2-5 mlo6-2 mlo12-1* triple mutant plant (right panels). The micrographs show a single confocal plane (upper panels), a snapshot from a time-series video (middle panels), and a minimal-intensity projection from the time series (bottom panels). Scale bars represent 20 μm. Quantification of the number of stationary GFP-PMR4-labeled intracellular dot-like compartments as calculated from minimal-intensity projection images (see Materials and methods for further details). Box plots represent the probability distribution of data as described in the Materials and methods chapter. The p-value was computed according to Wilcoxon–Mann–Whitney and indicates the statistical difference between the mobility of GFP-PMR4 in the Col-0 WT background and the *mlo2-5 mlo6-2 mlo12-1* background.

2.7 Interaction between MLO proteins and EXO70H4

Based on the similar alteration of trichome phenotype and the co-localisation of EXO70H4 and MLO2, MLO6, and MLO12, we hypothesised that these proteins may interact and be active in the same cellular pathway. We first tested this hypothesis using the Yeast Two-Hybrid system (Y2H). Due to its technical limitations with transmembrane proteins, we predicted candidate cytoplasmic domains and isolated the second intracellular loop and the C-terminal domain of MLO6 and tested the interaction with EXO70H4. We observed the growth of yeast colonies on selective media lacking Tryptophan and Leucine. When we grew the yeast on more restrictive media (-Leu, -Trp, -His), only colonies harbouring EXO70H4/MLO6-CT were observed, indicating a strong interaction with the cytoplasmic C-terminus of MLO6 **(Fig. 13G)**.

We conducted a plant luciferase complementation imaging assay (LCI) to confirm this interaction. In this assay, the amino-terminal (NLuc) and carboxyl-terminal (CLuc) fragments of firefly luciferase were joined to the proteins of interest, resulting in the restoration of luciferase activity (brightness) upon direct or indirect interaction of the two proteins **(H. Chen et al., 2008)**. By analysing co-expression data highlighting EXO70 genes that showed a high and positive correlation with genes encoding clade V MLO proteins (MLO2, MLO6, and MLO12) and taking into account tissue-specific and biotic stress data, we selected six genes from the Exo70.2 subfamily for the LCI assay (EXO70B2, EXO70D3, EXO70H1, EXO70H4, and EXO70H7). Additionally, we used the well-established interaction between MLO proteins and the cytosolic calcium sensor calmodulin as a positive control **(M. C. Kim et al., 2002) (Fig. 13)**.

The use of MLO2-NLuc led to a significant improvement in luminescence when co-expressed with CLuc-EXO70H1 (≈ 0.39) and -H4 (≈ 0.4), in contrast to the much lower value of ≈ 0.02 observed with CLuc-EXO70D3. The combination of MLO2-NLuc and CLuc-EXO70B2 resulted in a relative luminescence of ≈ 0.56, which was higher than the values obtained with MLO6-NLuc/CLuc-EXO70B2 (≈ 0.10), suggesting a

stronger interaction between MLO2 and EXO70B2. For MLO6-NLuc, the strongest relative luminescence was observed upon co-expression with CLuc-EXO70H4 (≈ 0.67), as expected from the results obtained with Y2H, while MLO12-NLuc showed enhanced relative luminescence in combination with CLuc-EXO70H1 (≈ 0.37) **(Fig. 13)**.

To further confirm the interaction between EXO70H4 and MLO6, we conducted in planta a Forster Resonance Energy Transfer (FRET) analysis using donor fluorescence lifetime imaging microscopy (FLIM). This method, which is widely accepted as the standard for FRET analysis of protein-protein interactions **(Lalonde et al., 2008)**, measures the decrease in donor fluorescence lifetime when an acceptor fluorophore is in close proximity (typically ¡10 nm) to the donor, indicating a close association between the two fluorophore-tagged proteins **(Bastiaens et al., 1999; Martin et al., 2018; Van Leeuwen et al., 2007)**. In our study, MLO6-GFP was used as the donor and mCherry-EXO70H4 as the acceptor molecule. Albertazzi et al. **(2009)** reported that the GFP-mCHerry pair has been well-suited for practical FRET-FLIM measurements in living cells. We used MLO6-GFP (donor alone) to serve as a negative control, while a GFP-mCherry fusion protein designed for intramolecular FRET was utilised as the positive control. All of the constructs were driven by the constitutive cauliflower mosaic virus 35S promoter and were transiently co-expressed with the p19 silencing suppressor in *N. benthamiana* leaves after the agroinfiltration.

The mean fluorescence lifetime of the MLO6-GFP negative control was approximately 2.18 ns, similar to the result obtained using EGFP alone, as reported in Martin *et al.* **(2018)**. The positive control, consisting of GFP-mCherry fusion protein, displayed a significantly reduced donor fluorescence lifetime of approximately 1.56 ns. When MLO6-GFP and mCherry-EXO70H4 were co-expressed, the resulting donor fluorescence lifetime was around 1.8 ns, which was statistically different from the positive and negative controls. This reduction in the donor fluorescence lifetime strongly suggests the interaction between EXO70H4 and MLO6 in plant cells cytoplasm **(Fig. 13E)**.

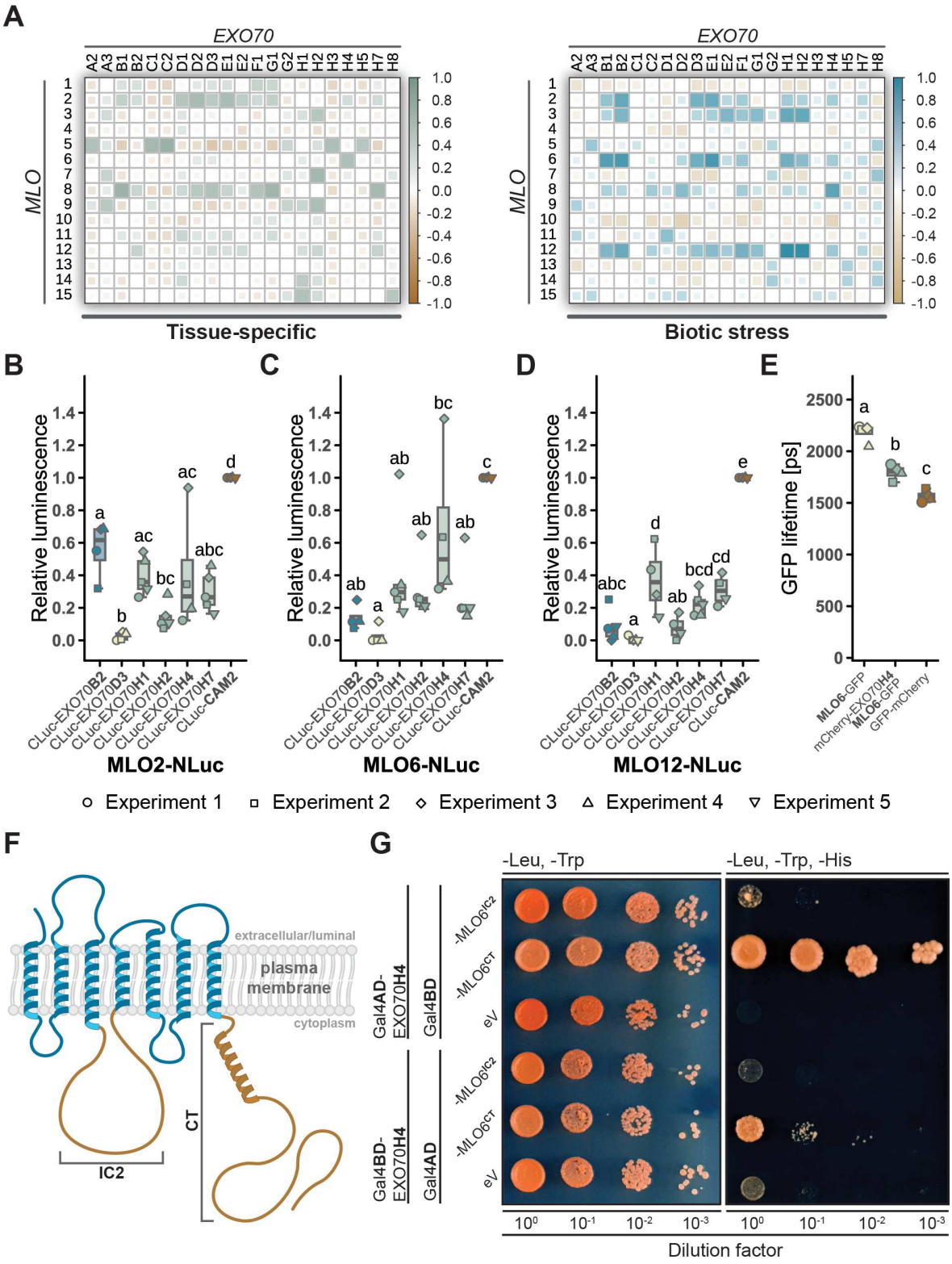

Figure 13: Interaction between clade V MLO proteins and different EXO70 proteins. **A** Tissue-specific or biotic stress-induced correlation of MLO and EXO70 transcript abundance. Transcript data (note that no data were available for EXO70A1 and EXO70H6) were retrieved from the Arabidopsis eFP browser (http://bar.utoronto.ca/efp/cgi-bin/efpWeb.cgi) on April 19, 2021.

Figure 13: (continued) Pearson correlation was calculated to assess the co-expression of individual MLO and EXO70 pairs. Squares illustrate Pearson correlation coefficients as indicated by the intensity scales on the right side of each graph. **B** to **D** Luciferase complementation imaging of different CLuc-EXO70 and MLO2/6/12-NLuc protein variant combinations was carried out by transient gene expression in *N. benthamiana*. For normalization, luminescence signals were divided by the signal obtained for the interaction of MLO-NLuc with CLuc-CAM2 (*A. thaliana* CALMODULIN 2; positive control) on the same leaf. Box plots represent the probability distribution of data as described in the Materials and methods chapter. Values are based on at least 4 independent experiments while individual data points represent the mean of 2 technical replicates each. Letters assign differences of statistical significance (pairwise Student's t-test corrected by FDR, $\alpha = 0.01$). **E** FRET-FLIM analysis of the interaction of mCherry-EXO70H4 with MLO6-GFP was performed by transient gene expression of constructs in *N. benthamiana* and determination of donor (GFP) fluorescence lifetimes. MLO6-GFP was used as a negative control, and GFP-mCherry as a positive control. Box plots represent the probability distribution of data as described in the Materials and methods chapter. Values shown were derived from 4 independent experiments with 3 cells and 5 regions of interest per cell analysed. Letters assign differences of statistical significance (pairwise Wilcoxon–Mann–Whitney test corrected by FDR, $\alpha = 0.05$). **F** Generic membrane topology of a clade V MLO protein. Protein domains that were subject to yeast two-hybrid analysis are shaded in brown. IC2, second intracellular loop; CT, carboxy terminus. G) Yeast two-hybrid experiment to test the interaction of EXO70H4 with MLO6IC2 or MLO6CT. *S. cerevisiae* cultures expressing recombinant EXO70H4 and MLO6 constructs were spotted on a medium deprived of (i) leucine (Leu) and tryptophan (Trp) or (ii) leucine, tryptophan, and histidine (His) in 4 different serial 1:10 dilutions. The images are representative of the outcome of 3 independent experiments. AD, activation domain; BD, binding domain; ev, empty vector.

2.8 Novel structure of MLO calcium channel (unpublished results

Based on the unpublished results obtained from EDS and the Raman spectra (shown in the sub-chapter 2.3), and considering the published results on the role of MLOs as calcium transporter channels, we utilised AlphaFold2 to test and model possible functional oligomerization of MLO proteins. We observed that full length MLO6 assembles into a hetero-trimer (MLO2 MLO6 MLO12) first and then also as a homo-trimer. Figure 14 (unpublished results) illustrates that the homo-trimer MLO6 (selected due to the pronounced phenotype in mlo6-2 mutant) forms a structure resembling well fitting channel, with the pore highlighted in purple **(Fig. 14A)**, which is not present in either monomer or homo-dimer MLO6 forms. Following these preliminary observations, all-atom molecular dynamics simulation were carried out to assess the stability of the formed channel when embedded into the lipid bilayer and the ability to transport calcium ions across the membrane. **(Fig. 14B)**.

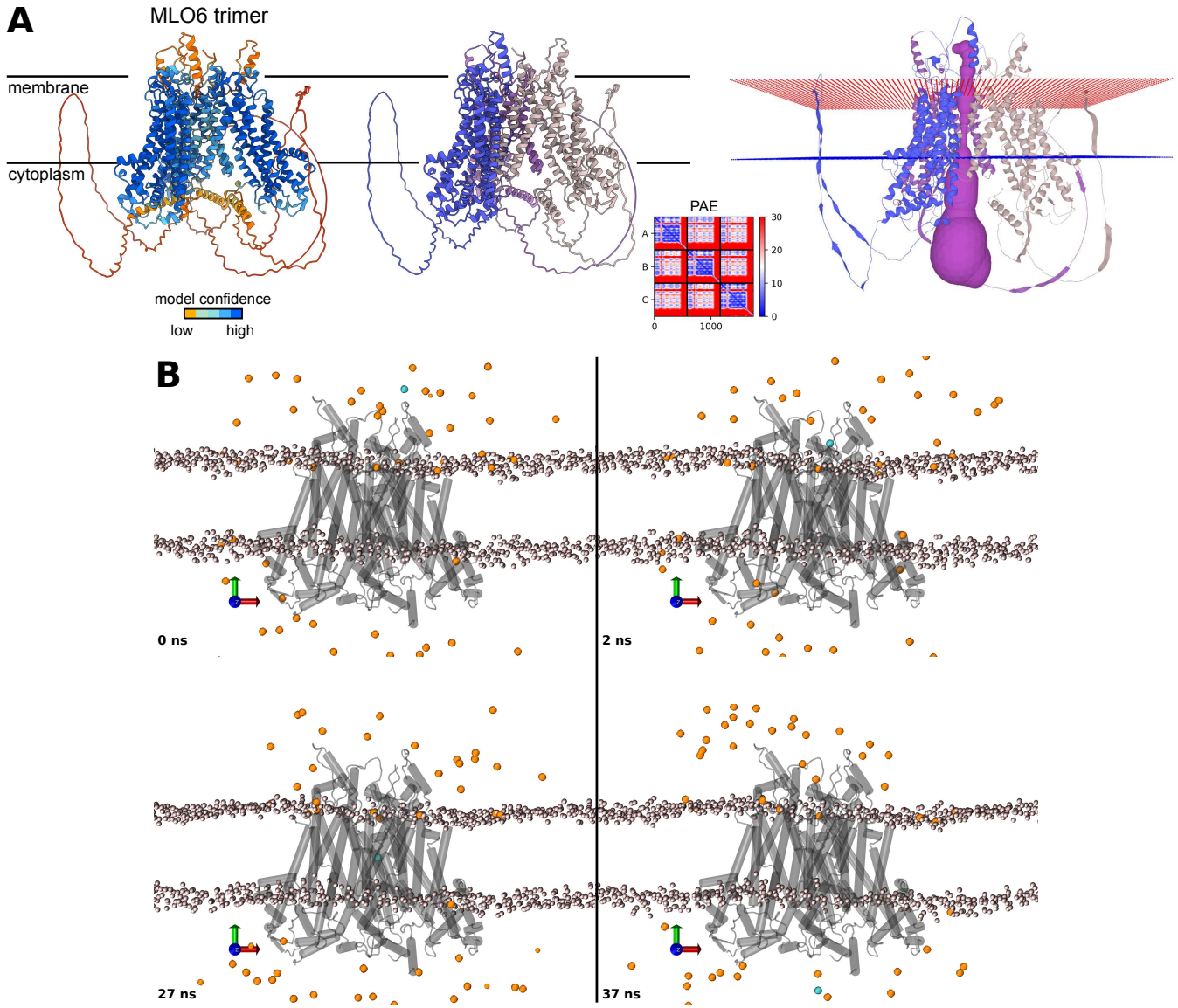

Figure 14: AlphaFold MLO6 homotrimer model. The channel pore is highlighted in purple in the right panel of A. In B, a time series 200 ns long highlights the transfer of a calcium ion (in cyan) from outside the membrane to the inside. The simulation was performed in 5 replicates by applying an external field of -750 mV for 500 ns.

2.9 Arabidopsis proteome analysis by proximity labelling (unpublished results)

Heterozygous 7 days old seedlings *exo84b-1* mutants transformed with UBQ::TurboID-GFP:EXO84B were utilised to analyse the Arabidopsis proteome under *P. syringae* stress; the experiment was designed as described in Fig. 15. Following biotynilation, a total of 135 proteins were labelled. Among all the proteins detected in the treated group, the autophagy related gene 18a (ATG18a) was selected for further investigation (**Fig. 16B**). Transient observations of UBQ::ATG18a:GFP and UBQ::mCherry:EXO84B in *N. benthamiana* demostrated the co-localisation of both protein (**Fig. 16A**), and FRET-FLIM analysis indicates that these two proteins are interacting under biotic stress (**Fig. 16C**)

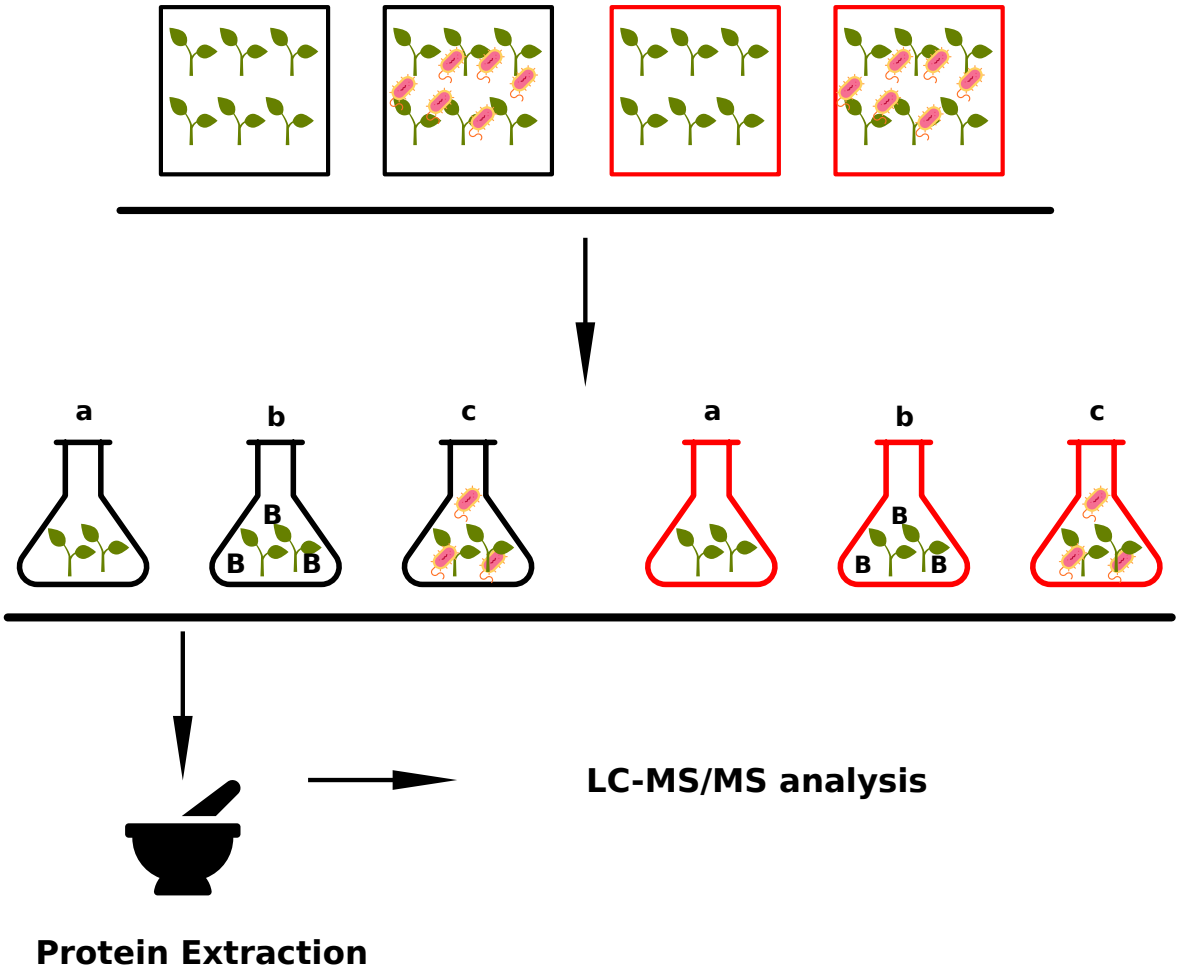

Figure 15: Schematic experimental design: COl-0 WT represented by black, UBQ::TurboID-GFP:EXO84B represented by red. Three experimental conditions were established for both Col-0 WT and plant carrying the TurboID construct: (a) plants incubated in liquid MS media on shaker for 6 h at 28° C; (b) plants incubated in liquid MS media with the addition of 100 μM on shaker for 6 h at 28° C; (c) plants incubated in liquid MS media with the addition of 100 μM and *P. syringae* (OD_{600} = 0.5) on shaker for 6 h at 28° C

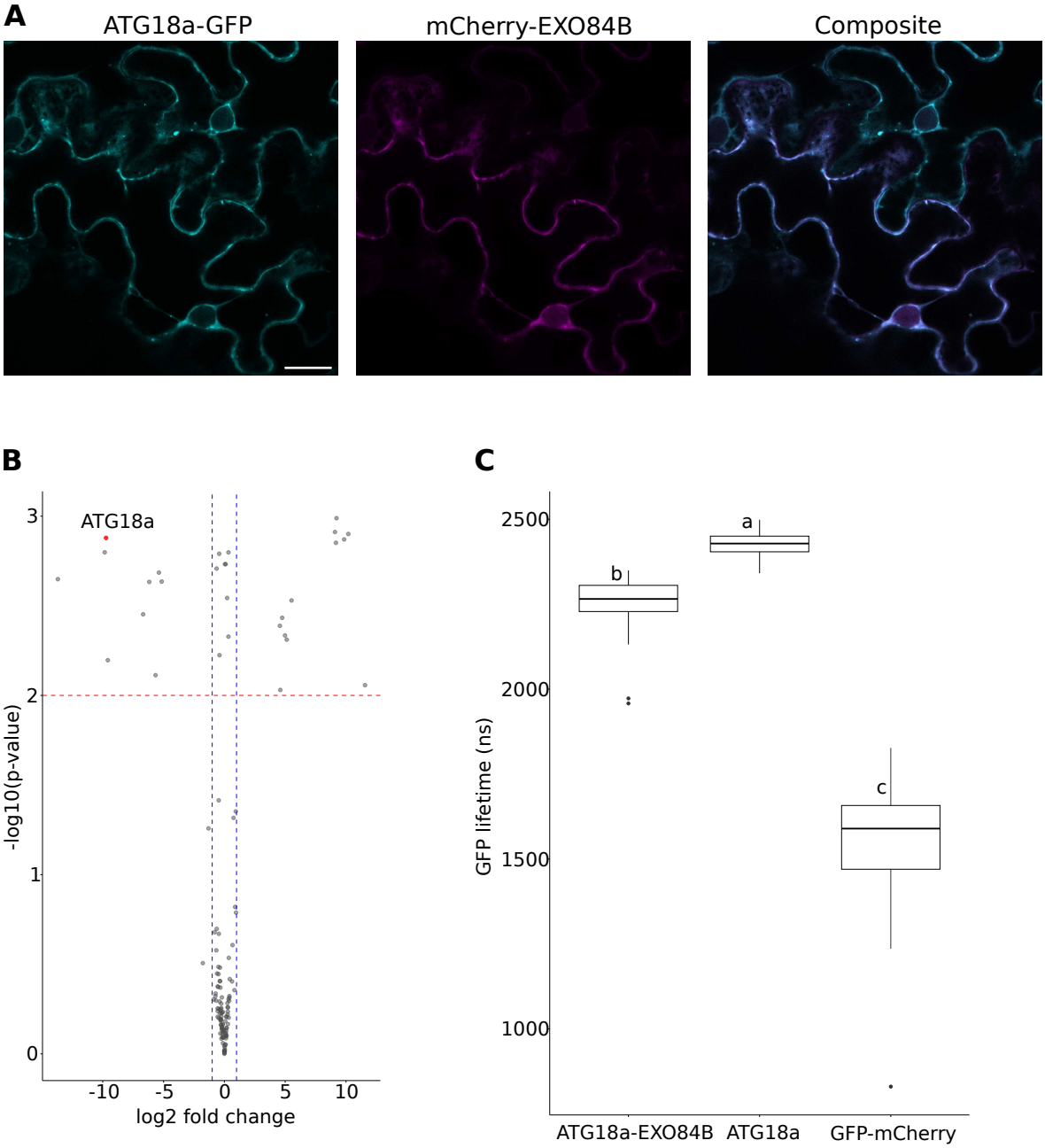

Figure 16: In **A** transient expression of ATG18a and EXO84B under UBQ promoter, scale bar represents 20 μm. **B** volcano plot illustrating differential protein expression. The x-axis display the log2-fold change in protein abundance detected in seedling treated with *P. syringae* (see Fig. 15) and control condition, whilst the y-axis display the -log10(p-value of each protein, indicating statistical significance (p-value = 0.01). **C** FRET-FLIM analysis of the interaction of mCherry-EXO84B with ATG18a-GFP in transient *N. benthamiana* expression, and determination of donor (GFP) fluorescence lifetime. ATG18a-GFP was utilised as negative control, and GFP-mCherry as a positive control. Box plot represents the probability distribution of data as described in the Material and methods chapter. Values shown were derived from 2 indipendent experiments with 3 cells and 5 regions of interest per cell analysed.

3. Discussion

The exocyst complex, a key regulator of polarised secretion in eukaryotes, is pivotal in delivering vesicles to specific plasma membrane domains. This process is essential for diverse cellular functions, including cell wall synthesis, cell polarity, and signalling. In trichomes, the EXO70 subunit, particularly EXO70H4, is instrumental in recruiting the exocyst complex to the plasma membrane, facilitating vesicle tethering and fusion used in cell wall development **(Kulich et al., 2015, 2018)**.

While MLO proteins were initially characterised for their role in powdery mildew resistance, recent research has unveiled their broader significance in plant physiology. MLO has been identified as a SNARE proteins interactor and plasma membrane calcium channel **(Gao et al., 2022; J.-G. Meng et al., 2020)**, suggesting a potential connection between exocytosis, given calcium's role in vesicle fusion and cell wall biosynthesis.

Here I discuss the relationship between MLO and the exocyst complex driving the secondary cell wall synthesis in A. thaliana trichomes in context of published findings. This sheds light on MLO's and exocyst multifaceted functions and integral role in fundamental cellular processes. In addition to the relationship between MLO and exocytosis, we show that MLO must form a trimer to be able to transport calcium, and also a new link between exocytosis and autophagy found through proximity-labelling

3.1 The intriguing collaboration between EXO70H4 and MLO genes in carving the trichome secondary cell wall

Based on our evaluation of the mlo triple mutant trichomes, it appears that the phenotype exhibited with regards to callose on the trichome is almost identical, to what was previously observed in *exo70h4-1* mutant trichomes **(Kulich et al., 2015)**. Previous research has suggested that EXO70H4 plays a vital role in the core deposition of callose, but there has been no confirmed relationship with MLO genes. Given that MLOs function as calcium channels, they might be located in specific areas of the trichome plasma membrane, helping to drive more targeted secretions.

Analysing and quantifying the parameters that determine the trichome phenotype, such as callose deposition, which, along with the cell wall's autofluorescence, are considered the primary discriminators between Col-0 WT and the *exo70h4-1* mutant, and cell wall thickness, which is influenced by the proper delivery to the plasma membrane of the various components used to build up the cell wall.

Callose deposition, in particular, was significantly disrupted in both MLO triple mutants **(Fig. 1)**. Notably, only those with the mutated MLO6 gene exhibited this phenotype among the single and double mutants. This finding is intriguing for two reasons: first, all three MLOs (MLO2, MLO6, MLO12) colocalise with EXO70H4; second, MLOs are known to function as calcium channels. Calcium plays a crucial role in regulating callose synthase activity, influencing callose deposition **(H. Kauss et al., 1990; Heinrich Kauss, 1985; Nedukha, 2015; Shikanai et al., 2020; Xiao et al., 2018)**. However, our results suggest that only MLO6 is significantly involved in the distribution of callose on *A. thaliana* trichomes. Knowing the role of MLOs as calcium channels and the fact that, in eukaryotes, calcium promotes vesicle fusion with the PM **(Barclay et al., 2005)**, along with recenti findings of interaction between

both MLOs and EXO70s with SNARE proteins, particularly VAMP721 **(Larson et al., 2020; J.-G. Meng et al., 2020)**, we hypothesize that PM-localised MLO calcium channels facilitate calcium-influx driven secretory events in specific localised regions. As shown in **Fig. 13**, the physical interaction between EXO70H4 and MLO6 protein may be crucial in determining the site of vesicle fusion, leading to polarised callose deposition due to a calcium gradient formed by MLOs. Given that MLOs function as calcium channels, they might be located in specific areas of the trichome PM, helping to drive more targeted secretion.

In trichomes, PMR4 and CalS9 are the two highly expressed callose synthase **(Jakoby et al., 2008)** and is known that EXO70H4 is responsible for the proper docking and delivery of PMR4 to the plasma membrane **(Kulich et al., 2015)**. The mislocalisation of PMR4 in *exo70h4-1* and the LOF *mlo* triple mutant emphasises a more intricate relationship between these proteins regarding callose synthase delivery and docking. We have seen that EXO70H4 is mislocalised in the *mlo* triple mutant, and a similar observation has been made with respect to MLO6 in *exo70h4-1* mutant. These observation indicates that EXO70H4 and MLO6 need each other for correct localisation and, cosequently, for correct delivery and docking of PMR4.

Regarding the cell wall thickness, it was observed that all mutants exhibit a thinner cell wall compared to Col-0 WT, which is consistent with the observation that MLO mutations can disrupt or influence the exocytosis of components used in the cell wall structure. As with callose, MLO6 plays the most critical role. However, when considering cell wall autofluorescence, there appears to be a second player and a collaboration between MLO2 and MLO6 rise, suggesting that not only EXO70H4 is responsible for delivering of phenolic compounds to the plasma membrane, as previously described **(Kulich et al., 2015)**, but it seems that this MLO2-MLO6 collaboration also disrupts the transport of vesicles containing phenolic compounds responsible for the cell wall autofluorescence.

This collaboration between MLO2 and MLO6 in regulating cell wall autofluo-

rescence suggests a more complex interaction between these proteins and EXO70H4 in trichome development to cell wall autofluorescence.

3.2 Cell wall trapping of EXO70H4 and MLOs

Our observations following plasmolysis indicate that both EXO70H4 and MLOs are trapped within the cell wall. As observed in Kubatova *et al.* **(2019)**, EXO70H4 appears to be trapped in pockets formed within the secondary cell wall. It has been established that EXO70H4 can bind phosphatidic acid, and that both phosphatidic acid, together with its interactor, and EXO70 are capable of bending the membrane in mammals **(Putta et al., 2016; Zhao et al., 2013)**, resulting in the formaation of rod-like structures observed in the trichome branches where both MLOs and EXO70H4 were observed. The formation of these rod-like structures may also contribute to developing the necessary calcium gradient to facilitate calcium carbonate formation (discussed afterwards)

3.3 Reactive Oxygen Species in trichome cell wall domain

Our data, presented in this thesis and the recently published article, show ROS production and localisation on the cell wall of trichomes in Col-0 WT near the OR. This phenotype is missing from all mutants investigated. It has been seen that under stress, ROS accumulates in trichomes of different species, such as mulberry **(Tewari et al., 2006)** or *A. thaliana*, under UV-B irradiation **(Bouché et al., 2003)**. Nevertheless, our experiments were performed under normal conditions and without the applied stress, whether biotic or abiotic. This implies the involvement of ROSs in regular Arabidopsis trichome maturation. It is currently not clear which mechanism is producing this ROSs. However ROSs might be produced in the wall e.g by ascor-

bate peroxidase and that they might be used as a substrate by wall peroxidases in the cross-linking of cell wall polysaccharides and phenolic compounds contributing to the trichome cell wall maturation **(Tenhaken, 2015)**.

This ROS production, close to the OR, correlates with the same pattern seen during the callose deposition in Col-0 WT trichomes, indicating a highly targeted and polarised process. This is due to the localised distribution of specific proteins that may be involved in ROS production, such as NADPH oxidases/RBOHs or wall peroxidases. In the case of Casparian strips, RBOH is phosphorylated by SCHENGEN1 in specific domains, resulting in localised production of ROS used by cell wall peroxidases for lignification of the Casparian strip **(Fujita et al., 2020)**.

Something similar may also occur in callose deposition in our *exocyst* and *mlo* mutants. Studies done under osmotic and heavy metal stress **(Lin 2013; Trinh 2014)** provide evidence of a possible functional connection between EXO70s/exocyst and ROS.

As we know, MLO proteins are best known for their role in the sensitivity to pathogens. It has been seen, particularly for MLO2, which can negatively regulate extracellular reactive oxygen species production, *mlo2* mutants show along with enhanced resistance to powdery mildew also tolerance to ozone, resulting in reduced cell death **(F. Cui et al., 2018)**. The absence of ROSs from the cell wall in our mutants, reinforces these observations, MLOs as negative regulators resulting in downregulation of cell wall ROS accumulation. In the case of trichomes we show that this happens in EXO70H4 dependent manner.

3.4 Trichomes are heavy metal accumulators in EXO70H4 and MLO dependent manner

Is established the role of HM as cofactors for some enzymes involved in cellular metabolism, and as observed in the case of ROS, their excess is toxic to the plant. Sev-

eral ion transporters play a key role in the transport of HMs within the plant organism, such as CPx-type ATPases, zinc-iron permeases (ZIP), and Nramp **(Williams et al., 2000)**. Over the years, plants have developed various strategies to combat heavy metals (HM), including pythochelators and biochemical synthesis to minimise toxic effects and restriction in the cell wall **(Ejaz et al., 2023)**.

Several studies indicate that trichomes are HM accumulators, particularly for plants from the Brassicaceae family. Brassica juncea can accumulate cadmium **(T. Li et al., 2023)**. In the case of *A. hallery* (and HM hyperaccumulator), HMs were seen to be present in the basal part of the trichome **(Roosens et al., 2008)**, resembling the callose ring/band or even that band observed for ROS deposition in Col-0 WT trichomes.

One way of trapping heavy metals in the trichome cell wall is the binding of certain metal cations, e.g. Pb or Cd, with the various functional groups of the cell wall components; for example, the carboxyl group in pectins **(Ejaz et al., 2023)**.

From recent proteomic data obtained from *A. thaliana* trichomes, it was found that COPT5 (copper transporter) is among the most enriched protein **(Huebbers et al., 2022)** together with ZIP proteins **(Jakoby et al., 2008)**. This HM transporter is most likely involved in the HMs transport and deposition in CW of trichomes. Based on our results, the absence of HM deposition in the cell wall, as determined by DAB staining of trichomes, suggests that both EXO70H4 and the investigated MLOs (MLO2, MLO6, MLO12) proteins are involved in eliminating excess of heavy metals and their inclusion into the cell wall, possibly by contributing to the PM localisation of HM transporters.

3.5 Biomineralization in trichomes

Biomineralisation is the biological process by which living organisms produce minerals that make tissues harder or stiffer. In the case of plants, the process occurs at the level of individual cells. In trichomes, the primary minerals that can be found to be deposited are silicon, calcium carbonate and calcium phosphate **(Ensikat et al., 2021)**, and their primary function is to harden and stiffen the cell wall.

Based on the results of Raman spectroscopy of trichome CW analyses presented here and recent discovery of MLO proteins as calcium channels, I focused on calcium carbonate deposition in this thesis. As observed from the spectra obtained by Raman spectroscopy, in comparison with Col-0 WT, mutants lack of calcium in their cell wall. All mutants analysed (*exo70h4-1*, *mlo2-5 mlo6-2 mlo12-1*, *mlo6-2*) exhibited this phenomenon. Along with compromised callose deposition this new defect certainly contributes to a thinner cell wall in mutants trichomes and enhanced fragility.

3.6 Active MLO calcium channel is an assembly of three subunits

Using computational approaches - AlphaFold and molecular dynamics simulation we have discovered that MLO proteins must form a trimer, both homo- or hetero-, to be able to transport calcium and that this trimer is stabilised when incorporated into the cell membrane.

These exciting new findings shed more light on how MLOs function as calcium transport channels. It is reasonable to assume that this is important for calcium carbonate deposit formation but how this is coordinated with EXO70H4 remains a topic for future investigation.

It is known that the difference between intracellular and extracellular calcium

is tremendous **(Gilroy et al., 1987)**. As possibly MLO functions as a channel for calcium - for calcium to move from the apoplast to intracellular/cytoplasm or from the intracellular stores (e.g. in the ER) to the apoplast to form the calcium carbonate. We hypothesised that MLO might be able to form a localised gradient of calcium/calcium maxima, perhaps also by its involvement in recruiting to the PM, especially to these rod-like structures where MLOs localisation was observed, of other calcium channels **(J.-G. Meng et al., 2020)** to create enough local free calcium concentration to have a transfer of the cations towards the cell wall allowing consequent formation of carbonate. A second hypothesis is that calcium carbonate or amorphous carbonate is formed inside the cell **(Blondeau et al., 2018)** and that MLO and EXO70H4 are involved in their shipment to the cell wall.

3.7 A novel link between exocytosis and autophagy in plants

ATG18 is involved in the formation and elongation of the phagophore, the precursor of the autophagosome, binds phosphatidylinosito 3-phosphate and the interaction with ATG2 and ATG9 promoting the transfer of lipids used for membrane expansions **(D. Mann et al., 2023; Rieter et al., 2013)**. In mammalian cells, EXO84 promotes the formation of the autophagosome by forming a complex with active ULK1 and Beclin1, essential for phagocytic formation **(Antonioli et al., 2017; Bodemann et al., 2011; Simicek et al., 2013)**, but also helps the turnover of exocyst compartments, as described by Zhang **(2023)**, and is known that *exo84b* mutants have compromised cell division **(Fendrych et al., 2010)**.

Similar to other autophagy genes, ATG18a has been observed to be involved in numerous biotic and abiotic stresses **(Lai et al., 2011; Zhu et al., 2024)**; however, there is limited research on EXO84B-related stress studies compared to other exocyst subunits. EXO84B interacts with other exocyst subunits, such as EXO70A1, which

are directly involved in stress- or autophagy-related responses **(Kulich et al., 2013; Pečenková et al., 2020)**. This newly discovered interaction between EXO84B and ATG18a may provide a novel link between exocytossi and autophagy. This connection potentially plays a pivotal role in maintaining cellular homeostasis and responding to environmental stimuli.

4. Conclusions

This thesis significantly advanced our understanding of the intricate relationship between EXO70H4/exocyst complex and MLO genes in regulating trichome secondary cell wall development and plant secondary cell wall biogenesis in general. Our findings elucidate the critical roles of these proteins in callose deposition, cell wall thickening, and modification affecting its autofluorescence. The observed interactions between EXO70H4 (and some other exocyst subunits) and MLOs suggest a complex regulatory network that governs trichome cell wall biosynthesis.

We found that EXO70H4 and MLO proteins, particularly MLO6, work collaboratively to ensure callose synthase (PMR4) delivery and function in trichomes cell wall maturation. The discovery of a novel phenotype, the lack of calcium carbonate in mutant trichomes, provided an opportunity to investigate MLO proteins as calcium channels and our *in silico* computations indicate that MLO proteins assemble into trimeric functional calcium channels.

While this study has shed light especially on the roles of EXO70H4 and MLO genes in trichome development, many questions remain unanswered. Given the large protein families of EXO70s and MLOs in *A. thaliana*, it is likely that other combinations of these proteins may function together in different cell types or tissues. Furthermore, the molecular mechanisms underlying MLO-mediated calcium transport require further exploration.

In addition to the novel findings regarding MLO and EXO70, this newly discovered link between EXO84B and ATG18a elucidates potential mechanisms for coordinating autophagy and exocytosis, thereby opening further research into plant stress responses.

5. Material and Methods

5.1 Plant material

The *A. thaliana* mutants used in this thesis are the following *exo70h4-1* (SALK_023593, **(Kulich et al., 2015)**), *mlo2-5 mlo2-6 mlo12-1* **(Consonni et al., 2006)** and *mlo2-6 mlo6-4 mlo12-8* **(Acevedo-Garcia et al., 2017)** triple mutants as well as the respective *mlo* single and double mutants are T-DNA/transposon insertion mutants in the Col-0 background ecotype. In the study context, a *mlo6* mutant was generated in the Col-0 background by CRISPR-Cas9. The *pmr4-1* **(J. Vogel et al., 2000)** are ethyl methasulsofonate-induced mutants. The following transgenic lines have been described before by Kulich *et al.* **(2018)**: mCherry-EXO70H4 under the control of the native EXO70H4 promotes in Col-0; GFP-PMR4 under the control of UBIQUITIN10 promoter in Col-0.

5.2 Plant Cultivation

A. thaliana and *N. benthamiana* plants were cultivated on Jiffy pellets (Jiffy Products Internationa BV, The Netherlands) at an average day/night temperature of 23/20° C and a photoperiod of 16/8 h/d light/darkness.

5.3 Generation of *mlo6* mutant by CRISPR-Cas9 based gene editing

To generate *mlo6-6*, the *mlo6* CRISPR mutant, an expression vector harbouring a 2-target gene-specific gRNA, was constructed based on a previously published system for multiplex gene editing **(Xing et al., 2014)**. Primers for the MLO6 gene-specific gRNAs were designed using the CRISPR-P web tool **(Lei et al., 2014)**, and were then used to amplify the target fragments from pCBC-DT1DT2 (https://www.addgene.org/50590/), which were then cloned into vector pHSE401 (https://www.addgene.org/62201/) by Golden Gate cloning **(Engler et al., 2008)**. The final vector expressing the gRNAs was transferred into **Agrobacterium tumefaciens** (strain GV3101) **(Koncz et al., 1986)** and *A. thaliana* Col-0 plants were transformed via the floral dip method **(Clough et al., 1998)**. Transgenic plants were selected based on hygromycin resistance, and the presence of the homozygous deletion was verified by Sanger DNA sequencing. The newly generated mlo6-6 mutant carries a CRISPR-Cas9-induced 1-bp deletion in a run of 3 consecutive T nucleotides at positions 786 to 788 (numbering is according to the MLO6 coding sequence; beginning of exon 7). This causes a frameshift leading to a premature stop codon in the MLO6 coding sequence 19 amino acids downstream of the mutational event.

5.4 Generation of plant expression constructs and transgenic lines

MLO2 and MLO6 cDNAs and MLO12 genomic sequences were amplified by PCR using suitable primers and integrated via BP recombination into Gateway-compatible pDONR221 entry vectors (Thermo Fisher Scientific). These MLO inserts and the EXO70H4 genomic sequence were co-shuttled via multisite Gateway recombination into plant expression vectors pK7m34GW (MLO2) or pH7m34GW (MLO6, MLO12)

(Karimi et al., 2005) under the control of either EXO70H4 or UBIQUITIN10 promoter. Similarly, an MLO6-GFP plant express construct under the control of the MLO6 promoter was established by multisite Gateway recombination. The resulting binary expression vectors were transferred to *A. tumefaciens* strain GV3101, and transgenic *A. thaliana* lines were generated via the floral dip method. The selection of transgenic lines was performed on suitable selection media.

5.5 Histochemical staining of trichomes for callose and autofluorescence assay

The callose staining in *A. thaliana* trichomes was carried out as previously described **(Kulich et al., 2018)**. Briefly, the third or fourth leaf of 3-week-old plants were washed for 3 to 4 hours in acetic acid:ethanol (1:3) solution and incubated overnight in aniline blue solution (0.01% (m/v) aniline blue in 150 mM potassium dihydrogen phosphate buffer, pH 9.5), trichomes were observed under UV illumination. The third or fourth visible leaf was used for the cell wall autofluorescence. The leaf was squeezed on the microscope slide, and the trichomes were brushed with a needle to stimulate the accumulation of autofluorescent phenolic compounds. Trichomes were observed under UV illumination after 5 to 10 min without cover glass.

5.6 Histochemical staining of trichomes for ROS and HM

The detection of hydrogen peroxide as a key representative of ROS was conducted as previously reported **(O'Brien et al., 2012)** using the third or fourth leaf of 3-week-old plants. The staining was performed 1 h after cutting to stabilise the ROS level in the whole leaf. Leaves were vacuum-infiltrated for 5 min with DAB solution (1mg/mL in 10 nM Na_2HPO_4, 0.05% (v/v) Tween 20) and then incubated on a shaker

for 5 h. Following the incubation, the leaves were transferred to 50 mL test tubes containing a bleaching solution (3:1:1 mixture of ethanol, acetic acid, and glycerol) and boiled for 15 to 20 min (until leaves were bleached entirely). Following bleaching, leaves were placed in 6-well plates and observed the following day.

For HM observation, 3-week-old A. thaliana plants were watered with a 1 mM zinc chloride solution for 4 consecutive days in 1 week and stained with dithizone as described previously **(Seregin et al., 1997)**. The staining solution was composed of 30 mg of dithizone dissolved in 20 mL of distilled water, 60 mL of acetone, and 8 drops of acetic acid. The leaves were stained for 1 h and observed the same day. Before observation, each leaf was rinsed in distilled water.

5.7 Quantification of neutral sugars and cellulose

The mass of neutral monosaccharides and cellulose in isolated and lyophilized trichomes was determined as described **(Yeats et al., 2016)**. In brief, alcohol-insoluble material was prepared from the dried trichomes and split into 2 samples. One sample was treated with a weak acid (4% sulfuric acid) to release matrix polysaccharide-derived sugars, while the other sample was treated with a strong acid (72% sulfuric acid) to swell cellulose. Afterwards, the solution was adjusted with distilled water to the concentration of the weak acid (4% sulfuric acid) to yield monosaccharides derived from cellulose and the matrix polymers. Subtraction of the 2 values allows for the quantification of crystalline cellulose. Monosaccharides were quantified using a Professional IC Vario high-performance anion-exchange chromatography system (Methrom, Herisau, Switzerland) equipped with a CarboPac PA20 column (Thermo Fisher Scientific, Waltham, Massachusetts, USA) and an amperometric detector (Methrom). The elution gradient of the monosaccharides is specified in Yeats et al. (**2016**).

5.8 Plasmolysis of leaf-attached trichomes

For plasmolysis, 4-week-old rosette leaves were incubated for 1.5 h in a 20% sucrose solution and then observed by confocal microscope.

5.9 FTIR spectroscopy

FTIR spectra were obtained from isolated and lyophilized trichomes using a JASCO4700 FTIR spectrometer (JASCO, Pfungstadt, Germany) equipped with an attenuated total reflection module (ATR) at a resolution of 1cm1. The region between 800 and 1800cm1 was selected from the average spectra (n = 10) to analyze differences in cell wall components **(Alonso-Simón et al., 2011)**. Subsequently, all spectra were normalized and baseline-corrected by using Spectra Manager (JASCO).

5.10 EDS analysis

For a semiquantitative energy-dispersive x-ray microanalysis (EDS) as previously described **(Kulich et al., 2018)**, four trichomes from eight leaves were selected for each of the three samples (Col-0, *exo70h4-1*, *mlo2-5 mlo6-1 mlo12-1*), air dried, and placed on a carbon pad. To maximize detection efficiency and accuracy of the analysis, trichomes were selected according to their shape and shadowing in x-ray maps using a solid-state detector of backscattered electrons and fast EDS mapping. Dried, chemical treatment-free, and conductive coating-free samples were imaged and analyzed using ESEM Quanta 650 FEG equipped with EDS silicon drift detector Bruker Quantax 400 XFlash 6/60 under beam energy 10 keV, beam current 100 pA, working distance 10 mm, and water vapor pressure 100 Pa. The ratio of silicon in the sample was calculated as the median values obtained from all trichomes for each sample.

5.11 Microscopy

The observation of callose and cell wall autofluorescence was done using a Nikon Eclipse 90i microscope with either a PlanApo 4x/0.2 objective (for the quantification of callose and cell wall autofluorescence) or a PlanApo 10x/0.45 objective (for imaging single trichomes) equipped with a Nikon DsFi 2 camera, for the observation of ROS, an Olympus IX71 microscope with LUCPlanFLN 40x/0.6 objective was used. For HM deposition, a Nikon Eclipse 90i microscope with a PlanApo 20x/0.75 objective was used. Trichome cell wall thickness was observed with an Olympus BX51 microscope with a UPlanSApo 60x/1.20 water immersion objective; brightfield micrographs were captured, and cell wall thickness was measured at the region of the OR.

A Zeiss LSM880 NLO with a C-Apochromat 40/1.2 W correction FCS M27 objective was used for confocal microscopy of trichomes. Excitation (in parentheses) and emission wavelengths were as follows: GFP (488 nm, argon laser) 508 to 540, chlorophyll (402 nm) 650 to 721 nm, mCherry (561 nm, Diode-Pumped Solid-State 561 laser) 597 to 641 nm.

5.12 FRET-FLIM analysis

We used MLO6-GFP, mCherry-EXO70H4, and a GFP-mCherry positive control, expressed under the control of the constitutive ProCaMV35S and under UBQ promoter for mCherry-EXO84B and ATG18a-GFP. *N. benthamiana* plants were used for transient gene expression, with *A. tumefaciens* harbouring the appropriate constructs and the p19 silencing suppressor plasmid **(Campe et al., 2016)**. For leaf infiltration of agrobacteria, bacterial cultures were grown overnight and resuspended in an infiltration medium (10 nM MES, pH 5.6, 10 mM $MgCl_2$, 150 μM acetosyringone), adjusted to an OD_{600} of 0.4. The analysis was performed at 2 d after agroinfiltration with a Zeiss LSM880 NLO confocal microscope as described above, equipped with a

hybrid single photon detector (HPM-100-40) connected to the Becker Hickl SPC-150 module (Becker Hickl GmbH, Berlin, Germany), and using a single band emission filter (AHF 525/50). The images were analysed using SPCImage software (**W. Becker, The bh TCSPC handbook. 10th edition (2023)** available on www.becker-hickl.com), and donor fluorescence lifetimes were calculated using pixels in the various regions of interest based on colour-coded lifetime images.

5.13 Yeast two-hybrid assay

For yeast two-hybrid assay, *S. cerevisiae* cells were transformed with plasmids expressing EXO70D3, EXO70H4, and either the IC2 or CT fragment of MLO6, respectively. The MLO6 IC2 fragment (MLO6IC2) consists of MLO6 amino acid residues 183 to 284, and the MLO6 CT fragment (MLO6CT) consists of MLO6 amino acid residues 433 to 583. For cloning of these constructs, EXO70D3, EXO70H4, AtMLO6IC2, and AtMLO6CT coding sequences were mobilised from pDONR207 entry clones via Gateway recombination into yeast two-hybrid vectors pGADT7 and pGBKT7 (Clonetech Laboratories Inc., Mountain View, California, USA). The recombinant plasmids were transformed by the LiAc/PEG method (**Yeast Protocols Handbook, Clonetech 2009**) into *S. cerevisiae* strain AH109. Yeast transformants expressing the recombinant proteins (see below) were spotted on a medium lacking leucine and tryptophan for growth control and on a medium lacking leucine, tryptophan, and histidine to detect putative interactions. For these tests, yeast cells were grown overnight in a liquid synthetic complete medium lacking leucine and tryptophan at 28 °C and 250 rpm. The cells were harvested the following day by 1 min of centrifugation at 3,000 × g and washed with sterile water before adjusting the OD_{600} of the solutions to 1. Ten-fold dilution series were established over 4 orders of magnitude and 3 or 4μL per dilution and construct combination were spotted onto the media mentioned above.

5.14 Raman microscopy

For the determination of the chemical composition of the trichome cell wall, samples were mounted on a quartz slide in 100 uL of 1% (m/v) solution of low-melting-point agarose (catalogue number 6351.5; Carl Roth, Germany) and observed by confocal Raman microscope was used (alpha300 RSA; WITec, Germany) equipped with Nikon CFI Achromat 60x/0.8 with a laser excitation of 531 nm (35 mW power at the focal plane). A Raman map of the whole trichome was acquired with ~230 lines/area with an integration time of 70 ms per cell voxel; for the single-point Raman spectra, ~50 points-acquisition were acquired with an integration time of 70 ms. Raman chemical maps were constructed by multivariate decomposition of the baseline components using Project Plus 5.1 software (WITec, Germany).

5.15 Proximity labelling

TurboID-GFP Gateway compatible construct was prepared from the TurboID plasmid obtained from AddGene. EXO84B used in Fendrych *et al.* **(2010)** together with TurboID-GFP, UBIQUITIN10 were used to prepare the expression vector in pH7m34GW used to transform heterozigous *exo84b-1* mutants via floral dip. 14 days old Arabidopsis seedling were transfered into flask containig 100 μM biotin and incubated for 6 h at 28° C on shaker; for the *P. syringae* treatment a DC3000 strain was used. After the protein extraction (protein extraction buffer described in Arora *et.al* **(2020)**, 500 μg of proteins were transfered to PD10-columns and eluted in PBS containing 0.5% SDS. After the elution protein extract was incubated overnight at 4° C with 100 μL slurry of streptavidin-Sepharose beads. Beads were washed with 6 mL PBS containing 2% SDS and then 3 times with 5 mL of PBS and then sent them to LC-MS analysis.

5.16 AlphaFold and molecular dynamics

For all-atom molecular dynamics simulation, we used AlphaFold2 **(Jumper et al., 2021)** generated structure models of MLO6 homo-trimer and CHARMM36m all-atom force-field **(J. Huang et al., 2017)**. The protein was inserted into a 15x15 nm symmetric membrane by PPM2.0 software **(Lomize et al., 2012)** in CHARMM-GUI **(Wu et al., 2014)**. The membrane was composed of 50% PC and 50% PE in both leaflet. The membrane-embedded protein was then solvated with TIP3 water and neutralized with 0.15 M KCl and 0.05 M multi-site calcium **(A. Zhang et al., 2020)**. This system was then energy minimized employing the steepest-descent algorithm for up 5000 steps and equilibrated for 1875 ps in 6 successive steps with progressive releaseing of the position restraints. The equilibrated system was then run for 100 ns with no position restraints to relax the input, after which position restraints of 1000 kJ $mol^{-}1$ $nm^{-}2$ were set on the protein backbone to prevent protein deformation due to the application of an external electric field. The production run was performed in 5 replicates, each with different starting velocities for 500 ns. An external field of -750 mV in the z-axis was applied to the system to facilitate the calcium transport. During production runs, the temperature was set to 303.15 K.

5.17 Image analysis

All micrographs of leaf-attached trichomes were processed using the Fiji platform as described below. To calculate the number of stable PM-associated GFP-PMR4- and MLO6-GFP-marked dots (compartments) in A. thaliana trichomes, we imaged the trichomes in a time-series experiment and subsequently performed the minimal projections command in the Fiji software **(Kulich et al., 2018; Schindelin et al., 2012)**. We then calculated the number of visible dots using the dot and ROI Manager tools. Colocalisation analysis of fluorophore-tagged proteins in mature rosette leaf trichomes was performed using Fiji JACoP (Just Another Colocalization Plugin; **(Bolte et al.,**

2006)). For each transgenic line, we examined 5 images from 4 different experimental replicates, consisting of 2 frames taken in immediate succession. Each frame combination was analysed to obtain Pearson's correlation coefficient, and based on this, the RBNCC (Replicate-Based Noise Corrected Correlation) coefficient was calculated as described before **(Daly et al., 2012)** to obtain a noise-corrected correlation indicator.

5.18 Plots and statistical analysis

R v.4.1.3 (R foundation, www.r-project.org/) was used for plotting, statistical analyses, and filtering of data during this study. Plotting was carried out using the ggplot2 library, whereas the dplyr library facilitated data processing, both included in the Tidyverse package **(Wickham et al., 2019)**. Box plots were assembled in the style of Tukey: The boundaries of the whiskers are defined by the lowest or highest value, respectively, within a 1.5 times interquartile range. The box marks the range between the first and third quartiles. Horizontal bars represent the median. Note that in the text, the arithmetic mean was used to compare different samples. Correlation analysis of these transcript data was facilitated by the corrplot package (**Wei and Simko 2021** https://github.com/taiyun/corrplot). We assessed the distribution of our data by quantile-quantile plots and by the Shapiro–Wilk test ($\alpha = 0.05$; **(Shapiro et al., 1965)**) and checked for homoscedasticity (equality of variances) by Levene's test ($\alpha = 0.05$; **(Gastwirth et al., 2009)**). Normally distributed data with similar variances were subjected to Student's t-test **(Student, 1908)**, whereas statistical differences between non-normally distributed samples were reviewed by the Wilcoxon–Mann–Whitney test **(H. B. Mann et al., 1947)**. Pearson's chi-square test **(Pearson, 1900)** assessed the statistical differences between nominal data. In the case of multiple comparison hypothesis testing, FDR was used to correct for the increased probability of type I errors **(Benjamini et al., 1995)**.

Bibliography

Abramson, Josh et al. (June 2024). "Accurate structure prediction of biomolecular interactions with AlphaFold 3". In: *Nature* 630.8016. Publisher: Nature Publishing Group, pp. 493–500. ISSN: 1476-4687. DOI: 10.1038/s41586-024-07487-w. URL: https://www.nature.com/articles/s41586-024-07487-w (visited on 08/13/2024).

Acevedo-Garcia, Johanna et al. (2017). "The powdery mildew-resistant Arabidopsis mlo2 mlo6 mlo12 triple mutant displays altered infection phenotypes with diverse types of phytopathogens". In: *Scientific Reports* 7.1. Number: 1, pp. 1–15. ISSN: 20452322. DOI: 10.1038/s41598-017-07188-7.

Albertazzi, Lorenzo et al. (Jan. 2009). "Quantitative FRET Analysis With the E ^{0} GFP-mCherry Fluorescent Protein Pair". In: *Photochemistry and Photobiology* 85.1, pp. 287–297. ISSN: 0031-8655, 1751-1097. DOI: 10.1111/j.1751-1097.2008.00435.x. URL: https://onlinelibrary.wiley.com/doi/10.1111/j.1751-1097.2008.00435.x (visited on 08/07/2024).

Alonso-Simón, Ana et al. (Aug. 2011). "The use of FTIR spectroscopy to monitor modifications in plant cell wall architecture caused by cellulose biosynthesis inhibitors". In: *Plant Signaling & Behavior* 6.8, pp. 1104–1110. ISSN: 1559-2324. DOI: 10.4161/psb.6.8.15793. URL: http://www.tandfonline.com/doi/abs/10.4161/psb.6.8.15793 (visited on 11/09/2024).

Antonioli, Manuela et al. (Jan. 2017). "Emerging Mechanisms in Initiating and Terminating Autophagy". In: *Trends in Biochemical Sciences* 42.1, pp. 28–41. ISSN: 09680004. DOI: 10.1016/j.tibs.2016.09.008. URL: https://linkinghub.elsevier.com/retrieve/pii/S0968000416301712 (visited on 11/05/2024).

Arora, Deepanksha et al. (Aug. 25, 2020). "Establishment of Proximity-dependent Biotinylation Approaches in Different Plant Model Systems". In: *The Plant Cell*. Publisher: American Society of Plant Biologists, tpc.00235.2020. ISSN: 1040-4651. DOI: 10.1105/tpc.20.00235. URL: http://www.plantcell.org/lookup/doi/10.1105/tpc.20.00235 (visited on 09/09/2020).

Bacete, Laura et al. (2018). "Plant cell wall-mediated immunity: cell wall changes trigger disease resistance responses". In: *The Plant Journal* 93.4. _eprint: https://onlinelibrary.wiley pp. 614–636. ISSN: 1365-313X. DOI: 10.1111/tpj.13807. URL: https://onlinelibrary.wiley.com/doi/abs/10.1111/tpj.13807 (visited on 03/27/2024).

Barclay, Jeff W. et al. (2005). "Calcium-dependent regulation of exocytosis". In: *Cell Calcium* 38.3, pp. 343–353. ISSN: 0143-4160. DOI: 10.1016/j.ceca.2005.06.012.

Bastiaens, Philippe I. H. et al. (Feb. 1999). "Fluorescence lifetime imaging microscopy: spatial resolution of biochemical processes in the cell". In: *Trends in Cell Biology* 9.2, pp. 48–52. ISSN: 0962-8924. DOI: 10.1016/S0962-8924(98)01410-X. URL: https://www.sciencedirect.com/science/article/pii/S096289249801410X (visited on 06/19/2023).

Benjamini, Yoav et al. (Jan. 1, 1995). "Controlling the False Discovery Rate: A Practical and Powerful Approach to Multiple Testing". In: *Journal of the Royal Statistical Society Series B: Statistical Methodology* 57.1, pp. 289–300. ISSN: 1369-7412, 1467-9868. DOI: 10.1111/j.2517-6161.1995.tb02031.x. URL: https://academic.oup.com/jrsssb/article/57/1/289/7035855 (visited on 09/24/2024).

Bidzinski, Przemyslaw et al. (2014). "Physiological characterization and genetic modifiers of aberrant root thigmomorphogenesis in mutants ofArabidopsis thaliana MILDEW LOCUS Ogenes". In: *Plant, Cell & Environment* 37.12, pp. 2738–2753. DOI: 10.1111/pce.12353. URL: http://dx.doi.org/10.1111/pce.12353.

Blondeau, Marine et al. (Aug. 6, 2018). "Amorphous Calcium Carbonate Granules Form Within an Intracellular Compartment in Calcifying Cyanobacteria". In: *Frontiers in Microbiology* 9. Publisher: Frontiers. ISSN: 1664-302X. DOI: 10.3389/fmicb.

2018.01768. URL: https://www.frontiersin.org/journals/microbiology/articles/10.3389/fmicb.2018.01768/full (visited on 09/16/2024).

Bodemann, Brian O. et al. (Jan. 2011). "RalB and the Exocyst Mediate the Cellular Starvation Response by Direct Activation of Autophagosome Assembly". In: *Cell* 144.2, pp. 253–267. ISSN: 00928674. DOI: 10.1016/j.cell.2010.12.018. URL: https://linkinghub.elsevier.com/retrieve/pii/S0092867410014364 (visited on 11/05/2024).

Bolte, S. et al. (Dec. 2006). "A guided tour into subcellular colocalization analysis in light microscopy". In: *Journal of Microscopy* 224.3, pp. 213–232. ISSN: 0022-2720, 1365-2818. DOI: 10.1111/j.1365-2818.2006.01706.x. URL: https://onlinelibrary.wiley.com/doi/10.1111/j.1365-2818.2006.01706.x (visited on 09/24/2024).

Bouché, Nicolas et al. (May 27, 2003). "Mitochondrial succinic-semialdehyde dehydrogenase of the γ-aminobutyrate shunt is required to restrict levels of reactive oxygen intermediates in plants". In: *Proceedings of the National Academy of Sciences* 100.11. Publisher: Proceedings of the National Academy of Sciences, pp. 6843–6848. DOI: 10.1073/pnas.1037532100. URL: https://www.pnas.org/doi/10.1073/pnas.1037532100 (visited on 09/12/2024).

Büschges, Rainer et al. (1997). "The Barley Mlo Gene: A Novel Control Element of Plant Pathogen Resistance". In: *Cell* 88.5, pp. 695–705. DOI: 10.1016/s0092-8674(00)81912-1. URL: http://dx.doi.org/10.1016/s0092-8674(00)81912-1.

Campe, Ruth et al. (Jan. 2016). "¡span style="font-variant:small-caps;"¿ABC¡/span¿ transporter ¡span style="font-variant:small-caps;"¿PEN¡/span¿ 3/ ¡span style="font-variant:small-caps;"¿PDR¡/span¿ 8/ ¡span style="font-variant:small-caps;"¿ABCG¡/span¿ 36 interacts with calmodulin that, like ¡span style="font-variant:small-caps;"¿PEN¡/span¿ 3, is required for Arabidopsis nonhost resistance". In: *New Phytologist* 209.1, pp. 294–306. ISSN: 0028-646X, 1469-8137. DOI: 10.1111/nph.13582. URL: https://nph.onlinelibrary.wiley.com/doi/10.1111/nph.13582 (visited on 09/24/2024).

Chen, Huamin et al. (Feb. 4, 2008). "Firefly Luciferase Complementation Imaging Assay for Protein-Protein Interactions in Plants". In: *Plant Physiology* 146.2, pp. 323–324. ISSN: 1532-2548. DOI: 10.1104/pp.107.111740. URL: https://academic.oup.com/plphys/article/146/2/323/6107098 (visited on 08/07/2024).

Chen, Zhongying et al. (2009). "Two Seven-Transmembrane Domain MILDEW RESISTANCE LOCUS O Proteins Cofunction inArabidopsisRoot Thigmomorphogenesis". In: *The Plant Cell* 21.7, pp. 1972–1991. DOI: 10.1105/tpc.108.062653. URL: http://dx.doi.org/10.1105/tpc.108.062653.

Clough, S. J. et al. (Dec. 1998). "Floral dip: a simplified method for Agrobacterium-mediated transformation of Arabidopsis thaliana". In: *The Plant Journal: For Cell and Molecular Biology* 16.6. Number: 6, pp. 735–743. ISSN: 0960-7412. DOI: 10.1046/j.1365-313x.1998.00343.x.

Consonni, Chiara et al. (June 2006). "Conserved requirement for a plant host cell protein in powdery mildew pathogenesis". In: *Nat. Genet.* 38.6, pp. 716–720. ISSN: 1061-4036. DOI: 10.1038/ng1806. URL: http://dx.doi.org/10.1038/ng1806.

Consonni, Chiara et al. (2010). "Tryptophan-Derived Metabolites Are Required for Antifungal Defense in the Arabidopsis mlo2 Mutant". In: *Plant Physiology* 152.3, pp. 1544–1561. DOI: 10.1104/pp.109.147660. URL: http://dx.doi.org/10.1104/pp.109.147660.

Cui, Fuqiang et al. (2018). "Arabidopsis MLO2 is a negative regulator of sensitivity to extracellular reactive oxygen species". In: *Plant Cell and Environment* 41.4. Number: 4, pp. 782–796. ISSN: 13653040. DOI: 10.1111/pce.13144.

Cui, Weier et al. (Apr. 2016). "Arabidopsis callose synthases CalS1/8 regulate plasmodesmal permeability during stress". In: *Nature Plants* 2.5, p. 16034. ISSN: 2055-0278. DOI: 10.1038/nplants.2016.34. URL: https://www.nature.com/articles/nplants201634 (visited on 12/31/2023).

Cvrčková, Fatima et al. (July 2012). "Evolution of the land plant exocyst complexes". In: *Front. Plant Sci.* 3, p. 159. ISSN: 1664-462X. DOI: 10.3389/fpls.2012.00159. URL: http://dx.doi.org/10.3389/fpls.2012.00159.

Daly, Craig J. et al. (2012). "Visualization and Analysis of Vascular Receptors Using Confocal Laser Scanning Microscopy and Fluorescent Ligands". In: *Receptor Binding Techniques*. Ed. by Anthony P. Davenport. Vol. 897. Series Title: Methods in Molecular Biology. Totowa, NJ: Humana Press, pp. 95–107. ISBN: 978-1-61779-908-2 978-1-61779-909-9. DOI: 10.1007/978-1-61779-909-9_5. URL: https://link.springer.com/10.1007/978-1-61779-909-9_5 (visited on 09/24/2024).

Devoto, A et al. (Dec. 1999). "Topology, subcellular localization, and sequence diversity of the Mlo family in plants". In: *J. Biol. Chem.* 274.49, pp. 34993–35004. ISSN: 0021-9258. DOI: 10.1074/jbc.274.49.34993. URL: http://dx.doi.org/10.1074/jbc.274.49.34993.

Dijk, Aalt Dirk Jan van et al. (Dec. 5, 2020). "Machine learning in plant science and plant breeding". In: *iScience* 24.1, p. 101890. ISSN: 2589-0042. DOI: 10.1016/j.isci.2020.101890. URL: https://www.ncbi.nlm.nih.gov/pmc/articles/PMC7750553/ (visited on 08/13/2024).

Donnelly, F. C. et al. (June 16, 2017). "Synthesis of CaCO3 nano- and micro-particles by dry ice carbonation". In: *Chemical Communications* 53.49. Publisher: The Royal Society of Chemistry, pp. 6657–6660. ISSN: 1364-548X. DOI: 10.1039/C7CC01420A. URL: https://pubs.rsc.org/en/content/articlelanding/2017/cc/c7cc01420a (visited on 06/26/2024).

Drdová, Edita Janková et al. (2013). "The exocyst complex contributes to PIN auxin efflux carrier recycling and polar auxin transport in Arabidopsis". In: *The Plant Journal* 73.5, pp. 709–719. ISSN: 1365-313X. DOI: 10.1111/tpj.12074. URL: https://onlinelibrary.wiley.com/doi/abs/10.1111/tpj.12074 (visited on 11/24/2023).

Dumanović, Jelena et al. (Jan. 6, 2021). "The Significance of Reactive Oxygen Species and Antioxidant Defense System in Plants: A Concise Overview". In: *Frontiers in Plant Science* 11. Publisher: Frontiers. ISSN: 1664-462X. DOI: 10.3389/fpls.2020.552969. URL: https://www.frontiersin.org/journals/plant-science/articles/10.3389/fpls.2020.552969/full (visited on 09/12/2024).

Ejaz, Ujala et al. (May 12, 2023). "Detoxifying the heavy metals: a multipronged study of tolerance strategies against heavy metals toxicity in plants". In: *Frontiers in Plant Science* 14. Publisher: Frontiers. ISSN: 1664-462X. DOI: 10.3389/fpls.2023.1154571. URL: https://www.frontiersin.org/journals/plant-science/articles/10.3389/fpls.2023.1154571/full (visited on 09/13/2024).

Elias, M et al. (2003). "The exocyst complex in plants". In: *Cell Biol. Int.* 27.3, pp. 199–201. ISSN: 1065-6995. DOI: 10.1016/s1065-6995(02)00349-9. URL: http://dx.doi.org/10.1016/s1065-6995(02)00349-9.

ELLIOTT, Candace et al. (Dec. 2004). "Conserved extracellular cysteine residues and cytoplasmic loop–loop interplay are required for functionality of the heptahelical MLO protein". In: *Biochemical Journal* 385.1, pp. 243–254. ISSN: 0264-6021. DOI: 10.1042/BJ20040993. URL: https://doi.org/10.1042/BJ20040993 (visited on 11/24/2023).

Engler, Carola et al. (Nov. 5, 2008). "A One Pot, One Step, Precision Cloning Method with High Throughput Capability". In: *PLoS ONE* 3.11. Ed. by Hany A. El-Shemy, e3647. ISSN: 1932-6203. DOI: 10.1371/journal.pone.0003647. URL: https://dx.plos.org/10.1371/journal.pone.0003647 (visited on 09/24/2024).

Enns, Linda C. et al. (June 2005). "Two callose synthases, GSL1 and GSL5, play an essential and redundant role in plant and pollen development and in fertility". In: *Plant Molecular Biology* 58.3, pp. 333–349. ISSN: 0167-4412, 1573-5028. DOI: 10.1007/s11103-005-4526-7. URL: http://link.springer.com/10.1007/s11103-005-4526-7 (visited on 12/31/2023).

Ensikat, Hans-Jürgen et al. (Nov. 19, 2021). "Distribution of Biominerals and Mineral-Organic Composites in Plant Trichomes". In: *Frontiers in Bioengineering and Biotechnology* 9. Publisher: Frontiers. ISSN: 2296-4185. DOI: 10.3389/fbioe.2021.763690. URL: https://www.frontiersin.org/journals/bioengineering-and-biotechnology/articles/10.3389/fbioe.2021.763690/full (visited on 07/15/2024).

Fendrych, Matyáš et al. (Sept. 2010). "The Arabidopsis Exocyst Complex Is Involved in Cytokinesis and Cell Plate Maturation". In: *The Plant Cell* 22.9. Number: 9, pp. 3053–3065. ISSN: 1040-4651. DOI: 10.1105/tpc.110.074351. URL: https://www.ncbi.nlm.nih.gov/pmc/articles/PMC2965533/ (visited on 08/22/2022).

Folkers, U et al. (Oct. 1997). "Cell morphogenesis of trichomes in Arabidopsis: differential control of primary and secondary branching by branch initiation regulators and cell growth". In: *Development* 124.19, pp. 3779–3786. ISSN: 0950-1991. DOI: 10.1242/dev.124.19.3779. URL: http://dx.doi.org/10.1242/dev.124.19.3779.

Fujita, Satoshi et al. (May 4, 2020). "SCHENGEN receptor module drives localized ROS production and lignification in plant roots". In: *The EMBO Journal* 39.9. Publisher: John Wiley & Sons, Ltd, e103894. ISSN: 0261-4189. DOI: 10.15252/embj.2019103894. URL: https://www.embopress.org/doi/full/10.15252/embj.2019103894 (visited on 09/12/2024).

Gao, Qifei et al. (July 2022). "A receptor–channel trio conducts Ca2+ signalling for pollen tube reception". In: *Nature* 607.7919, pp. 534–539. ISSN: 1476-4687. DOI: 10.1038/s41586-022-04923-7. URL: https://www.nature.com/articles/s41586-022-04923-7 (visited on 11/24/2023).

Gastwirth, Joseph L. et al. (Aug. 1, 2009). "The Impact of Levene's Test of Equality of Variances on Statistical Theory and Practice". In: *Statistical Science* 24.3. ISSN: 0883-4237. DOI: 10.1214/09-STS301. URL: https://projecteuclid.org/journals/statistical-science/volume-24/issue-3/The-Impact-of-Levenes-Test-of-Equality-of-Variances-on/10.1214/09-STS301.full (visited on 09/24/2024).

German, Liam et al. (Feb. 2023). "Callose metabolism and the regulation of cell walls and plasmodesmata during plant mutualistic and pathogenic interactions". In: *Plant, Cell & Environment* 46.2, pp. 391–404. ISSN: 0140-7791, 1365-3040. DOI: 10.1111/pce.14510. URL: https://onlinelibrary.wiley.com/doi/10.1111/pce.14510 (visited on 10/21/2024).

Gierlinger, Notburga (Aug. 9, 2018). "New insights into plant cell walls by vibrational microspectroscopy". In: *Applied Spectroscopy Reviews* 53.7. Publisher: Taylor & Francis _eprint: https://doi.org/10.1080/05704928.2017.1363052, pp. 517–551. ISSN: 0570-4928. DOI: 10.1080/05704928.2017.1363052. URL: https://doi.org/10.1080/05704928.2017.1363052 (visited on 02/08/2024).

Gill, Taqdeer et al. (June 1, 2022). "A Comprehensive Review of High Throughput Phenotyping and Machine Learning for Plant Stress Phenotyping". In: *Phenomics* 2.3, pp. 156–183. ISSN: 2730-5848. DOI: 10.1007/s43657-022-00048-z. URL: https://doi.org/10.1007/s43657-022-00048-z (visited on 08/13/2024).

Gilroy, S. et al. (June 1, 1987). "Calcium: a regulation system emerges in plant cells". In: *Development* 100.2, pp. 181–184. ISSN: 0950-1991. DOI: 10.1242/dev.100.2.181. URL: https://doi.org/10.1242/dev.100.2.181 (visited on 09/16/2024).

Grobei, Monica A. et al. (Oct. 2009). "Deterministic protein inference for shotgun proteomics data provides new insights into Arabidopsis pollen development and function". In: *Genome Research* 19.10, pp. 1786–1800. ISSN: 1088-9051, 1549-5469. DOI: 10.1101/gr.089060.108. URL: https://genome.cshlp.org/content/19/10/1786 (visited on 01/02/2024).

Gruner, Katrin et al. (2018). "A critical role for Arabidopsis MILDEW RESISTANCE LOCUS O2 in systemic acquired resistance". In: *Plant Journal* 94.6. Number: 6, pp. 1064–1082. ISSN: 1365313X. DOI: 10.1111/tpj.13920.

Guo, Chao et al. (Mar. 2022). "Mechanosensation triggers enhanced heavy metal ion uptake by non-glandular trichomes". In: *Journal of Hazardous Materials* 426, p. 127983. ISSN: 0304-3894. DOI: 10.1016/j.jhazmat.2021.127983. URL: https://www.sciencedirect.com/science/article/pii/S0304389421029526 (visited on 11/24/2023).

Guseman, Jessica M. et al. (May 2010). "Dysregulation of cell-to-cell connectivity and stomatal patterning by loss-of-function mutation in *Arabidopsis* CHORUS (*GLUCAN* SYNTHASE-LIKE 8)". In: *Development* 137.10, pp. 1731–1741. ISSN: 1477-9129, 0950-1991. DOI: 10.1242/dev.049197. URL: https://journals.

biologists.com/dev/article/137/10/1731/53169/Dysregulation-of-cell-to-cell-connectivity-and (visited on 01/02/2024).

Han, Xiao et al. (Jan. 2014). "Auxin-Callose-Mediated Plasmodesmal Gating Is Essential for Tropic Auxin Gradient Formation and Signaling". In: *Developmental Cell* 28.2, pp. 132–146. ISSN: 15345807. DOI: 10.1016/j.devcel.2013.12.008. URL: https://linkinghub.elsevier.com/retrieve/pii/S1534580713007351 (visited on 01/02/2024).

He, Bing et al. (Sept. 2007). "Exo70 interacts with phospholipids and mediates the targeting of the exocyst to the plasma membrane". In: *The EMBO Journal* 26.18, pp. 4053–4065. ISSN: 0261-4189. DOI: 10.1038/sj.emboj.7601834. URL: https://www.embopress.org/doi/full/10.1038/sj.emboj.7601834 (visited on 11/25/2023).

Heider, Margaret R et al. (July 2012). "Exorcising the exocyst complex". In: *Traffic* 13.7, pp. 898–907. ISSN: 1398-9219. DOI: 10.1111/j.1600-0854.2012.01353.x. URL: http://dx.doi.org/10.1111/j.1600-0854.2012.01353.x.

Hong, Z. et al. (Apr. 2001). "A novel UDP-glucose transferase is part of the callose synthase complex and interacts with phragmoplastin at the forming cell plate". In: *The Plant Cell* 13.4, pp. 769–779. ISSN: 1040-4651. DOI: 10.1105/tpc.13.4.769.

Hong, Zonglie et al. (Apr. 2001). "A Cell Plate–Specific Callose Synthase and Its Interaction with Phragmoplastin". In: *The Plant Cell* 13.4, pp. 755–768. ISSN: 1532-298X. DOI: 10.1105/tpc.13.4.755. URL: https://academic.oup.com/plcell/article/13/4/755/6009518 (visited on 01/02/2024).

Huang, Honglin et al. (June 25, 2019). "Mechanisms of ROS Regulation of Plant Development and Stress Responses". In: *Frontiers in Plant Science* 10. Publisher: Frontiers. ISSN: 1664-462X. DOI: 10.3389/fpls.2019.00800. URL: https://www.frontiersin.org/journals/plant-science/articles/10.3389/fpls.2019.00800/full (visited on 09/12/2024).

Huang, Jing et al. (Jan. 2017). "CHARMM36m: an improved force field for folded and intrinsically disordered proteins". In: *Nature Methods* 14.1. Publisher: Nature

Publishing Group, pp. 71–73. ISSN: 1548-7105. DOI: 10.1038/nmeth.4067. URL: https://www.nature.com/articles/nmeth.4067 (visited on 10/10/2024).

Huebbers, Jan W. et al. (Dec. 2022). "An advanced method for the release, enrichment and purification of high-quality Arabidopsis thaliana rosette leaf trichomes enables profound insights into the trichome proteome". In: *Plant Methods* 18.1, p. 12. ISSN: 1746-4811. DOI: 10.1186/s13007-021-00836-0. URL: https://plantmethods.biomedcentral.com/articles/10.1186/s13007-021-00836-0 (visited on 09/13/2024).

Hülskamp, M et al. (Feb. 1994). "Genetic dissection of trichome cell development in Arabidopsis". In: *Cell* 76.3, pp. 555–566. ISSN: 0092-8674. DOI: 10.1016/0092-8674(94)90118-x. URL: http://dx.doi.org/10.1016/0092-8674(94)90118-x.

Jacobs, Andrew K. et al. (Nov. 2003). "An Arabidopsis Callose Synthase, GSL5, Is Required for Wound and Papillary Callose Formation". In: *The Plant Cell* 15.11, pp. 2503–2513. ISSN: 1040-4651. DOI: 10.1105/tpc.016097. URL: https://doi.org/10.1105/tpc.016097 (visited on 11/24/2023).

Jakoby, Marc J et al. (Nov. 2008). "Transcriptional profiling of mature Arabidopsis trichomes reveals that NOECK encodes the MIXTA-like transcriptional regulator MYB106". In: *Plant Physiol.* 148.3, pp. 1583–1602. ISSN: 0032-0889. DOI: 10.1104/pp.108.126979. URL: http://dx.doi.org/10.1104/pp.108.126979.

Jørgensen, I Helms (Jan. 1992). "Discovery, characterization and exploitation of Mlo powdery mildew resistance in barley". In: *Euphytica* 63.1, pp. 141–152. ISSN: 0014-2336. DOI: 10.1007/BF00023919. URL: https://doi.org/10.1007/BF00023919.

Ju, Yan et al. (Nov. 2021). "Polarized NORTIA accumulation in response to pollen tube arrival at synergids promotes fertilization". In: *Dev. Cell* 56.21, 2938–2951.e6. ISSN: 1534-5807. DOI: 10.1016/j.devcel.2021.09.026. URL: http://dx.doi.org/10.1016/j.devcel.2021.09.026.

Jumper, John et al. (Aug. 2021). "Highly accurate protein structure prediction with AlphaFold". In: *Nature* 596.7873. Publisher: Nature Publishing Group, pp. 583–

589. ISSN: 1476-4687. DOI: 10.1038/s41586-021-03819-2. URL: https://www.nature.com/articles/s41586-021-03819-2 (visited on 08/13/2024).

Kalmbach, Lothar et al. (Apr. 2017). "Transient cell-specific EXO70A1 activity in the CASP domain and Casparian strip localization". In: *Nature Plants* 3.5, pp. 1–9. ISSN: 2055-0278. DOI: 10.1038/nplants.2017.58. URL: https://www.nature.com/articles/nplants201758 (visited on 11/25/2023).

Karimi, Mansour et al. (Mar. 2005). "Modular cloning in plant cells". In: *Trends in Plant Science* 10.3, pp. 103–105. ISSN: 13601385. DOI: 10.1016/j.tplants.2005.01.008. URL: https://linkinghub.elsevier.com/retrieve/pii/S1360138505000245 (visited on 11/06/2024).

Kaur, Jasleen et al. (2020). "Role of Trichomes in Plant Stress Biology". In: *Evolutionary Ecology of Plant-Herbivore Interaction*. Ed. by Juan Núñez-Farfán et al. Cham: Springer International Publishing, pp. 15–35. ISBN: 978-3-030-46012-9. DOI: 10.1007/978-3-030-46012-9_2. URL: https://doi.org/10.1007/978-3-030-46012-9_2 (visited on 11/24/2023).

Kauss, H. et al. (1990). "Ca2+ as a Signal in the Induction of Callose Synthesis". In: *Signal Perception and Transduction in Higher Plants*. Ed. by Raoul Ranjeva et al. Berlin, Heidelberg: Springer Berlin Heidelberg, pp. 117–131. ISBN: 978-3-642-83974-0.

Kauss, Heinrich (Jan. 1985). "Callose biosynthesis as a ca2+-regulated process and possible relations to the induction of other metabolic changes". In: *Journal of Cell Science* 1985 (Supplement_2), pp. 89–103. ISSN: 0021-9533. DOI: 10.1242/jcs.1985.Supplement_2.5. URL: https://doi.org/10.1242/jcs.1985.Supplement_2.5 (visited on 12/31/2023).

Kessler, Sharon A et al. (Nov. 2010). "Conserved molecular components for pollen tube reception and fungal invasion". In: *Science* 330.6006, pp. 968–971. ISSN: 0036-8075. DOI: 10.1126/science.1195211. URL: http://dx.doi.org/10.1126/science.1195211.

Kim, Dae In et al. (2016). "An improved smaller biotin ligase for BioID proximity labeling". In: *Molecular Biology of the Cell* 27.8. Number: 8, pp. 1188–1196. ISSN: 19394586. DOI: 10.1091/mbc.E15-12-0844.

Kim, Min C et al. (Mar. 2002). "Calmodulin interacts with MLO protein to regulate defence against mildew in barley". In: *Nature* 416.6879, pp. 447–451. ISSN: 0028-0836. DOI: 10.1038/416447a. URL: http://dx.doi.org/10.1038/416447a.

Koncz, Csaba et al. (Sept. 1986). "The promoter of TL-DNA gene 5 controls the tissue-specific expression of chimaeric genes carried by a novel type of Agrobacterium binary vector". In: *Molecular and General Genetics MGG* 204.3, pp. 383–396. ISSN: 0026-8925, 1432-1874. DOI: 10.1007/BF00331014. URL: http://link.springer.com/10.1007/BF00331014 (visited on 09/24/2024).

Kubátová, Zdeňka et al. (2019a). "Arabidopsis Trichome Contains Two Plasma Membrane Domains with Different Lipid Compositions Which Attract Distinct EXO70 Subunits". In: *International Journal of Molecular Sciences* 20.15, p. 3803. DOI: 10.3390/ijms20153803. URL: http://dx.doi.org/10.3390/ijms20153803.

Kubátová, Zdeňka et al. (2019b). "Arabidopsis trichome contains two plasma membrane domains with different lipid compositions which attract distinct EXO70 subunits". In: *International journal of molecular sciences* 20.15. Publisher: MDPI, p. 3803.

Kulich, Ivan et al. (2010). "Arabidopsis exocyst subunits SEC8 and EXO70A1 and exocyst interactor ROH1 are involved in the localized deposition of seed coat pectin". In: *New Phytologist* 188.2, pp. 615–625. ISSN: 1469-8137. DOI: 10.1111/j.1469-8137.2010.03372.x. URL: https://onlinelibrary.wiley.com/doi/abs/10.1111/j.1469-8137.2010.03372.x (visited on 11/23/2023).

Kulich, Ivan et al. (Nov. 2013). "Arabidopsis Exocyst Subcomplex Containing Subunit ¡span style="font-variant:small-caps;"¿EXO70B1¡/span¿ Is Involved in Autophagy-Related Transport to the Vacuole". In: *Traffic* 14.11, pp. 1155–1165. ISSN: 1398-9219, 1600-0854. DOI: 10.1111/tra.12101. URL: https://onlinelibrary.wiley.com/doi/10.1111/tra.12101 (visited on 11/05/2024).

Kulich, Ivan et al. (May 2015). "Cell wall maturation of Arabidopsis trichomes is dependent on exocyst subunit EXO70H4 and involves callose deposition". In: *Plant Physiol.* 168.1, pp. 120–131. ISSN: 0032-0889. DOI: 10.1104/pp.15.00112. URL: http://dx.doi.org/10.1104/pp.15.00112.

Kulich, Ivan et al. (2018). "Exocyst subunit EXO70H4 has a specific role in callose synthase secretion and silica accumulation". In: *Plant physiology* 176.3. Publisher: American Society of Plant Biologists, pp. 2040–2051.

Kusch, Stefan et al. (Mar. 2016). "Comprehensive Phylogenetic Analysis Sheds Light on the Diversity and Origin of the MLO Family of Integral Membrane Proteins". In: *Genome Biol. Evol.* 8.3, pp. 878–895. ISSN: 1759-6653. DOI: 10.1093/gbe/evw036. URL: http://dx.doi.org/10.1093/gbe/evw036.

Lai, Zhibing et al. (June 2011). "A critical role of autophagy in plant resistance to necrotrophic fungal pathogens". In: *The Plant Journal* 66.6, pp. 953–968. ISSN: 0960-7412, 1365-313X. DOI: 10.1111/j.1365-313X.2011.04553.x. URL: https://onlinelibrary.wiley.com/doi/10.1111/j.1365-313X.2011.04553.x (visited on 11/05/2024).

Lalonde, Sylvie et al. (2008). "Molecular and cellular approaches for the detection of protein–protein interactions: latest techniques and current limitations". In: *The Plant Journal* 53.4. _eprint: https://onlinelibrary.wiley.com/doi/pdf/10.1111/j.1365-313X.2007.03332.x, pp. 610–635. ISSN: 1365-313X. DOI: 10.1111/j.1365-313X.2007.03332.x. URL: https://onlinelibrary.wiley.com/doi/abs/10.1111/j.1365-313X.2007.03332.x (visited on 08/07/2024).

Larkin, John C. et al. (1993). "Arabidopsis GLABROUS1 Gene Requires Downstream Sequences for Function". In: *The Plant Cell* 5.12, pp. 1739–1748. ISSN: 1040-4651. DOI: 10.2307/3869690. URL: https://www.jstor.org/stable/3869690 (visited on 10/31/2023).

Larson, Emily R. et al. (Sept. 2020). "Synergy among Exocyst and SNARE Interactions Identifies a Functional Hierarchy in Secretion during Vegetative Growth". In: *The Plant Cell* 32.9, pp. 2951–2963. ISSN: 1040-4651, 1532-298X. DOI: 10.1105/tpc.

20.00280. URL: https://academic.oup.com/plcell/article/32/9/2951-2963/6115749 (visited on 10/21/2024).

LeCun, Yann et al. (May 2015). "Deep learning". In: *Nature* 521.7553. Publisher: Nature Publishing Group, pp. 436–444. ISSN: 1476-4687. DOI: 10.1038/nature14539. URL: https://www.nature.com/articles/nature14539 (visited on 08/13/2024).

Lei, Yang et al. (Sept. 2014). "CRISPR-P: A Web Tool for Synthetic Single-Guide RNA Design of CRISPR-System in Plants". In: *Molecular Plant* 7.9, pp. 1494–1496. ISSN: 16742052. DOI: 10.1093/mp/ssu044. URL: https://linkinghub.elsevier.com/retrieve/pii/S1674205214609527 (visited on 06/13/2023).

Li, Ting et al. (Oct. 12, 2023). "Expression in A. thaliana and cellular localization reveal involvement of BjNRAMP1 in cadmium uptake". In: *Frontiers in Plant Science* 14. Publisher: Frontiers. ISSN: 1664-462X. DOI: 10.3389/fpls.2023.1261518. URL: https://www.frontiersin.org/journals/plant-science/articles/10.3389/fpls.2023.1261518/full (visited on 09/13/2024).

Li, Xiaohui et al. (2023). "The EXO70 inhibitor Endosidin2 alters plasma membrane protein composition in Arabidopsis roots". In: *Frontiers in Plant Science* 14. ISSN: 1664-462X. URL: https://www.frontiersin.org/articles/10.3389/fpls.2023.1171957 (visited on 11/25/2023).

Liu, Jianglan et al. (Nov. 2007). "Phosphatidylinositol 4,5-Bisphosphate Mediates the Targeting of the Exocyst to the Plasma Membrane for Exocytosis in Mammalian Cells". In: *Molecular Biology of the Cell* 18.11, pp. 4483–4492. ISSN: 1059-1524. DOI: 10.1091/mbc.e07-05-0461. URL: https://www.molbiolcell.org/doi/full/10.1091/mbc.e07-05-0461 (visited on 11/25/2023).

Lomize, Mikhail A. et al. (Jan. 1, 2012). "OPM database and PPM web server: resources for positioning of proteins in membranes". In: *Nucleic Acids Research* 40 (D1), pp. D370–D376. ISSN: 0305-1048. DOI: 10.1093/nar/gkr703. URL: https://doi.org/10.1093/nar/gkr703 (visited on 10/10/2024).

Mair, Andrea et al. (Feb. 4, 2022). "Advances in enzyme-mediated proximity labeling and its potential for plant research". In: *Plant Physiology* 188.2. Number: 2 Pub-

lisher: Oxford Academic, pp. 756–768. ISSN: 0032-0889. DOI: 10.1093/PLPHYS/KIAB479. URL: https://academic.oup.com/plphys/article/188/2/756/6400265 (visited on 02/04/2022).

Mann, Daniel et al. (Dec. 6, 2023). "Atg18 oligomer organization in assembled tubes and on lipid membrane scaffolds". In: *Nature Communications* 14.1, p. 8086. ISSN: 2041-1723. DOI: 10.1038/s41467-023-43460-3. URL: https://www.nature.com/articles/s41467-023-43460-3 (visited on 11/05/2024).

Mann, H. B. et al. (Mar. 1947). "On a Test of Whether one of Two Random Variables is Stochastically Larger than the Other". In: *The Annals of Mathematical Statistics* 18.1, pp. 50–60. ISSN: 0003-4851. DOI: 10.1214/aoms/1177730491. URL: http://projecteuclid.org/euclid.aoms/1177730491 (visited on 09/24/2024).

Mao, Hailiang et al. (Dec. 2016). "A Framework for Lateral Membrane Trafficking and Polar Tethering of the PEN3 ATP-Binding Cassette Transporter". In: *Plant Physiology* 172.4, pp. 2245–2260. ISSN: 0032-0889. DOI: 10.1104/pp.16.01252. URL: https://doi.org/10.1104/pp.16.01252 (visited on 11/24/2023).

Martin, Kirsty J. et al. (Jan. 2018). "Accepting from the best donor; analysis of long-lifetime donor fluorescent protein pairings to optimise dynamic FLIM-based FRET experiments". In: *PLOS ONE* 13.1, e0183585. ISSN: 1932-6203. DOI: 10.1371/journal.pone.0183585. URL: https://journals.plos.org/plosone/article?id=10.1371/journal.pone.0183585 (visited on 06/19/2023).

Matsumura, Mamoru et al. (2022). "Mechanosensory trichome cells evoke a mechanical stimuli–induced immune response in Arabidopsis thaliana". In: *Nature communications* 13.1. Publisher: Nature Publishing Group UK London, p. 1216.

Meng, Jiang-Guo et al. (2020). "Integration of ovular signals and exocytosis of a Ca2 channel by MLOs in pollen tube guidance". In: *Nature Plants* 6.2, pp. 143–153. DOI: 10.1038/s41477-020-0599-1. URL: http://dx.doi.org/10.1038/s41477-020-0599-1.

Meng, Jiang-guo et al. (2020). "Ca 2 + channel by MLOs in pollen tube guidance". In: *Nature Plants* 15. Publisher: Springer US. ISSN: 2055-0278. DOI: 10.1038/s41477-020-0599-1. URL: http://dx.doi.org/10.1038/s41477-020-0599-1.

Mhamdi, Amna et al. (Aug. 9, 2018). "Reactive oxygen species in plant development". In: *Development* 145.15, dev164376. ISSN: 0950-1991. DOI: 10.1242/dev.164376. URL: https://doi.org/10.1242/dev.164376 (visited on 09/12/2024).

Mittler, Ron et al. (Oct. 2022). "Reactive oxygen species signalling in plant stress responses". In: *Nature Reviews Molecular Cell Biology* 23.10. Publisher: Nature Publishing Group, pp. 663–679. ISSN: 1471-0080. DOI: 10.1038/s41580-022-00499-2. URL: https://www.nature.com/articles/s41580-022-00499-2 (visited on 09/12/2024).

Mohnen, Debra (June 2008). "Pectin structure and biosynthesis". In: *Current Opinion in Plant Biology* 11.3, pp. 266–277. ISSN: 1369-5266. DOI: 10.1016/j.pbi.2008.03.006.

Nedukha, O. M. (Jan. 2015). "Callose: Localization, functions, and synthesis in plant cells". In: *Cytology and Genetics* 49.1, pp. 49–57. ISSN: 1934-9440. DOI: 10.3103/S0095452715010090. URL: https://doi.org/10.3103/S0095452715010090 (visited on 12/31/2023).

Nishimura, Marc T et al. (Aug. 2003). "Loss of a callose synthase results in salicylic acid-dependent disease resistance". In: *Science* 301.5635, pp. 969–972. ISSN: 0036-8075. DOI: 10.1126/science.1086716. URL: http://dx.doi.org/10.1126/science.1086716.

O'Brien, Jose A. et al. (Sept. 1, 2012). "Reactive oxygen species and their role in plant defence and cell wall metabolism". In: *Planta* 236.3, pp. 765–779. ISSN: 1432-2048. DOI: 10.1007/s00425-012-1696-9. URL: https://doi.org/10.1007/s00425-012-1696-9 (visited on 09/12/2024).

Ortmannová, Jitka et al. (Jan. 2022). "Arabidopsis EXO70B2 exocyst subunit contributes to papillae and encasement formation in antifungal defence". In: *Journal of Experimental Botany* 73.3. Ed. by Jacqueline Monaghan, pp. 742–755. ISSN: 0022-

0957, 1460-2431. DOI: 10.1093/jxb/erab457. URL: https://academic.oup.com/jxb/article/73/3/742/6402053 (visited on 11/24/2023).

Pantazopoulou, Chrysoula K. et al. (Sept. 2023). "Mechanodetection of neighbor plants elicits adaptive leaf movements through calcium dynamics". In: *Nature Communications* 14.1, p. 5827. ISSN: 2041-1723. DOI: 10.1038/s41467-023-41530-0. URL: https://www.nature.com/articles/s41467-023-41530-0 (visited on 11/24/2023).

Pattanaik, Sitakanta et al. (2014). "An overview of the gene regulatory network controlling trichome development in the model plant, Arabidopsis". In: *Frontiers in Plant Science* 5. ISSN: 1664-462X. URL: https://www.frontiersin.org/articles/10.3389/fpls.2014.00259 (visited on 11/24/2023).

Pearson, Karl (July 1900). "X. *On the criterion that a given system of deviations from the probable in the case of a correlated system of variables is such that it can be reasonably supposed to have arisen from random sampling*". In: *The London, Edinburgh, and Dublin Philosophical Magazine and Journal of Science* 50.302, pp. 157–175. ISSN: 1941-5982, 1941-5990. DOI: 10.1080/14786440009463897. URL: https://www.tandfonline.com/doi/full/10.1080/14786440009463897 (visited on 09/24/2024).

Pečenková, Tamara et al. (Mar. 2011). "The role for the exocyst complex subunits Exo70B2 and Exo70H1 in the plant–pathogen interaction". In: *Journal of Experimental Botany* 62.6, pp. 2107–2116. ISSN: 1460-2431, 0022-0957. DOI: 10.1093/jxb/erq402. URL: https://academic.oup.com/jxb/article-lookup/doi/10.1093/jxb/erq402 (visited on 11/05/2024).

Pečenková, Tamara et al. (June 26, 2020). "Redundant and Diversified Roles Among Selected Arabidopsis thaliana EXO70 Paralogs During Biotic Stress Responses". In: *Frontiers in Plant Science* 11, p. 960. ISSN: 1664-462X. DOI: 10.3389/fpls.2020.00960. URL: https://www.frontiersin.org/article/10.3389/fpls.2020.00960/full (visited on 11/05/2024).

Peiffer, Michelle et al. (2009). "Plants on early alert: glandular trichomes as sensors for insect herbivores". In: *New Phytologist* 184.3, pp. 644–656. ISSN: 1469-8137. DOI: 10.1111/j.1469-8137.2009.03002.x. URL: https://onlinelibrary.wiley.com/doi/abs/10.1111/j.1469-8137.2009.03002.x (visited on 11/24/2023).

Persson, Staffan et al. (Sept. 30, 2024). *Pupylation-based proximity labelling reveals regulatory factors in cellulose biosynthesis in Arabidopsis*. ISSN: 2693-5015. DOI: 10.21203/rs.3.rs-3849556/v1. URL: https://www.researchsquare.com/article/rs-3849556/v1 (visited on 10/31/2024).

Piffanelli, Pietro et al. (July 2002). "The barley MLO modulator of defense and cell death is responsive to biotic and abiotic stress stimuli". In: *Plant Physiol.* 129.3, pp. 1076–1085. ISSN: 0032-0889. DOI: 10.1104/pp.010954. URL: http://dx.doi.org/10.1104/pp.010954.

Podgórska, Anna et al. (Aug. 22, 2017). "Extra-Cellular But Extra-Ordinarily Important for Cells: Apoplastic Reactive Oxygen Species Metabolism". In: *Frontiers in Plant Science* 8. Publisher: Frontiers. ISSN: 1664-462X. DOI: 10.3389/fpls.2017.01353. URL: https://www.frontiersin.org/journals/plant-science/articles/10.3389/fpls.2017.01353/full (visited on 10/24/2024).

Putta, Priya et al. (Nov. 2016). "Phosphatidic acid binding proteins display differential binding as a function of membrane curvature stress and chemical properties". In: *Biochimica et Biophysica Acta (BBA) - Biomembranes* 1858.11, pp. 2709–2716. ISSN: 00052736. DOI: 10.1016/j.bbamem.2016.07.014. URL: https://linkinghub.elsevier.com/retrieve/pii/S000527361630267X (visited on 10/22/2024).

Qadota, Hiroshi et al. (Apr. 1996). "Identification of Yeast Rho1p GTPase as a Regulatory Subunit of 1,3-β-Glucan Synthase". In: *Science* 272.5259, pp. 279–281. ISSN: 0036-8075, 1095-9203. DOI: 10.1126/science.272.5259.279. URL: https://www.science.org/doi/10.1126/science.272.5259.279 (visited on 01/02/2024).

Richmond, Todd A. et al. (Oct. 2000). "The Cellulose Synthase Superfamily". In: *Plant Physiology* 124.2, pp. 495–498. ISSN: 1532-2548, 0032-0889. DOI: 10.1104/pp.124.

2.495. URL: https://academic.oup.com/plphys/article/124/2/495/6098861 (visited on 01/02/2024).

Rieter, Ester et al. (Jan. 15, 2013). "Atg18 function in autophagy is regulated by specific sites within its β-propeller". In: *Journal of Cell Science* 126.2, pp. 593–604. ISSN: 1477-9137, 0021-9533. DOI: 10.1242/jcs.115725. URL: https://journals.biologists.com/jcs/article/126/2/593/54213/Atg18-function-in-autophagy-is-regulated-by (visited on 11/05/2024).

Roosens, Nancy H. C. J. et al. (May 1, 2008). "Using Arabidopsis to explore zinc tolerance and hyperaccumulation". In: *Trends in Plant Science* 13.5. Publisher: Elsevier, pp. 208–215. ISSN: 1360-1385. DOI: 10.1016/j.tplants.2008.02.006. URL: https://www.cell.com/trends/plant-science/abstract/S1360-1385(08)00095-2 (visited on 09/13/2024).

Rossi, Guendalina et al. (2020). "Exocyst structural changes associated with activation of tethering downstream of Rho/Cdc42 GTPases". In: *Journal of Cell Biology* 219.2. Publisher: The Rockefeller University Press.

Roux, Kyle J. et al. (2012). "A promiscuous biotin ligase fusion protein identifies proximal and interacting proteins in mammalian cells". In: *Journal of Cell Biology* 196.6. Number: 6, pp. 801–810. ISSN: 00219525. DOI: 10.1083/jcb.201112098.

Scheller, Henrik Vibe et al. (2010). "Hemicelluloses". In: *Annual Review of Plant Biology* 61, pp. 263–289. ISSN: 1545-2123. DOI: 10.1146/annurev-arplant-042809-112315.

Schindelin, Johannes et al. (June 2012). "Fiji: an open-source platform for biological-image analysis". In: *Nat. Methods* 9.7, pp. 676–682. ISSN: 1548-7091. DOI: 10.1038/nmeth.2019. URL: http://dx.doi.org/10.1038/nmeth.2019.

Seregin, I V et al. (Nov. 1997). "Histochemical Investigation of Cadmium and Lead Distribution in Plants". In: *Russ. J. Plant Physiol.* 44.6, pp. 791–796. ISSN: 1021-4437. URL: http://dx.doi.org/ (visited on 01/25/2022).

Sevilem, Iris et al. (Jan. 2013). "Cell-to-cell communication via plasmodesmata in vascular plants". In: *Cell Adhesion & Migration* 7.1, pp. 27–32. ISSN: 1933-6918,

1933-6926. DOI: 10.4161/cam.22126. URL: http://www.tandfonline.com/doi/abs/10.4161/cam.22126 (visited on 01/02/2024).

Shapiro, S. S. et al. (Dec. 1, 1965). "An analysis of variance test for normality (complete samples)". In: *Biometrika* 52.3, pp. 591–611. ISSN: 0006-3444, 1464-3510. DOI: 10.1093/biomet/52.3-4.591. URL: https://academic.oup.com/biomet/article-lookup/doi/10.1093/biomet/52.3-4.591 (visited on 09/24/2024).

Shikanai, Yusuke et al. (Apr. 2020). "Callose Synthesis Suppresses Cell Death Induced by Low-Calcium Conditions in Leaves1". In: *Plant Physiology* 182.4, pp. 2199–2212. ISSN: 0032-0889. DOI: 10.1104/pp.19.00784. URL: https://www.ncbi.nlm.nih.gov/pmc/articles/PMC7140939/ (visited on 12/31/2023).

Simicek, Michal et al. (Oct. 2013). "The deubiquitylase USP33 discriminates between RALB functions in autophagy and innate immune response". In: *Nature Cell Biology* 15.10, pp. 1220–1230. ISSN: 1465-7392, 1476-4679. DOI: 10.1038/ncb2847. URL: https://www.nature.com/articles/ncb2847 (visited on 11/05/2024).

Smith, Ewen et al. (Dec. 17, 2004). *Modern Raman Spectroscopy – A Practical Approach*. 1st ed. Wiley. ISBN: 978-0-471-49668-7 978-0-470-01183-6. DOI: 10.1002/0470011831. URL: https://onlinelibrary.wiley.com/doi/book/10.1002/0470011831 (visited on 06/04/2024).

Student (Mar. 1908). "The Probable Error of a Mean". In: *Biometrika* 6.1, p. 1. ISSN: 00063444. DOI: 10.2307/2331554. URL: https://www.jstor.org/stable/2331554?origin=crossref (visited on 09/24/2024).

Synek, Lukás et al. (Oct. 2006). "AtEXO70A1, a member of a family of putative exocyst subunits specifically expanded in land plants, is important for polar growth and plant development". In: *Plant J.* 48.1, pp. 54–72. ISSN: 0960-7412. DOI: 10.1111/j.1365-313X.2006.02854.x. URL: http://dx.doi.org/10.1111/j.1365-313X.2006.02854.x.

Synek, Lukáš et al. (2021). "Plasma membrane phospholipid signature recruits the plant exocyst complex via the EXO70A1 subunit". In: *Proceedings of the National Academy of Sciences* 118.36. Publisher: National Acad Sciences, e2105287118.

Szymanski, D B et al. (Apr. 1998). "Control of GL2 expression in Arabidopsis leaves and trichomes". In: *Development* 125.7, pp. 1161–1171. ISSN: 0950-1991. DOI: 10.1242/dev.125.7.1161. URL: http://dx.doi.org/10.1242/dev.125.7.1161.

Tenhaken, Raimund (Jan. 7, 2015). "Cell wall remodeling under abiotic stress". In: *Frontiers in Plant Science* 5. Publisher: Frontiers. ISSN: 1664-462X. DOI: 10.3389/fpls.2014.00771. URL: https://www.frontiersin.org/journals/plant-science/articles/10.3389/fpls.2014.00771/full (visited on 09/12/2024).

TerBush, D R et al. (Dec. 1996). "The Exocyst is a multiprotein complex required for exocytosis in Saccharomyces cerevisiae". In: *EMBO J.* 15.23, pp. 6483–6494. ISSN: 0261-4189. URL: https://www.ncbi.nlm.nih.gov/pubmed/8978675.

Tewari, Rajesh Kumar et al. (May 2006). "Antioxidant responses to enhanced generation of superoxide anion radical and hydrogen peroxide in the copper-stressed mulberry plants". In: *Planta* 223.6, pp. 1145–1153. ISSN: 0032-0935. DOI: 10.1007/s00425-005-0160-5.

Thiele, Knut et al. (Apr. 2009). "The timely deposition of callose is essential for cytokinesis in Arabidopsis". In: *The Plant Journal* 58.1, pp. 13–26. ISSN: 0960-7412, 1365-313X. DOI: 10.1111/j.1365-313X.2008.03760.x. URL: https://onlinelibrary.wiley.com/doi/10.1111/j.1365-313X.2008.03760.x (visited on 01/02/2024).

Töller, Armin et al. (June 2008). "Dual function of Arabidopsis glucan synthase-like genes *GSL8* and *GSL10* in male gametophyte development and plant growth". In: *The Plant Journal* 54.5, pp. 911–923. ISSN: 0960-7412, 1365-313X. DOI: 10.1111/j.1365-313X.2008.03462.x. URL: https://onlinelibrary.wiley.com/doi/10.1111/j.1365-313X.2008.03462.x (visited on 01/02/2024).

Van Leeuwen, Wessel et al. (Dec. 2007). "Visualization of phosphatidylinositol 4,5-bisphosphate in the plasma membrane of suspension-cultured tobacco BY-2 cells and whole Arabidopsis seedlings". In: *The Plant Journal* 52.6, pp. 1014–1026. ISSN: 0960-7412, 1365-313X. DOI: 10.1111/j.1365-313X.2007.03292.x. URL: https:

//onlinelibrary.wiley.com/doi/10.1111/j.1365-313X.2007.03292.x (visited on 08/07/2024).

Varner, Joseph E. et al. (Jan. 27, 1989). "Plant cell wall architecture". In: *Cell* 56.2, pp. 231–239. ISSN: 0092-8674. DOI: 10.1016/0092-8674(89)90896-9. URL: https://www.sciencedirect.com/science/article/pii/0092867489908969 (visited on 03/27/2024).

Verma, Desh Pal S. et al. (2001). "Plant callose synthase complexes". In: *Plant Molecular Biology* 47.6, pp. 693–701. ISSN: 01674412. DOI: 10.1023/A:1013679111111. URL: http://link.springer.com/10.1023/A:1013679111111 (visited on 01/02/2024).

Vogel, J et al. (Feb. 2000). "Isolation and characterization of powdery mildew-resistant Arabidopsis mutants". In: *Proc. Natl. Acad. Sci. U. S. A.* 97.4, pp. 1897–1902. ISSN: 0027-8424. DOI: 10.1073/pnas.030531997. URL: http://dx.doi.org/10.1073/pnas.030531997.

Vogel, John P et al. (Sept. 2002). "PMR6, a Pectate Lyase–Like Gene Required for Powdery Mildew Susceptibility in Arabidopsis". In: *Plant Cell* 14.9, pp. 2095–2106. ISSN: 1040-4651. DOI: 10.1105/tpc.003509. URL: https://academic.oup.com/plcell/article-abstract/14/9/2095/6009825 (visited on 04/19/2022).

Vogel, John P et al. (Dec. 2004). "Mutations in PMR5 result in powdery mildew resistance and altered cell wall composition". In: *Plant J.* 40.6, pp. 968–978. ISSN: 0960-7412. DOI: 10.1111/j.1365-313X.2004.02264.x. URL: http://dx.doi.org/10.1111/j.1365-313X.2004.02264.x.

Vukašinović, Nemanja et al. (2017). "Microtubule-dependent targeting of the exocyst complex is necessary for xylem development in Arabidopsis". In: *New Phytologist* 213.3, pp. 1052–1067. ISSN: 1469-8137. DOI: 10.1111/nph.14267. URL: https://onlinelibrary.wiley.com/doi/abs/10.1111/nph.14267 (visited on 11/23/2023).

Wang, Bin et al. (Apr. 2022). "The function and biosynthesis of callose in high plants". In: *Heliyon* 8.4. DOI: 10.1016/j.heliyon.2022.e09248. URL: https://www.ncbi.nlm.nih.gov/pmc/articles/PMC8991245/ (visited on 12/31/2023).

Wang, Wei et al. (July 2020). "The Arabidopsis exocyst subunits EXO70B1 and EXO70B2 regulate FLS2 homeostasis at the plasma membrane". In: *New Phytologist* 227.2, pp. 529–544. ISSN: 0028-646X. DOI: 10.1111/nph.16515. URL: https://nph.onlinelibrary.wiley.com/doi/full/10.1111/nph.16515 (visited on 11/26/2023).

Wang, Xiaojing et al. (Feb. 2021). "Analysis and review of trichomes in plants". In: *BMC Plant Biology* 21.1, p. 70. ISSN: 1471-2229. DOI: 10.1186/s12870-021-02840-x. URL: https://doi.org/10.1186/s12870-021-02840-x (visited on 10/31/2023).

Wickham, Hadley et al. (Nov. 21, 2019). "Welcome to the Tidyverse". In: *Journal of Open Source Software* 4.43, p. 1686. ISSN: 2475-9066. DOI: 10.21105/joss.01686. URL: https://joss.theoj.org/papers/10.21105/joss.01686 (visited on 09/24/2024).

Williams, Lorraine E et al. (May 2000). "Emerging mechanisms for heavy metal transport in plants". In: *Biochimica et Biophysica Acta (BBA) - Biomembranes* 1465.1, pp. 104–126. ISSN: 00052736. DOI: 10.1016/S0005-2736(00)00133-4. URL: https://linkinghub.elsevier.com/retrieve/pii/S0005273600001334 (visited on 09/13/2024).

Wolter, M et al. (May 1993). "The mlo resistance alleles to powdery mildew infection in barley trigger a developmentally controlled defence mimic phenotype". In: *Mol. Gen. Genet.* 239.1, pp. 122–128. ISSN: 0026-8925. DOI: 10.1007/BF00281610. URL: http://dx.doi.org/10.1007/BF00281610.

Wu, Emilia L. et al. (2014). "CHARMM-GUI Membrane Builder toward realistic biological membrane simulations". In: *Journal of Computational Chemistry* 35.27. _eprint: https://onlinelibrary.wiley.com/doi/pdf/10.1002/jcc.23702, pp. 1997–2004.

ISSN: 1096-987X. DOI: 10.1002/jcc.23702. URL: https://onlinelibrary.wiley.com/doi/abs/10.1002/jcc.23702 (visited on 10/10/2024).

Xiao, D. et al. (Mar. 2018). "Changes in nitric oxide levels and their relationship with callose deposition during the interaction between soybean and *Soybean* mosaic virus". In: *Plant Biology* 20.2. Ed. by A. Pineda, pp. 318–326. ISSN: 1435-8603, 1438-8677. DOI: 10.1111/plb.12663. URL: https://onlinelibrary.wiley.com/doi/10.1111/plb.12663 (visited on 01/02/2024).

Xing, Hui-Li et al. (Nov. 2014). "A CRISPR/Cas9 toolkit for multiplex genome editing in plants". In: *BMC Plant Biology* 14.1, p. 327. ISSN: 1471-2229. DOI: 10.1186/s12870-014-0327-y. URL: https://doi.org/10.1186/s12870-014-0327-y (visited on 06/13/2023).

Yang, Kezhen et al. (2020). "Cell polarity: Regulators and mechanisms in plants". In: *Journal of Integrative Plant Biology* 62.1, pp. 132–147. ISSN: 1744-7909. DOI: 10.1111/jipb.12904. URL: https://onlinelibrary.wiley.com/doi/abs/10.1111/jipb.12904 (visited on 11/24/2023).

Yeats, Trevor et al. (2016). "Rapid Determination of Cellulose, Neutral Sugars, and Uronic Acids from Plant Cell Walls by One-step Two-step Hydrolysis and HPAEC-PAD". In: *BIO-PROTOCOL* 6.20. ISSN: 2331-8325. DOI: 10.21769/BioProtoc.1978. URL: https://bio-protocol.org/e1978 (visited on 11/09/2024).

Žárský, Viktor et al. (Jan. 2020). "Three subfamilies of exocyst EXO70 family subunits in land plants: early divergence and ongoing functional specialization". In: *J. Exp. Bot.* 71.1, pp. 49–62. ISSN: 0022-0957. DOI: 10.1093/jxb/erz423. URL: http://dx.doi.org/10.1093/jxb/erz423.

Zhang, Aihua et al. (Feb. 17, 2020). "The Ca2+ permeation mechanism of the ryanodine receptor revealed by a multi-site ion model". In: *Nature Communications* 11.1. Publisher: Nature Publishing Group, p. 922. ISSN: 2041-1723. DOI: 10.1038/s41467-020-14573-w. URL: https://www.nature.com/articles/s41467-020-14573-w (visited on 10/10/2024).

Zhang, Tong et al. (Aug. 14, 2023). "Exo84c interacts with VAP27 to regulate exocytotic compartment degradation and stigma senescence". In: *Nature Communications* 14.1, p. 4888. ISSN: 2041-1723. DOI: 10.1038/s41467-023-40729-5. URL: https://www.nature.com/articles/s41467-023-40729-5 (visited on 11/05/2024).

Zhao, Yuting et al. (Aug. 12, 2013). "Exo70 Generates Membrane Curvature for Morphogenesis and Cell Migration". In: *Developmental Cell* 26.3. Publisher: Elsevier, pp. 266–278. ISSN: 1534-5807. DOI: 10.1016/j.devcel.2013.07.007. URL: https://www.cell.com/developmental-cell/abstract/S1534-5807(13)00415-2 (visited on 10/22/2024).

Zhong, Ruiqin et al. (Feb. 2015). "Secondary Cell Walls: Biosynthesis, Patterned Deposition and Transcriptional Regulation". In: *Plant and Cell Physiology* 56.2, pp. 195–214. ISSN: 0032-0781. DOI: 10.1093/pcp/pcu140. URL: https://doi.org/10.1093/pcp/pcu140 (visited on 12/18/2023).

Zhu, Xi et al. (Aug. 27, 2024). "Identification of autophagy-related genes ATG18 subfamily genes in potato (Solanum tuberosum L.) and the role of StATG18a gene in heat stress". In: *Frontiers in Plant Science* 15, p. 1439972. ISSN: 1664-462X. DOI: 10.3389/fpls.2024.1439972. URL: https://www.frontiersin.org/articles/10.3389/fpls.2024.1439972/full (visited on 11/05/2024).